

## 7. SITE 1092<sup>1</sup>

Shipboard Scientific Party<sup>2</sup>

### BACKGROUND AND OBJECTIVES

Site 1092 (proposed site SubSAT-3B) is located on the northern Meteor Rise at a water depth of 1974 m (Fig. F1, p. 35; in the “Leg 177 Summary” chapter). The Meteor Rise is one of the dominant topographic features in the southeast Atlantic and marks the westward limit of the Agulhas Basin (Fig. F5, p. 39; in the “Leg 177 Summary” chapter). This oval-shaped, aseismic plateau consists of basement highs alternating with depositional basins and is the conjugate feature of the Islas Orcadas Rise in the western South Atlantic.

Much of the impetus for drilling Site 1092 came from a late Neogene sedimentary record obtained during Ocean Drilling Program (ODP) Leg 114 at Site 704, located only 34 nmi to the southeast. Site 704 was drilled to 671.7 meters below seafloor (mbsf) and recovered sediment of lower Oligocene to Quaternary age that was characterized by (1) the presence of carbonate throughout, (2) minor proportions of terrigenous matter that can be related to individual ice-rafting episodes, (3) the continuous presence of all calcareous and siliceous microfossil groups, and (4) a relatively good paleomagnetic stratigraphy. Until Leg 177, Site 704 was one of the few sites available from the Southern Ocean that had sufficient stratigraphic continuity and carbonate content to be suitable for Pliocene–Pleistocene paleoclimatic studies (Hodell and Venz, 1992; Hodell, 1993). One of the shortcomings of Site 704, however, is that it was drilled in a small sedimentary basin on the southern Meteor Rise that is surrounded by three basement highs that have provided material for downslope transport. For example, Parasound profiles near Site 704 revealed clear evidence for the top of a turbidite sequence beginning at ~25 mbsf. In addition, the soft, water-saturated sediment of Site 704 was easily disturbed during coring and handling in the exceptionally high seas experienced during Leg 114. We targeted Site 1092 in the hope that many of the short-

---

<sup>1</sup>Examples of how to reference the whole or part of this volume.

<sup>2</sup>Shipboard Scientific Party addresses.

comings of Site 704 could be overcome by our recent ODP drilling initiative on Meteor Rise.

A detailed geophysical survey was conducted of the northern Meteor Rise with efforts focused on a broad shallow area that is protected from the undesirable effects of downslope transport (Fig. F1). Site 1092 was selected on the basis of the uniformity and thickness of the upper seismic reflectors (Figs. F2, F3). Core PS2083-3 (Bathmann et al., 1992), located approximately 1.4 nmi to the northwest of Site 1092, obtained 10.61 m of sediment consisting of alternating diatom-bearing foraminifer mud, foraminifer ooze, and diatom mud deposited with an average sedimentation rate of 10 to 15 m/m.y.

Site 1092 is located in the Polar Front Zone (PFZ), ~3° north of the present-day position of the Polar Front. The shallow water depth (1974 m) places the site above the regional carbonate lysocline and calcium carbonate compensation depth and within a mixing zone between North Atlantic Deep Water (NADW) and Circumpolar Deep Water (CDW) (Fig. F2 in the “Leg 177 Summary” chapter). Together with Sites 704 (2532 m) and 1091 (4363 m), Site 1092 (1974 m) forms a depth transect on the Meteor Rise that can be used to study changes in the flux of NADW and its effect on the chemistry of CDW.

The primary objective at Site 1092 was to recover a carbonate-bearing, upper Miocene–Pleistocene sedimentary sequence that could be used to study (1) past migrations in the position of the PFZ, (2) changes in the mixing ratios of upper NADW and CDW in the Southern Ocean and its relation to high-latitude climate change, (3) the response of the Southern Ocean environment to the initiation of Northern Hemisphere glaciation, (4) marine proxies indicating the changes in the Antarctic cryosphere during the early and early late Pliocene when the climate was warmer than present, and (5) paleoceanographic changes in the subantarctic South Atlantic during the late Miocene (Müller et al., 1991; Wright et al., 1991).

## OPERATIONS

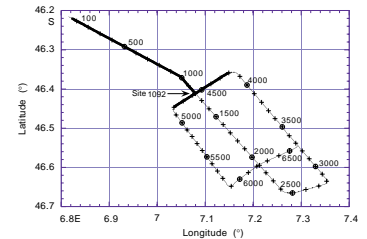
With a tail wind and low seas, the transit to Site 1092 on the Meteor Rise, 63 nmi to the northeast of Site 1091, was accomplished with an average speed of 11.6 kt. After the positioning approach had been completed and bow thrusters lowered, a positioning beacon was launched at 1145 hr on 7 January.

### Hole 1092A

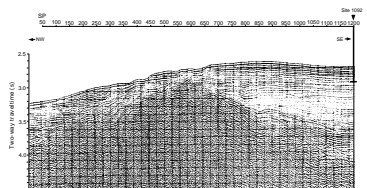
The drill bit was positioned at 1986 meters below rig floor (mbrf) for the initial core, and an 8-m core established the seafloor depth at 1987.5 mbrf. Continuous advanced hydraulic piston corer (APC) coring continued through Core 20H. Good environmental operating conditions permitted very good core recovery despite several core-liner failures, but the weather began to deteriorate as total depth (TD) was approached.

Withdrawal overpull on Core 19H was 30 kips, but Core 20H (188.5 mbsf TD) could not be pulled free with a force of 100 kips. It was necessary to drill over the core barrel for 5 m to free it. Vessel heave had increased to nearly 2 m by that time, and the APC assembly sustained severe damage from the drillover operation. Coring operations were

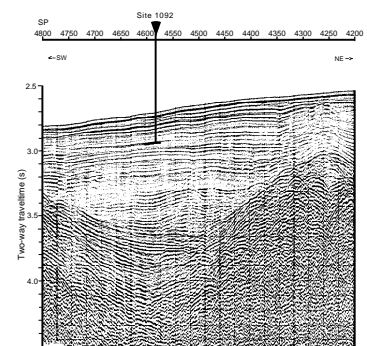
F1. Track line and shotpoints for the site survey of Site 1092, p. 21.



F2. Seismic line (northwest–southeast) showing the location and penetration depth of Site 1092, p. 22.



F3. Seismic line (northeast–southwest) showing the location and penetration depth of Site 1092, p. 23.



terminated because most scientific objectives and effective APC refusal had been reached.

### Hole 1092B

The ship was offset 10 m laterally. To achieve stratigraphic overlap, the new hole was spudded with the bit 4 m higher than for Core 177-1092A-1H. Core recovery indicated a seafloor depth about 3.5 m shallower than at Hole 1092A. Weather and motion conditions were less favorable for Hole 1092B, and core recovery and quality were diminished by an increase in core-liner failures and other motion-related factors. Overall recovery was good, but there were gaps in the recovered section. The coring depth target was reached with Core 18H at 168.9 mbsf, and the drill string was withdrawn for a respud.

### Hole 1092C

Coring began at 2115 hr on 8 January. Results improved with time and depth as the weather abated and vessel-motion conditions improved. The target depth of 165.5 mbsf was reached with Core 18H.

### Hole 1092D

The first three holes at Site 1092 had failed to achieve complete stratigraphic coverage of the section because of lost and disturbed cores at a relatively shallow depth. Thus, a fourth hole was requested to cover the interval equivalent to 36–64.5 mbsf in Hole 1092C.

When the bit had been pulled clear of the seafloor, the vessel was offset to a location near the center of the three positions determined for the first three holes. The new location was closest to Hole 1092B and, therefore, the seafloor depth of that hole was assumed. Hole 1092D was spudded at 0840 hr on 9 January and the hole was drilled ahead to 36.4 mbsf. From there, three consecutive APC cores were taken to a TD of 64.9 mbsf. Coring results were good and the scientific objectives of the site were achieved.

The drill string was recovered, and the bottom-hole assembly connections were inspected magnetically for cracks. The vessel was under way at 1818 hr on 9 January.

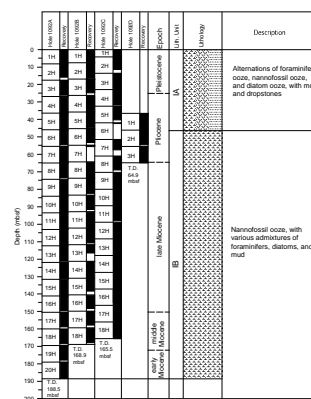
## LITHOSTRATIGRAPHY

### Overview

Site 1092 was drilled to a TD of 188.5 mbsf, recovering sediments of Pleistocene to early Miocene age (Fig. F4). The sediments consist of pale brown-green to pure white nannofossil ooze with mixtures of diatom and foraminifer oozes and muds. Smear-slide analyses reveal that nannofossil abundance ranges from trace amounts to 98%, whereas foraminifer percentages vary between 0% and 70% (see “Site 1092 Smear Slides,” p.59).

Nannofossils are the overall dominant lithologic (biogenic) component at this site. They alternate and are intermixed with foraminifers, diatoms, and mud, particularly in the upper 63 meters composite depth (mcd) of the sedimentary column. In this interval, foraminifer, foraminifer-bearing, diatom, and diatom-bearing varieties of nannofossil

F4. Lithologic summary of Site 1092, p. 24.



ooze alternate with ooze dominated by foraminifers and diatoms. Below 63 mcd, nannofossils are the predominant lithologic component and are replaced by diatoms or foraminifers in only a few intervals. The dominance of calcareous components is illustrated in Figure F5. The mud content of the entire sedimentary column is low, less than 20% based on smear-slide examination and X-ray diffraction (XRD) analyses (Fig. F5). Dropstones are present throughout the upper 63 mcd of the sedimentary column, although their exact placement within a core (in place or downhole contaminant?) is uncertain.

Recovery at this site was very good, reaching 96.6% in Hole 1092A, 85.6% in Hole 1092B, 91.1% in Hole 1092C, and 99.2% in Hole 1092D.

### X-ray Diffraction Results

XRD measurements were performed on the noncarbonate fraction of 35 samples from Hole 1092A (Table T1, also in ASCII format in the TABLES directory). Opal content inferred from XRD measurements shows downhole fluctuations between 0 and 90 wt% (Fig. F5). Opal abundance was expressed as bulk sediment opal concentration using bulk carbonate concentrations measured in the same sample intervals (see “Geochemistry,” p. 14). Bulk opal percentages are inversely correlated with bulk carbonate concentrations. In Quaternary and Pliocene sediments, bulk opal varies between 10 and 60 wt%, with a peak value of 80 wt% at the Pliocene/Pleistocene boundary (~33 mcd). Below a hiatus at ~65 mcd (early Pliocene), spanning a short time interval, and a series of hiatuses at the Miocene/Pliocene transition (~70–75 mcd), bulk opal abundances drop continuously to near 0 wt%. Proportions of the lithogenic fraction are below 15% in most intervals of the section. Higher lithogenic concentrations of up to 18%, associated with elevated values in magnetic susceptibility (see “Physical Properties,” p. 15), appear below the Pliocene/Pleistocene boundary.

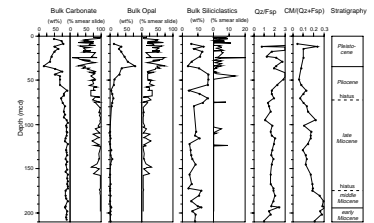
Quartz/feldspar values show maximal amplitudes and reach highest values in the Pliocene and Quaternary section; they remain constant at ~2.0 below the short hiatus at ~65 mcd. Clay minerals/(quartz+feldspar) values increase from 0.1 to 0.2 in the Miocene sediments below the hiatus. A pronounced downhole shift to values around 0.3 marks another hiatus (~176–177 mcd) that coincides with a sediment change from greenish white to reddish white nannofossil ooze and a further decrease of quartz/feldspar values toward 1.0. The long-term fluctuations of quartz/feldspar values and clay minerals/(quartz+feldspar) values, which are not discernible on smear slides, reveal a trend that is similar to the one observed at Site 1088, and probably reflect a downhole decrease in the grain size of lithogenic particles.

### Description of the Lithostratigraphic Unit

#### Unit I

One lithostratigraphic unit was recognized and was subdivided into two subunits (IA and IB) (Figs. F4, F5) on the basis of visual color variations on Hole 1092A core photographs. The transition between these two subunits is gradual. In Hole 1092C, the boundary falls somewhere within Core 177-1092C-6H, which had only 10 cm recovery (used for biostratigraphy). Subunit IA extends, therefore, to the bottom of Core 177-1092C-5H and Subunit IB begins at the top of Core 177-1092C-7H.

F5. Carbonate, opal, and mud contents, and mineral ratios at Site 1092, p. 25.



T1. X-ray diffraction data for Site 1092, p. 42.



### ***Subunit IA***

Intervals: 177-1092A-1H through 5H (0–46.0 mbsf; 2.55–53.89 mcd); 177-1092B-1H through 6H-4, 20 cm (0–50.1 mbsf; 0.55–53.89 mcd); 177-1092C-1H through 5H (0–42.0 mbsf; 0–46.05 mcd); 177-1092D-1H through 2H-4, 74 cm (36.4–51.1 mbsf; 38.47–53.89 mcd)

Age: Pleistocene to late Pliocene

Subunit IA consists of alternations of foraminifer, nannofossil, and diatom ooze with various mixtures of all biogenic components plus admixtures of mud, particularly in the foraminifer- and diatom-rich sediment types. Dropstones and smaller sized ice-rafted debris (IRD) are scattered throughout but are concentrated in the pale tan to tan diatom/foraminifer-rich varieties that additionally contain 5%–10% (and in places more) mud.

Calcium carbonate is present throughout Subunit IA. Carbonate concentrations, based on coulometric analyses, vary between 17 and 95 wt% (Fig. F5). A good correlation exists between calcium carbonate concentrations estimated by smear-slide analyses and those inferred from coulometric titration (Fig. F5). The darker (i.e., pale tan to tan) diatom- and mud-rich sediment types presumably represent glacial intervals and contain ~55 wt% carbonate or less (by coulometry). Carbonate contents of 60 wt% or more occur in white to greenish white sediments that presumably represent interglacial intervals.

### ***Subunit IB***

Intervals: 177-1092A-6H through 20H (46.0–188.5 mbsf; 53.89–210.84 mcd); 177-1092B-6H-4, 20 cm, through 18H (50.1–168.9 mbsf; 53.89–184.81 mcd); 177-1092C-7H through 18H (51.5–165.5 mbsf; 56.97–185.29 mcd); 177-1092D, 2H-4, 74 cm through Core 3H (51.1–64.9 mbsf; 53.89–68.92 mcd)

Age: late Pliocene to early Miocene in Hole 1092A; late Pliocene to middle Miocene in Holes 1092B and 1092C; late Pliocene in Hole 1092D, which ends at the Miocene/Pliocene transition

Subunit IB consists of nannofossil ooze, with variable amounts of foraminifers and diatoms down to ~100 mbsf in Hole 1092A (~112 mcd). Below this level, nannofossil ooze is the only major lithologic type; diatoms and foraminifers are minor admixtures. Mud is a minor component of these sediments. Rare dropstones occur in the upper portion of this subunit (e.g., at interval 177-1092D-3H-4, 8 cm). Many samples are completely free of terrigenous components, at least as determined by smear-slide analysis, particularly near the bases of the drill holes. Faint laminations, mottling, and rare burrows occur throughout this subunit.

## **CHRONOSTRATIGRAPHY**

### **Composite Depth**

Multisensor track (MST) and color reflectance data (650–750 nm) collected from Holes 1092A–1092D were used to determine depth offsets in the composite section. Gamma-ray attenuation (GRA) bulk density and magnetic susceptibility data were collected at 2- to 4-cm intervals on cores recovered from Holes 1092A–1092D. Color reflec-

tance data were collected at 4- to 6-cm intervals on cores from Holes 1092A–1092D (see “Physical Properties,” p. 15; “Lithostratigraphy,” p. 3; both for details about these MST and color reflectance data sets).

The composite data show that the cores from Site 1092 provide a continuous overlap to 188 mcd (base of Core 177-1092A-18H). The data used to construct the composite section and determine core overlaps are presented on a composite depth scale in Figures F6, F7, and F8. The depth offsets that comprise the composite section for Holes 1092A–1092D are given in Table T2 (also in ASCII format in the TABLES directory).

Stretching and compression of sedimentary features in aligned cores indicates distortion of the cored sequence. Because much of the distortion occurred within individual cores on depth scales of <9 m, it was not possible to align every feature in the MST and color reflectance records accurately by simply adding a constant to the mbsf core depth. Within-core scale changes will require postcruise processing to align smaller sedimentary features. Only after allowing variable adjustments of peaks within each core can an accurate estimate of core gaps be made.

Following construction of the composite depth section for Site 1092, a single spliced record was assembled for the aligned cores over the upper 188 mcd using cores from all four holes. The composite depths were aligned so that tie points between adjacent holes occurred at exactly the same depths in mcd. Intervals having significant disturbance or distortion were avoided if possible. The Site 1092 splice (Table T3, also in ASCII format in the TABLES directory) can be used as a sampling guide to recover a single sedimentary sequence between 0 and 188 mcd. Spliced records of magnetic susceptibility and GRA bulk density are shown in Figure F9.

## Biostratigraphy

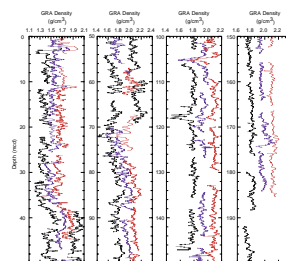
### Calcareous Nannofossils

Sediments recovered at Site 1092 provide a Pleistocene–early Miocene record. Pleistocene calcareous nannofossils are abundant to common, showing good to moderate preservation. The Pleistocene assemblages do not show a clear stratigraphic range of *Emiliania huxleyi* and *Pseudoemiliania lacunosa* in Hole 1092A, probably because of disturbance during recovery and/or reworking. However, the Pleistocene record of Hole 1092B provides good biostratigraphic resolution. Pliocene and Miocene intervals are characterized by the absence of biostratigraphic marker species, a fact which prevents an accurate biozonation. One or two samples per section were examined from Site 1092. Besides the standard zonations of Martini (1971) and Okada and Bukry (1980), we include Pleistocene events and age calibrations by Raffi et al. (1993) and Wei (1993). For the Miocene interval, the biochronology proposed by Berggren et al. (1995) is used. Tables T4 and T5 (both also in ASCII format in the TABLES directory), and Figure F10, summarize the main calcareous nannofossil biostratigraphic results.

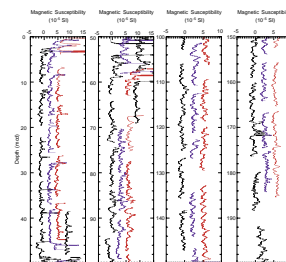
#### Pleistocene

The Pleistocene interval is represented from 0 to ~34 mcd at Site 1092 (Figs. F10, F11). The first occurrence (FO) of medium *Gephyrocapsa* (4–5.5  $\mu\text{m}$ ) approximates the Pliocene/Pleistocene boundary between 32.01 and 32.51 mcd (Fig. F10). The acme of *E. huxleyi* is recorded

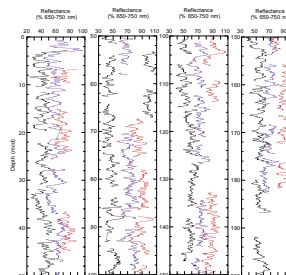
F6. Smoothed GRA bulk density data for Site 1092, p. 26.



F7. Smoothed magnetic susceptibility data for Site 1092, p. 27.



F8. Smoothed color reflectance data for Site 1092, p. 28.



T2. Composite depths for Site 1092, p. 43.

T3. Site 1092 splice tie points, p. 44.

between 0.65 and 1.15 mcd (base of Subzone NN21b). The FO of *E. huxleyi* is present from 1.72 to 2.15 mcd (Subzone NN21a) in Hole 1092A, whereas it is recognized at the top of Hole 1092A (Table T4). The last occurrence (LO) of *P. lacunosa* is present between 2.75 and 3.31 mcd, defining the base of Zone NN20. The LO and FO of *Reticulofenestra asanoi* are recognized at Site 1092 from 7.55 to 8.69 and from 12.05 to 13.55 mcd, respectively. The reentrance of medium *Gephyrocapsa* (4–5.5  $\mu\text{m}$ ) is recognized from 8.69 to 10.90 mcd in Hole 1092B, although this event is not identified in Hole 1092A because the species is almost absent above 14.0 mbsf (Table T4). The LO of *Gephyrocapsa* >5.5  $\mu\text{m}$  is observed from 14.65 to 16.05 mcd, whereas the FO of this species is present from 24.54 to 25.54 mcd. The LO of *Calcidiscus macintyreii* is not identified at Site 1092 because the species is very rare and its stratigraphic range is discontinuous (Table T4; Fig. F10).

### Pliocene

Characteristic late Pliocene assemblages are not observed at Site 1092. As a result, the standard biozones (NN16–18) are not identified because marker species such as *Discoaster pentaradiatus*, *Discoaster brouweri*, and *Discoaster tamalis* are absent. The LO of *Reticulofenestra pseudoumbilicus* (base of Zone NN16) is present from 61.39 to 62.39 mcd, and the FO of *P. lacunosa* (within Zones NN14–15; Rio et al., 1990) is recorded between 64.19 and 65.19 mcd (Fig. F10). The acme of small *Gephyrocapsa* is recognized between 62.39 and 64.19 mcd, close to the LO of *R. pseudoumbilicus* (Table T4). According to Marino (1994), the acme of small *Gephyrocapsa* approximates the early/late Pliocene boundary.

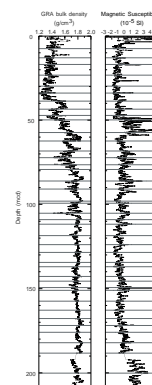
### Miocene

A transitional interval between the Pliocene and Miocene is defined between 70 and 75 mcd at Site 1092 (Figs. F10, F11). No calcareous nannofossil markers are identified that constrain the Miocene/Pliocene boundary. The closest middle/late Miocene boundary nannofossil event is the LO of *Coccolithus miopelagicus* (Zone NN8) that is present between 170.22 and 174.15 mcd, below the base of Chron 5n (156.04–157.04 mcd) (Table T4; Fig. F11). The presence of the last common occurrence (LCO) of *Cyclicargolithus floridanus*, the LO of *Coronocyclus nitescens*, and the LO of *Calcidiscus premacintyreii* in a short interval (between 176.73 and 179.85 mcd) suggests a hiatus of ~3 m.y. spanning the interval between Zones NN7 and NN5 (Fig. F10). The early/middle Miocene boundary is approximated by the FO of *C. premacintyreii* (Zone NN4) between 194.84 and 196.34 mcd. A lower Miocene assemblage is observed from below 196.34 mcd to the bottom of Hole 1092A. *Reticulofenestra bisecta*, a species whose disappearance was recognized at Site 1090 (23.9 Ma, base of Zone NN1), is absent in the deepest samples studied at Site 1092 (210.69 mcd). This indicates that the interval recovered is younger than 23.9 Ma (Zones NN1–2) (Table T4; Fig. F10).

### Planktic Foraminifers

The planktic foraminifer content is high in all studied core-catcher (CC) samples and the planktic foraminifers are, with only a few exceptions, well preserved. The planktic foraminifer fauna at Site 1092 can be divided into two major assemblages: a Pliocene–Pleistocene assemblage and a Miocene assemblage. The Pliocene–Pleistocene assemblage is dominated by *Neogloboquadrina pachyderma* (sinistral) with major contri-

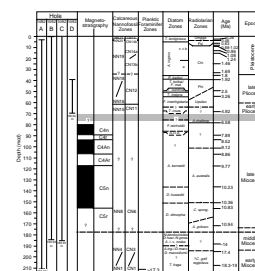
F9. Spliced magnetic susceptibility and GRA bulk density for Site 1092, p. 29.



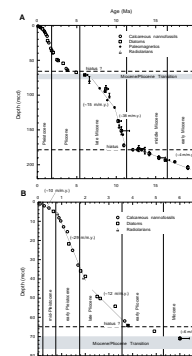
T4. Main calcareous nannofossil species in Holes 1092A and 1092B, p. 45.

T5. Biostratigraphic age assignments for Site 1092, p. 48.

F10. Bio- and magnetostratigraphic correlations and age designations for Site 1092, p. 30.



F11. Age-depth plots of biostratigraphic and paleomagnetic events at Site 1092, p. 31.



butions from *Globigerina bulloides*, *Globigerina quinqueloba*, *Globorotalia puncticulata*, and *Globorotalia puncticuloides* (Table T6, also in ASCII format in the TABLES directory). The Miocene assemblage is dominated by *G. bulloides*, *Globorotalia scitula*, and *Neogloboquadrina continousa*. The taxonomic concept of *N. continousa* applied to the Miocene of Site 1092 includes four- and five-chambered specimens. Future shore-based work will show if this group may be subdivided into *N. continousa* and *Neogloboquadrina mayeri*. Zonal subdivision is difficult because of the absence of several marker species; it is clear, however, that Sample 177-1092A-20H-CC, 13–18 cm (188.35 mbsf), is of early Miocene age (>17.3 Ma; Berggren et al., 1995) because of the presence of *Catapsydrax dissimilis*.

### Benthic Foraminifers and *Bolboforma*

Benthic foraminifers at Site 1092 are generally abundant and vary from poor to good in their state of preservation. Well preserved *Bolboforma* specimens are found intermittently downhole from Sample 177-1092A-14H-CC, 10–15 cm (131.11 mbsf, 147.23 mcd), notably within the middle Miocene interval.

Benthic foraminifers typically constitute less than 5% of the total foraminifer fauna from the >63- $\mu\text{m}$  fraction studied. Benthic foraminifer abundances are variable, reaching a maximum of 1265 specimens/cm<sup>3</sup> in Sample 177-1092B-1H-CC, 7–12 cm (10.55 mcd) (Table T7, also in ASCII format in the TABLES directory). Higher abundances below ~170 mcd coincide with a general decrease in sediment accumulation rates throughout the middle Miocene (Fig. F11). No barren intervals occur, suggesting that a continuous benthic foraminifer isotopic record should be relatively easy to obtain from this site.

Quantitative estimates of relative species abundance were made from Hole 1092A, with counts of up to 231 specimens/sample. Species richness is variable, with a maximum of 37 taxa recorded in Sample 177-1092A-20H-CC, 13–18 cm, and a minimum of 13 taxa in Sample 177-1092A-3H-CC, 9–14 cm (Table T7). Not all of this variability can be accounted for by sample size (see “Biostratigraphy,” p. 10, in the “Explanatory Notes” chapter), and a trend of increasing species richness is evident downhole (Table T7), notably in the early to middle Miocene. Such trends in species richness have been noted previously (e.g., at ODP Sites 747, 748, and 751 by Mackensen, 1992) and coincide with deep-water benthic foraminifer  $\delta^{18}\text{O}$  increases that have been attributed to a combination of ice growth and deep-water cooling (e.g., Shackleton and Kennett, 1975).

Three main benthic foraminifer assemblages are recognized at Site 1092, although there is clearly potential to further subdivide the assemblages after more detailed sampling.

#### Assemblage 1: Pliocene–Pleistocene

Assemblage 1 is present from the mudline down to Sample 177-1092A-7H-CC, 15–20 cm (73.51 mcd), and is dominated by *Globocassidulina subglobosa*, *Melonis barleanum*, *Melonis pompiliodes*, and *Pullenia bulloides*. The large, well-sorted foraminifer tests and high abundances throughout the upper 30 mcd at Site 1092 suggest that the Pleistocene sediments have undergone some winnowing.

#### Assemblage 2: middle to late Miocene

Assemblage 2 is present between Samples 177-1092A-8H-CC, 11–16 cm (83.17 mcd), and 18H-CC, 0–7 cm (188.35 mcd), and is dominated by

---

T6. Major planktic foraminifer species at Site 1092, p. 56.

---



---

T7. Benthic foraminifers at Site 1092, p. 58.

---

*Cibicidoides mundulus*, *Epistominella exigua*, and *Gyroidinoides soldanii*. Important additional taxa include *Laticarinina pauperata*, *Pullenia subcarinata*, *Stilostomella lepidula*, and *Uvigerina hispidocostata*. The LO of a single specimen of *Rectuvigerina senni* in Sample 177-1092A-13H-CC, 10–15 cm (135.77 mcd), indicates a middle Miocene age and does not fit well with the other stratigraphic evidence, which indicates a late Miocene age. Closer sampling in this interval will determine whether or not this age assignment for *R. senni* should be revised.

Abundant, well-preserved *Bolboforma* specimens are recorded in Samples 177-1092A-14H-CC, 10–15 cm (147.23 mcd), and 16H-CC, 14–19 cm (169.09 mcd), and are tentatively assigned to the *B. compressispinosa* Zone of Qvale and Spiegler (1989). The LCO of *B. compressispinosa* at Site 747 corresponds to an age of ~11.5 Ma (Mackensen and Spiegler, 1992), again suggesting that this interval at Site 1092 requires further investigation, because the other stratigraphic evidence clearly indicates younger ages.

### Assemblage 3: early Miocene

Assemblage 3 is present in Samples 177-1092A-19H-CC and 20H-CC, and is dominated by *S. lepidula*, *Martinotiella* sp., *G. subglobosa*, *G. soldanii*, and *C. mundulus*. Additional taxa which are not observed uphole include *Rectuvigerina multicoستا*, *Bulimina* cf. *simplex*, and an unidentified species of *Melonis* that is relatively abundant. The significant changes in the benthic foraminifer assemblages below ~190 mcd support the interpreted hiatus at this depth. An early Miocene age, however, is indicated by the co-occurrence of *U. hispidocostata* and *Nuttallides umbonifera*, similar to the middle early Miocene assemblages described by Mackensen (1992) from ODP Leg 120.

### Diatoms

For biostratigraphic age assignments, we used the zonations proposed by Gersonde and Bárcena (1998) and Gersonde et al. (1998) for the last 2 m.y. and the Neogene, respectively. All diatom stratigraphic information from the four holes was combined and converted to the mcd scale (Tables T5, T8, T9; all also in ASCII format in the TABLES directory).

Diatoms are generally common to abundant and preservation is moderate to good in the top ~45 mcd, an interval that is Pleistocene in age. Below this level we observe strongly variable abundance and preservation ranging from rare to abundant and poor to good, respectively, until ~65 mcd. The following ~10-m-thick interval, representing the Pliocene/Miocene transition, contains generally well-preserved diatom assemblages with common to abundant diatoms. The calcareous Miocene sequences below ~75 contain only trace to rare amounts of diatoms. However, acid-cleaned samples from this interval contain moderate to well-preserved assemblages that are useful for biostratigraphic age assignment and paleoenvironmental interpretation (Table T8). During examination of the diatom assemblages, we also encountered silicoflagellates in rare to trace numbers, as well as sporadic occurrences of *Actiniscus* species (Table T8).

### Biostratigraphy

Low sedimentation rates in the upper and middle Pleistocene intervals (~10 m/m.y.) and broad sample spacing did not allow us to subdivide the *Thalassiosira lentiginosa* Zone into its three subzones. The

---

T8. Diatom, silicoflagellate, ebridian, *Actiniscus*, sponge spicule, and phytolith occurrence, Site 1092, p. 60.

---

---

T9. Control points used to calculate sedimentation rates at Site 1092, p. 72.

---



base of the *T. lentiginosa* Zone was identified at 4.81 mcd. Because *Thalassiosira elliptipora*, the marker taxon for the *Actinocyclus ingens* Subzone c, was observed only intermittently, we combined Subzones b and c of the *A. ingens* zone. The FO of *Fragilariopsis barronii*, which defines the boundary between Subzones a and b of the *A. ingens* Zone, is noted at 21.74 mcd. Assemblages assigned to the upper Pliocene *Proboscia barboi* Zone, which corresponds with the Olduvai Subchron, were found between 35.8 and 38.3 mcd. Below this interval, the *Thalassiosira kolbei*–*Fragilariopsis matuyamae* Zone, which ranges from 2 to 2.5 Ma, is recognized to 49.1 mcd. The sediments representing the lower Pleistocene *A. ingens* Zone and the upper Pliocene *P. barboi* and *T. kolbei*–*F. matuyamae* Zones were deposited at a significantly higher sedimentation rate (~29 m/m.y.) than the mid- and upper Pleistocene sequences (Fig. F11). The intervals 49.1–50.1 and 50.1–54.2 mcd are marked by lower sedimentation rates, corresponding with the *Thalassiosira vulnifica* and the *Thalassiosira insigna* Zones, respectively. However, the presence of one or more hiatuses cannot be ruled out. Hiatuses punctuating this time interval have also been observed at Site 1091 (see “Chronostratigraphy,” p. 6, in the “Site 1091” chapter). The FO of *Fragilariopsis interfrigidaria*, which defines the base of the *F. interfrigidaria* Zone, was identified at 64.3 mcd. This zone straddles the early/late Pliocene boundary and has its base at 3.8 Ma. The diatom assemblages found below the *F. interfrigidaria* Zone to ~71 mcd do not allow a clear biostratigraphic age assignment. The nominate taxon of the underlying *Fragilariopsis barronii* Zone, which has its FO at 4.4 Ma, was not encountered in the samples studied. However, *Thalassiosira inura*, which has its FO at ~4.8 Ma, was noted to a depth of 67.2 mcd. This could be interpreted as indicating the base of the *T. inura* Zone at that depth. Alternatively, it might indicate the presence of a hiatus between the sediments assigned to the *F. interfrigidaria* and the *T. inura* Zones. We could not identify the underlying *Thalassiosira oestrupii* Zone, which straddles the Pliocene/Miocene boundary, because the nominate taxon whose LO defines the base of this zone was not present. However, the assemblages between 67.2 and 75.5 mcd contain taxa such as *Fragilariopsis praeinterfrigidaria*, *F. reinholdii*, *F. aurica*, and *F. clementia*, all known to occur in the earliest Pliocene and the latest Miocene. The uppermost portion of the *F. reinholdii* Zone, which is below the *T. oestrupii* Zone, is marked by the LO of *Hemidiscus triangularis*, which was placed by Harwood and Maruyama (1992) below the Miocene/Pliocene boundary at ~5.9 Ma. This taxon, which has a distinctive morphology, was found in Samples 177-1092C-8H-CC, 13–20 cm (75.45 mcd), and 177-1092A-8H-1, 120–122 cm (75.65 mcd). These samples are also characterized by common occurrences of fragments of the large diatom *Neobrunia mirabilis*. A similar assemblage was reported from ODP Site 701 (Shipboard Scientific Party, 1988), from a ~30-m-thick sedimentary interval tentatively correlated with the middle portion of late Miocene Chron C3A (Clement and Hailwood, 1991). This indicates that the Miocene/Pliocene transition falls in the interval between 67.2 and 75.6 mcd and is marked by one or more hiatuses, which is also indicated by magnetostratigraphy (see “Paleomagnetism,” p. 13).

The FO of *F. reinholdii*, the nominate taxon of the latest Miocene diatom zone, was found in a sample at 86.04 mcd. This interval was tentatively placed in a normal polarity interval of Chron C4, probably C4n.2n, which ranges from 7.65 to 8.07 Ma (see “Paleomagnetism,” p. 13). This suggests that the FO of *F. reinholdii* at Site 1092 is not at ~6.4

Ma as proposed by Harwood and Maruyama (1992) for southern high-latitude areas, but it is close to its FO in the equatorial Pacific at 8.2 Ma, a datum reported by Barron (1992). This is supported by the proximity of the FO of *Actinocyclus ingens* var. *ovalis* and FO of *F. reinholdii* at ~86.8 mcd. The datum of the FO of *A. ingens* var. *ovalis* has been placed in the reversed polarity interval of Chron C4 (Gersonde and Burckle, 1990). However, because of the broad spacing of acid-cleaned samples available for shipboard investigations, we have not been able to accurately identify the range of the FO of *A. ingens* var. *ovalis* at Site 1092. The same is true for the diatom age assignments for the Miocene interval below 90 mcd. Despite the broad sample spacing, it was possible to identify diatom zones in relation to the magnetostratigraphy. The base of the early late Miocene *Asteromphalus kennettii* and *Denticulopsis hustedtii* Zones was placed at ~137 and 151 mcd on the basis of the FO of *A. kennettii* and the LO of *Denticulopsis dimorpha*, respectively. The underlying *D. dimorpha* Zone was identified based on the presence of *D. meridionalis* and the abundant to dominant occurrence of the nominate species between ~150 and ~172 mcd. According to Harwood and Maruyama (1992), *D. meridionalis* is restricted to the upper portion of the *D. dimorpha* Zone. The age assignment on the basis of the three late Miocene diatom zones agrees well with the paleomagnetic correlation of these zones with Chrons C4A and C5 see “**Biostratigraphy**,” p. 10, in the “Explanatory Notes” chapter).

Below the interval assigned to the *D. dimorpha* Zone, we could not find markers of the late middle Miocene *Denticulopsis praedimorpha*–*Nitzschia denticuloides* and *D. praedimorpha* Zones. This indicates the presence of a hiatus that spans a time interval from the lower *D. dimorpha* Zone, close to the late/middle Miocene boundary, to the middle Miocene time period represented by the *N. denticuloides* and the *Denticulopsis hustedtii*–*Nitzschia grossepunctata* Zones. This interpretation agrees with the paleomagnetic stratigraphy as well as the radiolarian and calcareous nannofossil biostratigraphic age assignments. Physical properties measurements indicate distinct changes in resistivity and blue reflectance (450–550 nm) at 178–179 mcd, which may indicate a hiatus in the record of Site 1092 (Fig. F16).

Below the hiatus in the upper portion of the middle Miocene, diatoms indicate ages in the *N. denticuloides*, *D. hustedtii*–*N. grossepunctata*, and *Actinocyclus ingens* var. *nodus* Zones to a depth of 187 mcd. These zones represent the middle and lower portion of the middle Miocene between ~12.8 and ~14.4 Ma. They are underlain by sediments assigned to the lowermost middle Miocene *A. ingens*–*Denticulopsis maccollumii* and *D. maccollumii* Zones, which straddle the middle/early Miocene boundary between ~192.5 and ~194 mcd. This assignment is based on the presence of the nominate taxa. The co-occurrence of *Thalassiosira fraga*, *Nitzschia maleinterpretaria*, and *Azpeitia tabularis* between 202.5 and 209 mcd, places this interval in the middle *T. fraga* Zone, from ~18.3 to 19 Ma. The broad spacing of acid-cleaned samples makes it difficult to determine if the lower Miocene record is punctuated by hiatuses, or if this section was deposited at low sedimentation rates.

## Radiolarians

Radiolarian biostratigraphy at Site 1092 is based on the examination of 34 CC samples (Table T10, also in ASCII format in the TABLES directory). Radiolarians at Site 1092 are highly variable both in abundance and preservation. Samples from above ~80 mcd yield well-

---

T10. Main components of the radiolarian assemblages at Site 1092, p. 74.

---

preserved and abundant radiolarian assemblages, whereas those from the lower portion generally contain poorly to moderately preserved radiolarian assemblages of rare to common abundance. Radiolarian assemblages indicate that the recovered sequence is Pleistocene to early Miocene in age and that hiatuses occur at ~70 and ~180 mcd.

The uppermost sample (177-1092C-1H-CC, 7–12 cm [3.99 mcd]), is correlative to the Psi Zone based on the presence of *Stylatractus universus*. The boundary between the Psi and underlying Chi Zone can be placed above Sample 177-1092B-1H-CC, 0–7 cm (7.90 mcd). The base of the Chi Zone is placed at ~39 mcd (Table T9). Below the base of the Chi Zone, *Eucyrtidium calvertense*, diagnostic of the Phi Zone, and *Helotholus vema*, defining the Upsilon Zone, co-occur to a depth of ~63 mcd. This suggests reworking of *H. vema* into the Phi Zone, so that the distinction of the Phi and Upsilon Zones is not possible at Site 1092. The latest Miocene to earliest Pliocene Tau Zone, defined by the absence of *H. vema* and *Amphymenium challengerae*, is not recognized. This agrees with the diatom evidence that indicates a hiatus in this interval. Sample 177-1092A-7H-CC, 15–20 cm (73.51 mcd), contains few specimens of *A. challengerae*, which has a short range from 6.10 to 6.58 Ma. This sample is, therefore, correlative to the late Miocene *Amphymenium challengerae* Zone, and the base of the zone at 6.58 Ma can be placed at 78.34 mcd (Table T9). Zonal assignment of Samples 177-1092A-8H-CC through 177-1092C-10H-CC (80.11–97.42 mcd), characterized by the co-occurrence of *Lamprocyclus aegles* and *Stichocorys peregrina*, remains uncertain because of the lack of index species. Samples 177-1092A-10H-CC, 15–20 cm (104.17 mcd), and 177-1092B-13H-CC, 10–15 cm (126.97 mcd), yield *Cycladophora spongothorax*, and Sample 177-1092C-14H-CC, 15–20 cm (142.74 mcd), contains *Acrosphaera australis*. Thus, the interval from 104.17 to 142.74 mcd can be assigned to the late Miocene *Acrosphaera australis* Zone. The underlying interval from Sample 177-1092A-14H-CC, 10–15 cm (147.23 mcd), to Sample 177-1092B-17H-CC, 23–28 cm (174.82 mcd), is characterized by continuous occurrences of *Cyrtocapsella japonica*, which is common in middle Miocene strata of the northwestern Pacific and was also found at Site 1088. Two samples in this interval, 177-1092A-16H-CC, 14–19 cm (169.09 mcd), and 177-1092B-17H-CC, 23–28 cm (174.82 mcd), contain *Actinomma golownini*, which ranges in age from 13.61 to 10.77 Ma and suggests that this interval is correlative to the middle Miocene *Actinomma golownini* Zone or middle–late Miocene *Cycladophora spongothorax* Zone. The interval from 184.56 to 210.69 mcd, below Sample 177-1092B-18H-CC, 25–30 cm, is characterized by the presence of *Cycladophora gollii regipileus*, *Cyrtocapsella longithorax*, and *C. tetrapera*. These species indicate that the interval is of early Miocene age, younger than 19.11 Ma, and possibly correlative to the *Cycladophora gollii regipileus* Zone. As a result, it is possible to infer the presence of a hiatus from the early middle to late early Miocene, in agreement with other biostratigraphic data (Fig. F10).

The radiolarian assemblages from the Pleistocene Psi Zone to the late Miocene *Amphymenium challengerae* Zone are composed of characteristic species of the Antarctic region. However, those from the middle to upper Miocene interval below the *Amphymenium challengerae* Zone are different from hitherto known Antarctic faunas. These assemblages are composed of the genus *Didymocyrtis* and *Cyrtocapsella japonica*, indicating warmer conditions than are typical for the Antarctic region.

## Paleomagnetism

Archive halves of APC cores recovered at Site 1092 were measured using the shipboard pass-through magnetometer. Measurements were made at 5-cm intervals. Sections obviously affected by drilling disturbance were not measured. Hole 1092A was measured after alternating-field demagnetization at peak fields of 0 (natural remanent magnetization [NRM]), 5, 10, 15, 20, and 25 mT. Holes 1092B and 1092D were measured after peak fields of 0, 10, 20, and 25 mT. Hole 1092C was measured after peak fields of 0, 10, and 20 mT.

At Site 1092, NRM intensities vary around  $5 \times 10^{-4}$  A/m for most of the cored intervals. Two intervals of higher intensities were found between 42 and 53 mbsf ( $\sim 3 \times 10^{-3}$  A/m) and below 165 mbsf in Hole 1092A ( $\sim 2 \times 10^{-3}$  A/m).

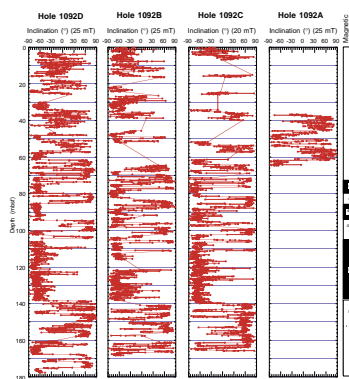
The inclination records are highly discontinuous in the upper 60 mbsf at all holes due to drilling-induced disturbance in the poorly consolidated nannofossil oozes. Below 70 mbsf in Holes 1092A–1092C, the inclination records indicate relatively well-defined polarity zones to a depth of 150 mbsf (Fig. F12; Table T5). The tentative polarity interpretation given in Figure F12 is based on the records from Holes 1092A and 1092D. However, unambiguous interpretations of the exact depth of polarity transitions cannot be made from shipboard data. Therefore, correlation of polarity zones to the geomagnetic polarity time scale must await detailed shore-based magnetic and biostratigraphic studies to confirm the exact position and identity of the polarity transitions.

## Stratigraphic Summary

A 210.74-mcd thick Pleistocene to early Miocene record was recovered at Site 1092. Holes 1092A–1092D were cored with the APC to 188.5, 168.9, 165.5, and 64.9 mbsf, respectively. Hole 1092D is a spot core drilled to ensure a continuous sedimentary section in the upper part of the cored interval. The combined MST and color reflectance data provide a nearly continuous section to 188 mcd (base of Core 177-1092A-18H) (Figs. F6, F7, F8).

All biostratigraphic datums, including calcareous nannofossil, diatom, and radiolarian events, and available magnetostratigraphic interpretations yield consistent age assignments throughout the record at Site 1092. The sedimentation rates in the carbonate-dominated sequences range between  $\sim 10$  and  $\sim 29$  m/m.y. for the Pliocene–Pleistocene, and between  $\sim 4$  and  $\sim 38$  m/m.y. for the Miocene (Fig. F11; Table T9). The upper and mid-Pleistocene sediments are restricted to the upper 5 mcd and were deposited at 10 m/m.y. This low sedimentation rate might be related to the occurrence of short hiatuses and/or sediment winnowing, as indicated by the presence of well-sorted foraminifer assemblages. A distinct increase in sedimentation rates is observed to a depth of  $\sim 45$  mcd, and can be related to sediments of early Pleistocene and latest Pliocene age. In the late Pliocene (below 45 mcd), estimated sedimentation rates drop to  $\sim 12$  m/m.y. (Fig. F11B). A similar Pleistocene–upper Pliocene sedimentation pattern was also observed at Sites 1090 and 1091. The early Pliocene is disturbed by a hiatus at  $\sim 65$  mcd, which spans approximately from 3.8 to 4.6 Ma (Figs. F10, F11). Disturbance caused by one or more hiatuses is also observed in the sediments spanning the Pliocene/Miocene boundary. For this reason, a preliminary Miocene/Pliocene boundary has been placed in a transition zone between 70 and 75 mcd. Below  $\sim 80$  mcd, the magnetostratigraphic data show distinct

F12. Inclination of the remanent magnetization after AF demagnetization at Holes 1092A–1092D, p. 32.



variations in magnetic inclination that have been interpreted using the biostratigraphic record (Fig. F10). Resulting sedimentation rates are ~15 m/m.y. between ~7 and 10 Ma, and increase to ~38 m/m.y. in the early late Miocene (Fig. F11). A hiatus at ~178 mcd, which spans the earliest late Miocene to middle Miocene time interval, lasted from ~11 to 13 Ma. The middle and lower Miocene sediments below this hiatus were deposited at an average rate of 4 m/m.y. However, it is possible that one or more hiatuses punctuate the early middle and early Miocene record at Site 1092. The base of Site 1092 is in the lower Miocene, representing an age of ~19 Ma.

The sedimentation pattern at Site 1092 closely resembles that observed at Site 704, located only 61 km to the southeast of Site 1092. However, the sedimentation rates at Site 1092 are considerably lower throughout the entire section. Late and mid-Pleistocene sedimentation rates at Site 704 are ~45 m/m.y. and increase to as high as ~100 m/m.y. in the early Pleistocene and latest Pliocene (Hailwood and Clement, 1991). At Site 1092, we observe an increase from ~10 to ~29 m/m.y. during this time period. Between the middle late Pliocene and the base of the early Pliocene, sedimentation rates are ~20 m/m.y. at Site 704, whereas the incomplete record at Site 1092 precludes the estimation of sedimentation rates at present. At both Sites 704 and 1092, the Pliocene/Miocene transition is disturbed by one or more hiatuses. Sedimentation rates at Site 704 average 27 m/m.y. for the late and middle late Miocene and increase to ~48 m/m.y. in the early late Miocene. A similar two-fold increase of sedimentation rate was observed at Site 1092, where late-middle late Miocene and early late Miocene rates are ~15 and ~38 m/m.y., respectively. At both sites, a prominent hiatus is found in the middle Miocene. However, sedimentation rates in the early middle and early Miocene at Site 704 (~30 m/m.y.) are distinctly higher than those calculated for Site 1092 (~4 m/m.y.). This might be further indication that the oldest record at Site 1092 is also disturbed by one or more hiatuses.

## GEOCHEMISTRY

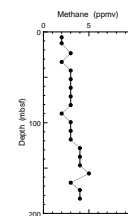
### Volatile Hydrocarbons

As a part of the shipboard safety and pollution program, volatile hydrocarbons (methane, ethane, and propane) were measured in the sediments of Site 1092 from every core in Hole 1092A using the standard ODP headspace sampling techniques (Table T11; Fig. F13). Headspace methane concentrations were quite low (2–5 parts per million by volume [ppmv]) throughout the sedimentary sequence. Ethane, propane, and other higher molecular weight hydrocarbons were not observed.

### Interstitial Water Chemistry

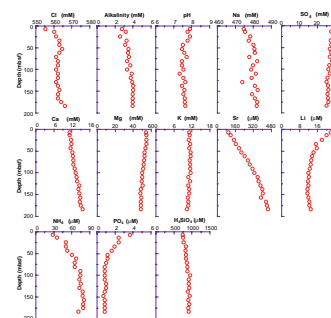
Shipboard chemical analyses of the interstitial water from Site 1092 followed the procedures for Sites 1088–1091. Twenty interstitial water samples from Hole 1092A were taken (one per core) to a depth of 183 mbsf (Table T12; Fig. F14).

The downhole gradients in most of the dissolved species are gradual and unremarkable. The maximum in Cl<sup>-</sup> of ~563 mM is reached at ~33 mbsf and is somewhat broader and less intense than those observed at neighboring Sites 1091 and 1093. This difference is probably the result of



T11. Concentrations of methane at Site 1092, p. 76.

F13. Concentration of methane vs. depth at Site 1092, p. 33.



T12. Interstitial water chemistry at Site 1092, p. 77.

F14. Interstitial water chemistry profiles vs. depth at Site 1092, p. 34.



the absence of diatom mats at Site 1092, yielding lower sedimentation rates and higher diffusion rates in the upper 100 mbsf. The major cations (Ca, Mg, and Sr) behave in a manner similar to that seen in Sites 1088 and 1090, and, qualitatively, the behavior is similar to that of Site 1089 below its Ca<sup>+2</sup> minimum. Silicate rises very gradually to values near 1000  $\mu\text{M}$ , consistent with biogenic sedimentation and little influence from clays, zeolites, or cherts. Generally speaking, the agreement is excellent between these results and those obtained previously at nearby Site 704 (Froelich et al., 1991). One exception is a significant offset between the chloride profiles of the two sites, a difference for which we have no obvious explanation.

The redox characteristics of Site 1092 can be characterized as generally oxic or suboxic throughout the section. Sulfate reduction rates are very low as indicated by the absence of H<sub>2</sub>S (by scent) and the minor decreases in sulfate concentrations to ~26 mM at the bottom of the section. Ammonium increases moderately downhole to a relatively constant value of ~75  $\mu\text{M}$  below 90 mbsf. Phosphate concentrations are low throughout the section, registering barely above detection limits below 50 mbsf. Mn<sup>+2</sup> was below detection limits for all samples, and Fe<sup>+2</sup> was not measured at this site.

### Solid Phase Analysis

The shipboard solid phase analysis at Site 1092 consisted of measurements of inorganic carbon throughout the sedimentary sequence of Hole 1092A, and preliminary measurements of total carbon (TC), total nitrogen (TN), and total sulfur in selected samples from Cores 177-1092A-1H through 10H (Table T13; Fig. F15; for methods see “Geochemistry,” p. 18, in the Explanatory Notes” chapter). Calcium carbonate (CaCO<sub>3</sub>) contents in Hole 1092A range from 16.7 to 94.6 wt%, with an average value of 80.2 wt%. Above 50 mbsf, a minimum value (16.7 wt%) of CaCO<sub>3</sub> concentrations was observed at 29 mbsf within the section of nannofossil- and foraminifer-bearing diatom ooze (see “Lithostratigraphy,” p. 3). CaCO<sub>3</sub> contents are consistently very high (average value of 88 wt%) from 50 mbsf to the bottom of the section.

Total organic carbon (TOC) contents vary between 0 and 0.7 wt%, with an average value of 0.16 wt%. Most TOC concentrations, taken as the difference between TC and carbonate carbon measurements, are below 0.1 wt%. Many samples have concentrations below the detection limits of the shipboard analytical technique, because these sediments are mainly composed of calcareous microfossils. TN contents are generally low (0 to 0.07 wt%). Sulfur was not detected. TOC/TN values vary between 0.5 and 11.0, indicating a predominance of marine organic material. However, these low TOC/TN values are probably underestimated because of the low TOC contents of the sediment. Pyrolysis analyses were not performed because of the low organic-carbon content of the sediments.

## PHYSICAL PROPERTIES

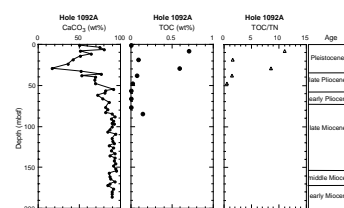
GRA bulk density, magnetic susceptibility, natural gamma-ray (NGR) emission, and *P*-wave velocity were measured with the MST on whole-core sections recovered from Site 1092. Color reflectance and resistivity were measured on the working half of all split APC cores using the

---

T13. Analytical results of IC, CaCO<sub>3</sub>, TC, TOC, TN, TS, and TOC/TN at Site 1092, p. 79.

---

F15. CaCO<sub>3</sub>, TOC, and TOC/TN vs. depth at Hole 1092A, p. 35.



Oregon State University Split Core Analysis Track (OSU-SCAT) (see “[Explanatory Notes](#)” chapter). Other physical properties measurements conducted on discrete core samples included moisture, density, and *P*-wave velocity. Measured parameters were initial wet bulk mass ( $M_b$ ), dry mass ( $M_d$ ), and dry volume ( $V_d$ ). Velocity was measured on split-core sections using the *P*-wave velocity sensor 3 (PWS3). Table [T14](#) and Figure [F16](#) summarize the physical properties measurements performed at Site 1092.

### Multisensor Track and Split Core Analysis Track

All physical properties measured at Site 1092 generally covary. As with previous Leg 177 sites, downhole variations in physical properties are controlled largely by changes in the proportion of carbonate vs. siliceous sedimentary components. GRA bulk densities and discrete-sample bulk densities generally agree very well (Fig. [F17](#)). Porosity determined gravimetrically on discrete samples (moisture and density [MAD] method) and sediment resistivity show the expected inverse relationship. Low porosities (high resistivities) are associated with intervals of high carbonate content. As was observed at Site 1091, carbonate-rich intervals exhibit bright reflectance with little divergence between the blue, red, or near-infrared bands. In contrast, diatom-rich intervals exhibit a greater contrast between blue and red reflectance. In Figure [F16](#) reflectance in the blue band (450–550 nm) is shown for all holes at Site 1092. In Hole 1092A, between 65 and 105 mcd, reflectance values were approximately 5% lower on average than in Holes 1092B–1092D. The reason for this has been attributed to an insufficient number of calibration points in this interval. Correction of these data may be possible.

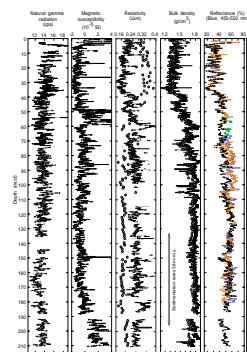
In the upper 35 mcd of Site 1092, physical properties exhibit rhythmic variability related to alternation between diatom-rich and carbonate-rich layers. In the upper 20 mcd, there is cyclicity with a period of ~2 m. Between 20 and 35 mcd, the period of cyclicity increases to ~4 m (Fig. [F18](#)), probably as a result of increased sedimentation rates in this interval (see “[Chronostratigraphy](#),” p. 5). Increased sedimentation rates are consistent with the trends in bulk density and magnetic susceptibility, both of which increase below 35 mcd.

At 35 mcd, the large amplitude alternations between siliceous and carbonate dominance end, followed by a transition zone between 35 and 50 mcd where a carbonate-dominated lithology begins (see “[Lithostratigraphy](#),” p. 3). This transition is clearly visible in the suite of physical properties measurements shown in Figure [F18](#), especially in the red/blue values where, after an initial sudden decrease, values gradually approach 1.0 (high carbonate content) by 50 mcd.

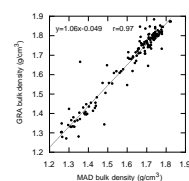
Magnetic susceptibility increases in the interval between 49 and 59 mcd. This would suggest an increase in terrigenous content that may have resulted from decreased sedimentation rates and/or increased terrigenous influx. Mud content determined by smear-slide analysis is low (see “[Lithostratigraphy](#),” p. 3) and can, therefore, not be linked to the magnetic susceptibility. In fact, alternations between finer grained foraminifer/nannofossil layers and coarse foraminifer-rich layers (see “[Lithostratigraphy](#),” p. 3), in conjunction with the low mud content, may suggest some winnowing in this interval. The cores contain numerous large dropstones in this interval (see “[Lithostratigraphy](#),” p. 3), which are most likely the cause of the increased magnetic susceptibility.

T14. Physical properties measurements conducted at Site 1092, p. 80.

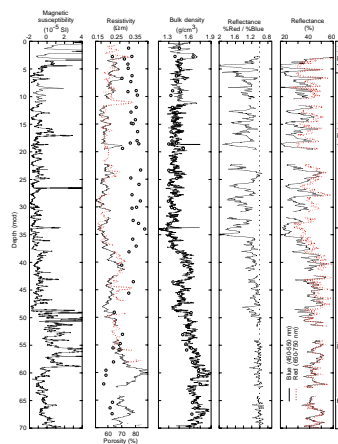
F16. Site 1092 NGR, magnetic susceptibility, porosity, resistivity, bulk density, and blue reflectance, p. 36.



F17. Relationship between GRA and MAD bulk density at Site 1092, p. 37.



F18. Variations of magnetic susceptibility, porosity, resistivity, bulk density, and reflectance in the upper 70 mcd, p. 38.



Between 60 and 110 mcd, there is progressively less downhole variation in the suite of measured physical properties. Below ~110 mcd, density is ~1.8 g/cm<sup>3</sup>. Reflectance and resistivity also increase (porosity decreases), corresponding to the increase in carbonate content in the same depth interval (see “[Geochemistry](#),” p. 14; “[Lithostratigraphy](#),” p. 3). Below 110 mcd, downhole variations in physical properties are of much lower amplitude than above this depth. This is especially true of bulk density values, which are very uniform between 110 and 190 mcd.

Near the base of the section, around 188 mcd, there is a gap in the record resulting from incomplete recovery. The last two cores (177-1092A-19H and 20H) show a clear change in physical properties (Figs. [F16](#), [F19](#)), and biostratigraphic evidence suggests a hiatus around 190 mcd (see “[Chronostratigraphy](#),” p. 5). GRA bulk density drops to ~1.7 g/cm<sup>3</sup>, porosity increases, and magnetic susceptibility increases notably. Smear-slide analysis (see “[Lithostratigraphy](#),” p. 3) indicates higher foraminifer content relative to nannofossils, which can explain the decrease in density and lower porosity. The increase in magnetic susceptibility requires either an increase in terrigenous material or a change in its mineralogical composition, which may be indicated by the higher clay mineral to quartz plus feldspar content of the lithogenic fraction (see “[Lithostratigraphy](#),” p. 3). The red/blue reflectance values increase in Cores 177-1092-19H and 20H (Fig. [F19](#)), indicating that a noncarbonate component becomes significant. The rarity of diatoms, however, cannot be the cause. Instead, the redder color may be related to iron oxides, and this is consistent with the greater magnetic susceptibility.

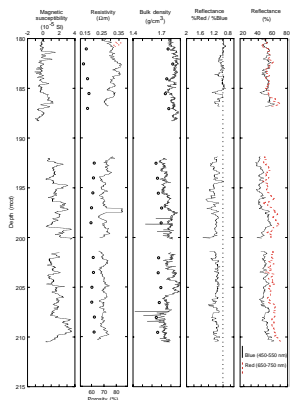
### P-wave Velocity

Figure [F20](#) shows *P*-wave velocities measured with the PWS3 velocimeter and *P*-wave logger (PWL). PWS3 velocities generally reflect the trends in bulk density described above. Higher velocities were observed in the upper 65 mcd of Site 1092 than at any previous Leg 177 site. This is presumably a result of the higher concentration of ice-rafted terrigenous grains. Below 65 mcd, where IRD is much less common (see “[Lithostratigraphy](#),” p. 3), velocities are more similar to those of other carbonate-rich sediments from other Leg 177 sites. The PWL velocities obtained from the MST were problematic in that values were considerably lower than those of the PWS3 and showed a clear bimodal distribution (Fig. [F20](#)). The reason for this was a defective threshold adjustment knob, resulting in the inaccurate auto-picking of *P*-wave traveltimes by the PWL. The problem was corrected during the first few cores logged at Site 1093.

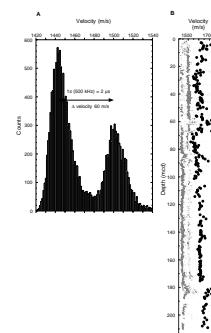
### Thermal Conductivity

A total of 91 thermal conductivity measurements were taken from Holes 1092A–1092C (Table [T15](#), also in ASCII format in the [TABLES](#) directory). The values range between 0.69 and 1.23 W/(m·K), the widest range measured among Sites 1088–1092. The distinct bimodal distribution of values (Fig. [F21](#)) reflects a sudden decrease of porosity from ~80% to ~60%, as well as a change in lithology, in the depth interval between 40 and 60 mcd. The lower values, with an average between 0.7 and 0.8 W/(m·K), represent the diatom ooze intervals within Subunit IA (see “[Lithostratigraphy](#),” p. 3). The higher values, clustering

F19. Variations of magnetic susceptibility, porosity, resistivity, bulk density, and reflectance in 180–215 mcd, [p. 39](#).

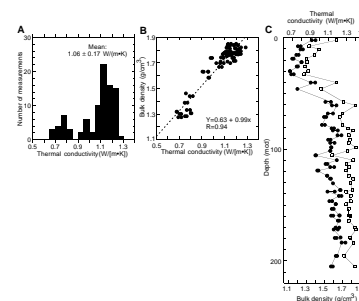


F20. Distribution and downhole variation of *P*-wave velocity, [p. 40](#).



T15. Thermal conductivity measurements at Site 1092, [p. 81](#).

F21. Thermal conductivity measurements at Site 1092, [p. 41](#).



between 1.1 and 1.2 W/(m·K), characterize the calcareous ooze of Sub-unit IB.

## REFERENCES

- Barron, J.A., 1992. Neogene diatom datum levels in the equatorial and North Pacific. In Ishizaki, K., and Saito, T. (Eds.), *The Centenary of Japanese Micropaleontology*: Tokyo (Terra Sci. Publ.), 413–425.
- Bathmann, U., Schulz-Baldes, M., Fahrbach, E., Smetacek, V., and Hubberten, H.-W., 1992. The Expeditions ANTARKTIS IX/1-4 1990/1991. *Rep. Polar Res.*, 100.
- Berggren, W.A., Kent, D.V., Swisher, C.C., III, and Aubry, M.-P., 1995. A revised Cenozoic geochronology and chronostratigraphy. In Berggren, W.A., Kent, D.V., Aubry, M.-P., and Hardenbol, J. (Eds.), *Geochronology, Time Scales and Global Stratigraphic Correlation*. Spec. Publ.—Soc. Econ. Paleontol. Mineral. (Soc. Sediment. Geol.), 54:129–212.
- Clement, B.M., and Hailwood, E.A., 1991. Magnetostratigraphy of sediments from Sites 701 and 702. In Ciesielski, P.F., Kristoffersen, Y., et al., *Proc. ODP, Sci. Results*, 114: College Station, TX (Ocean Drilling Program), 359–366.
- Froelich, P.N., Mortlock, R.A., Mefferd, M., and Powers, J., 1991. Interstitial-water chemistry: abyssal South Atlantic and East Georgia Basins, Islas Orcadas and Meteor Rises. In Ciesielski, P.F., Kristoffersen, Y., et al., *Proc. ODP, Sci. Results*, 114: College Station, TX (Ocean Drilling Program), 719–731.
- Gersonde, R., and Bárcena, M.A., 1998. Revision of the late Pliocene–Pleistocene diatom biostratigraphy for the northern belt of the Southern Ocean. *Micropaleontology*, 44:1–15.
- Gersonde, R., and Burckle, L.H., 1990. Neogene diatom biostratigraphy of ODP Leg 113, Weddell Sea (Antarctic Ocean). In Barker, P.F., Kennett, J.P., et al., *Proc. ODP, Sci. Results*, 113: College Station, TX (Ocean Drilling Program), 761–789.
- Gersonde, R., Spiess, V., Flores, J. A., Hagen, R., and Kuhn, G., 1998. The sediments of Gunnerus Ridge and Kainan Maru Seamount (Indian sector of Southern Ocean). *Deep-Sea Res. Part I*, 45:1515–1540.
- Hailwood, E.A., and Clement, B.M., 1991. Magnetostratigraphy of Sites 703 and 704, Meteor Rise, southeastern South Atlantic. In Ciesielski, P.F., Kristoffersen, Y., et al., *Proc. ODP, Sci. Results*, 114: College Station, TX (Ocean Drilling Program), 367–386.
- Harwood, D.M., and Maruyama, T., 1992. Middle Eocene to Pleistocene diatom biostratigraphy of Southern Ocean sediments from the Kerguelen Plateau, Leg 120. In Wise, S.W., Jr., Schlich, R., et al., *Proc. ODP, Sci. Results*, 120: College Station, TX (Ocean Drilling Program), 683–733.
- Hodell, D.A., 1993. Late Pleistocene paleoceanography of the South Atlantic sector of the Southern Ocean: Ocean Drilling Program Hole 704A. *Paleoceanography*, 8:47–67.
- Hodell, D.A., and Venz, K., 1992. Toward a high-resolution stable isotopic record of the Southern Ocean during the Pliocene–Pleistocene (4.8 to 0.8 Ma). In Kennett, J.P., Warnke, D.A. (Eds.), *The Antarctic Paleoenvironment: A Perspective on Global Change* (Pt. 1). Am. Geophys. Union, Antarct. Res. Ser., 56:265–310.
- Mackensen, A., 1992. Neogene benthic foraminifers from the southern Indian Ocean (Kerguelen Plateau): biostratigraphy and paleoecology. In Wise, S.W., Jr., Schlich, R., et al., *Proc. ODP, Sci. Results*, 120: College Station, TX (Ocean Drilling Program), 649–673.
- Mackensen, A., and Spiegler, D., 1992. Middle Eocene to early Pliocene *Bolboforma* (algae?) from the Kerguelen Plateau, southern Indian Ocean. In Wise, S.W., Jr., Schlich, R., et al., *Proc. ODP, Sci. Results*, 120: College Station, TX (Ocean Drilling Program), 675–682.
- Marino, M., 1994. Biostratigrafia integrata a nannofosili calcari e foraminiferi planctonici di alcune successioni terrigene pliocenico-superiori del Bacino di Sant' Arcangelo (Appennino meridionale). *Boll. Soc. Geol. Ital.*, 113:329–354.



- Martini, E., 1971. Standard Tertiary and Quaternary calcareous nannoplankton zonation. In Farinacci, A. (Ed.), *Proc. 2nd Int. Conf. Planktonic Microfossils Roma*: Rome (Ed. Tecnosci.), 2:739–785.
- Müller, D.W., Hodell, D.A., and Ciesielski, P.F., 1991. Late Miocene to earliest Pliocene (9.8–4.5 Ma) Paleoceanography of the subantarctic Southeast Atlantic: stable isotopic, sedimentologic, and microfossil evidence. In Ciesielski, P.F., Kristoffersen, Y., et al., *Proc. ODP, Sci. Results*, 114: College Station, TX (Ocean Drilling Program), 459–474.
- Okada, H., and Bukry, D., 1980. Supplementary modification and introduction of code numbers to the low-latitude coccolith biostratigraphic zonation (Bukry, 1973; 1975). *Mar. Micropaleontol.*, 5:321–325.
- Qvale, G., and Spiegler, D., 1989. The stratigraphic significance of *Bolboforma* (algae, Chrysophyta) in Leg 104 samples from the Vøring Plateau. In Eldholm, O., Thiede, J., Taylor, E., et al., *Proc. ODP, Sci. Results*, 104: College Station, TX (Ocean Drilling Program), 487–495.
- Raffi, I., Backman, J., Rio, D., and Shackleton, N.J., 1993. Plio-Pleistocene nannofossil biostratigraphy and calibration to oxygen isotopes stratigraphies from Deep Sea Drilling Project Site 607 and Ocean Drilling Program Site 677. *Paleoceanography*, 8:387–408.
- Rio, D., Raffi, I., and Villa, G., 1990. Pliocene-Pleistocene calcareous nannofossil distribution patterns in the Western Mediterranean. In Kastens, K.A., Mascle, J., et al., *Proc. ODP, Sci. Results*, 107: College Station, TX (Ocean Drilling Program), 513–533.
- Shackleton, N.J., and Kennett, J.P., 1975. Paleotemperature history of the Cenozoic and the initiation of Antarctic glaciation: oxygen and carbon isotope analyses in DSDP Sites 277, 279, and 281. In Kennett, J.P., Houtz, R.E., et al., *Init. Repts. DSDP*, 29: Washington (U.S. Govt. Printing Office), 743–755.
- Shipboard Scientific Party, 1988. Preliminary results of subantarctic South Atlantic Leg 114 of the Ocean Drilling Program. In Ciesielski, P.F., Kristoffersen, Y., et al., *Proc. ODP, Init. Repts.*, 114: College Station, TX (Ocean Drilling Program), 797–804.
- Wei, W., 1993. Calibration of Upper Pliocene-Lower Pleistocene nannofossil events with oxygen isotope stratigraphy. *Paleoceanography*, 8:85–99.
- Wright, J.D., Miller, K.G., and Fairbanks, R.G., 1991. Evolution of modern deepwater circulation: evidence from the late Miocene Southern Ocean. *Paleoceanography*, 6:275–290.

Figure F1. Track line and shotpoints for the site survey of Site 1092 conducted during *Thompson* Cruise TTN057. The bold portion of the track line corresponds to the segments of the seismic profile displayed in Figures F2, p. 22, (northwest–southeast line) and F3, p. 23, (northeast–southwest line).

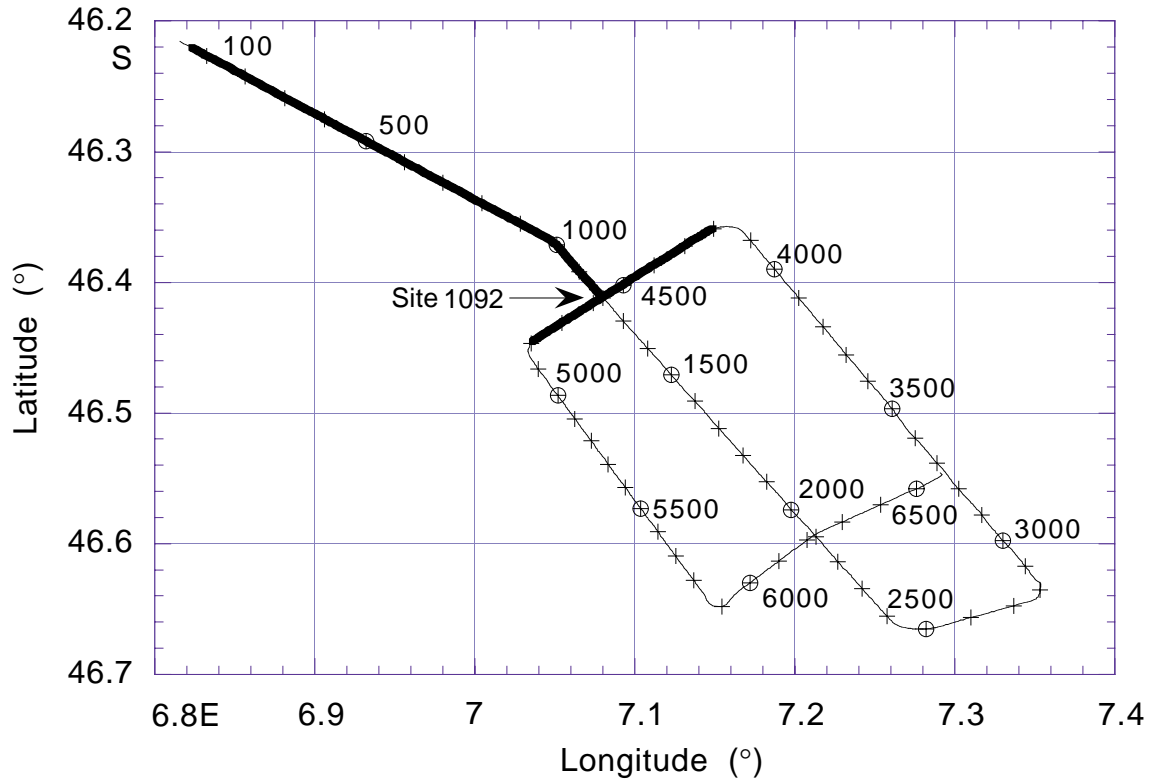


**Figure F2.** Single-channel seismic line (oriented northwest–southeast) collected during site-survey *Thompson* Cruise TTN057 showing the location and penetration depth of Site 1092. SP = shotpoint.

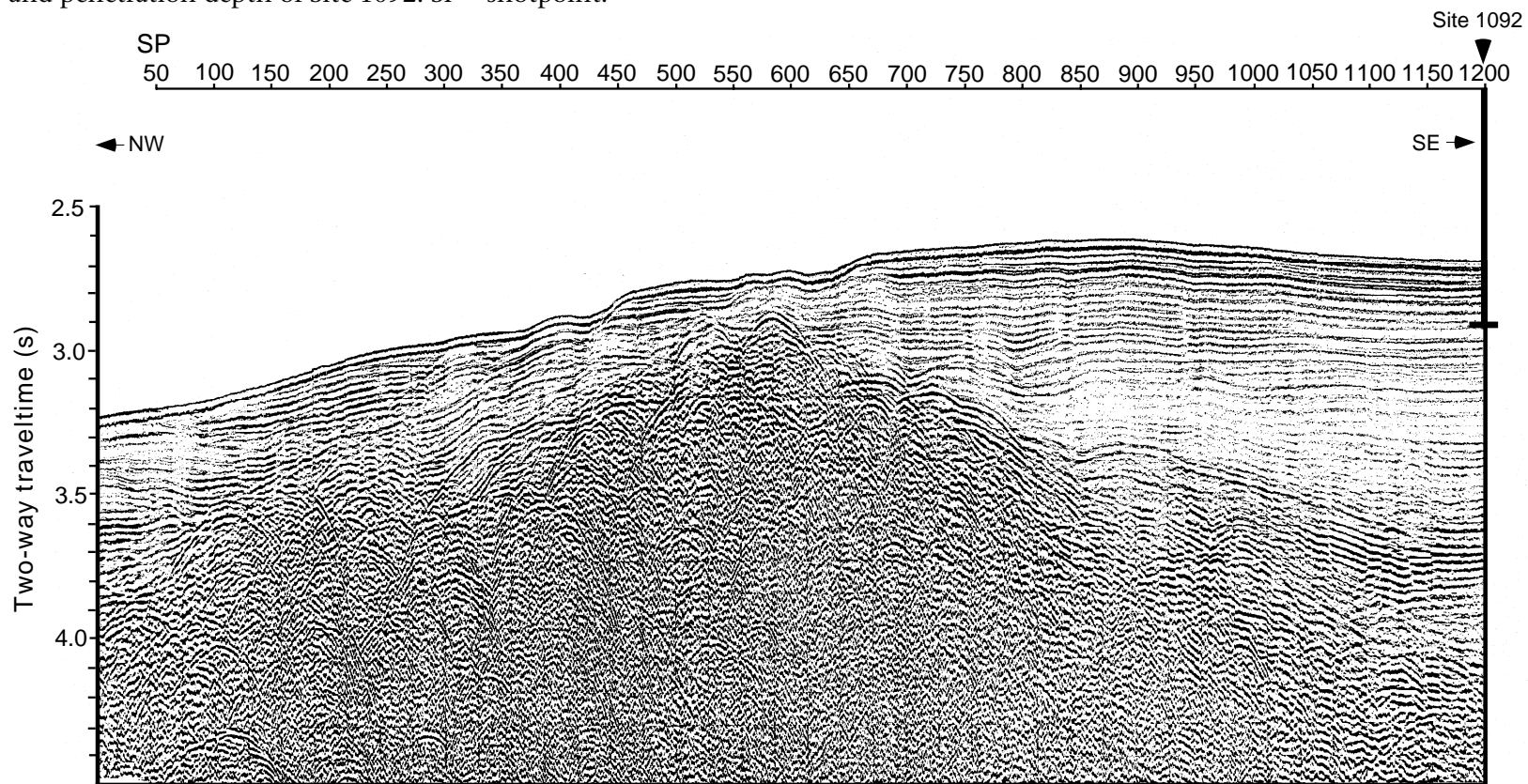


Figure F3. Single-channel seismic line (oriented northeast–southwest) collected during site-survey *Thompson* Cruise TTN057 showing the location and penetration depth of Site 1092. SP = shotpoint.

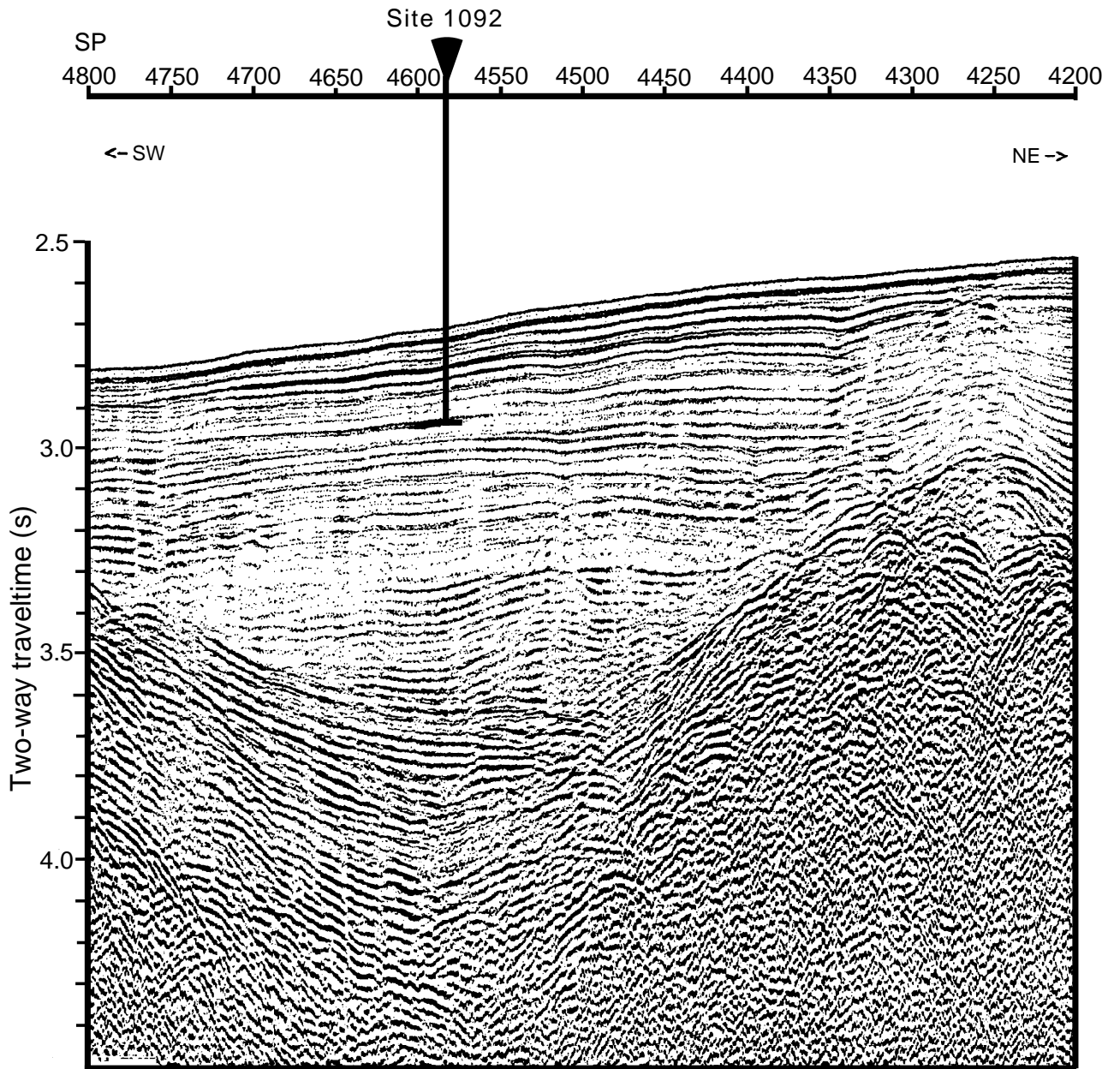
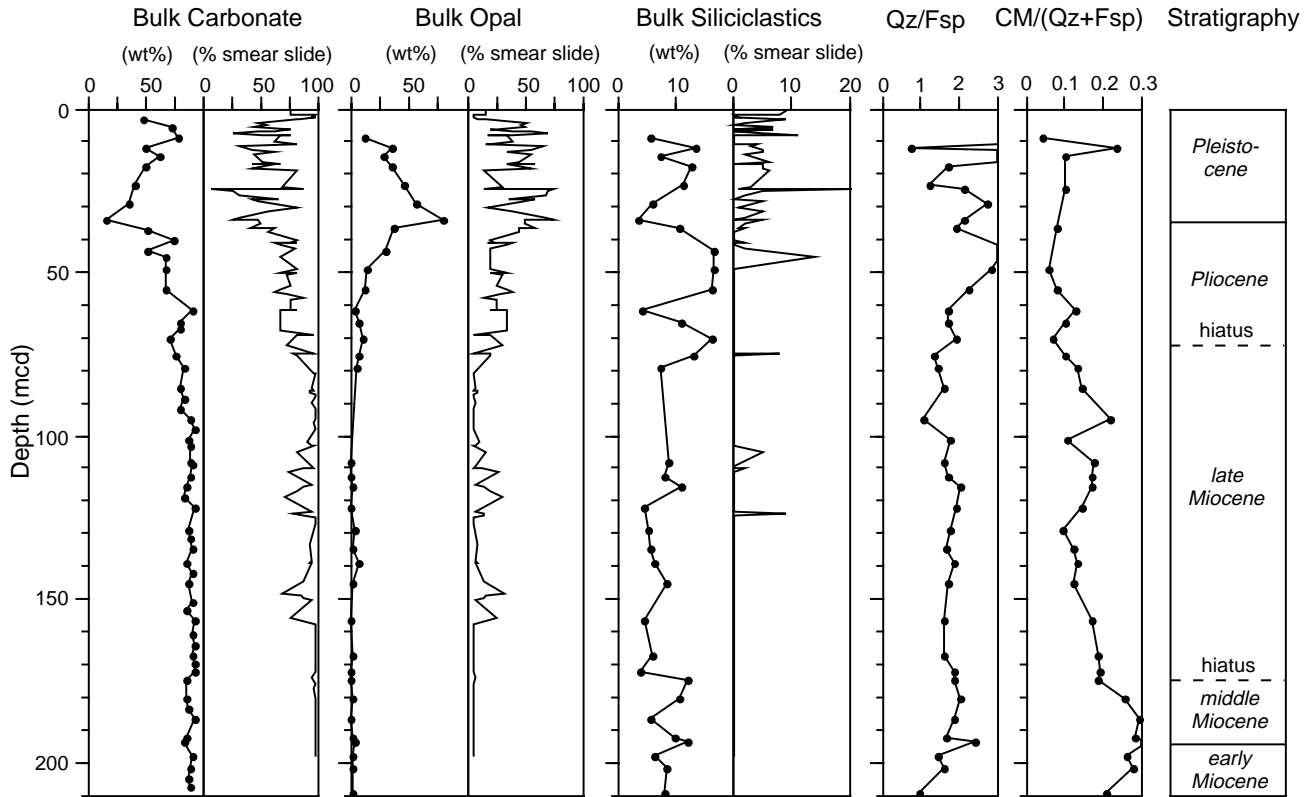


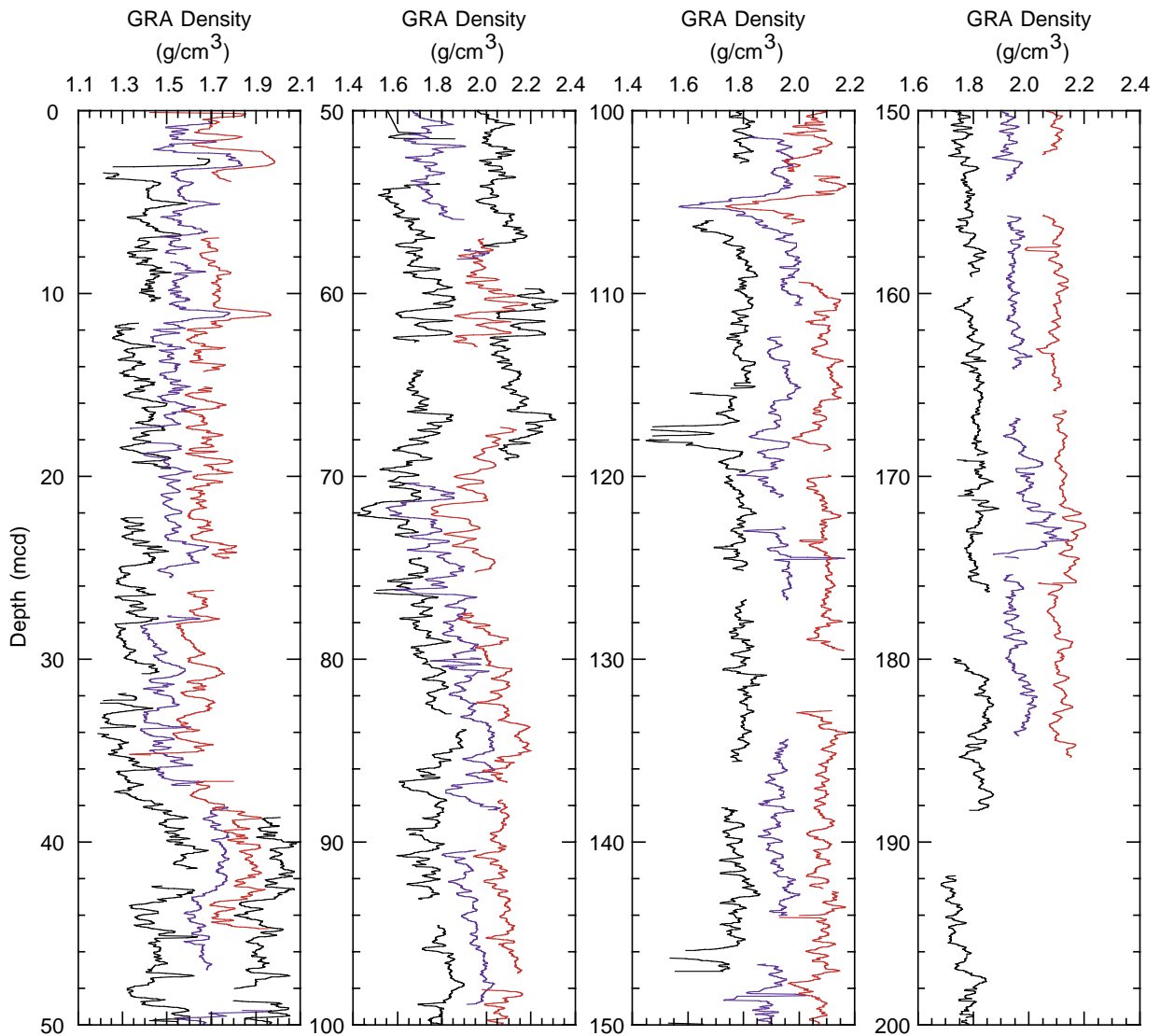




Figure F5. Summary diagram of smear-slide and XRD estimates of total carbonate, opal, and mud (i.e., bulk siliciclastics) contents, and quartz/feldspar and clay minerals/(quartz+feldspar) values for Site 1092. Qz = quartz, Fsp = feldspar, CM = clay minerals.



**Figure F6.** Smoothed (5-point average) GRA bulk density data for Site 1092. Holes 1092A (left curve), 1092B (second from left curve), 1092C (second from right curve), and 1092D (right curve) are horizontally offset from each other by a constant ( $0.15 \text{ g/cm}^3$ ). Data from the top 20 cm of each core have been removed. Note the difference in horizontal range between the two panels on the left and the two panels on the right ( $1.0$  vs.  $0.8 \text{ g/cm}^3$ ).



**Figure F7.** Smoothed (5-point average) magnetic susceptibility data (converted from instrument units to SI units) for Site 1092. Holes 1092A (left curve), 1092B (second from left curve), 1092C (second from right curve), and 1092D (right curve) are horizontally offset from each other by a constant ( $3 \times 10^{-5}$  SI units). Data from the top 20 cm of each core have been removed. Note the difference in horizontal range between the two panels on the left and the two panels on the right (20% vs. 15%).

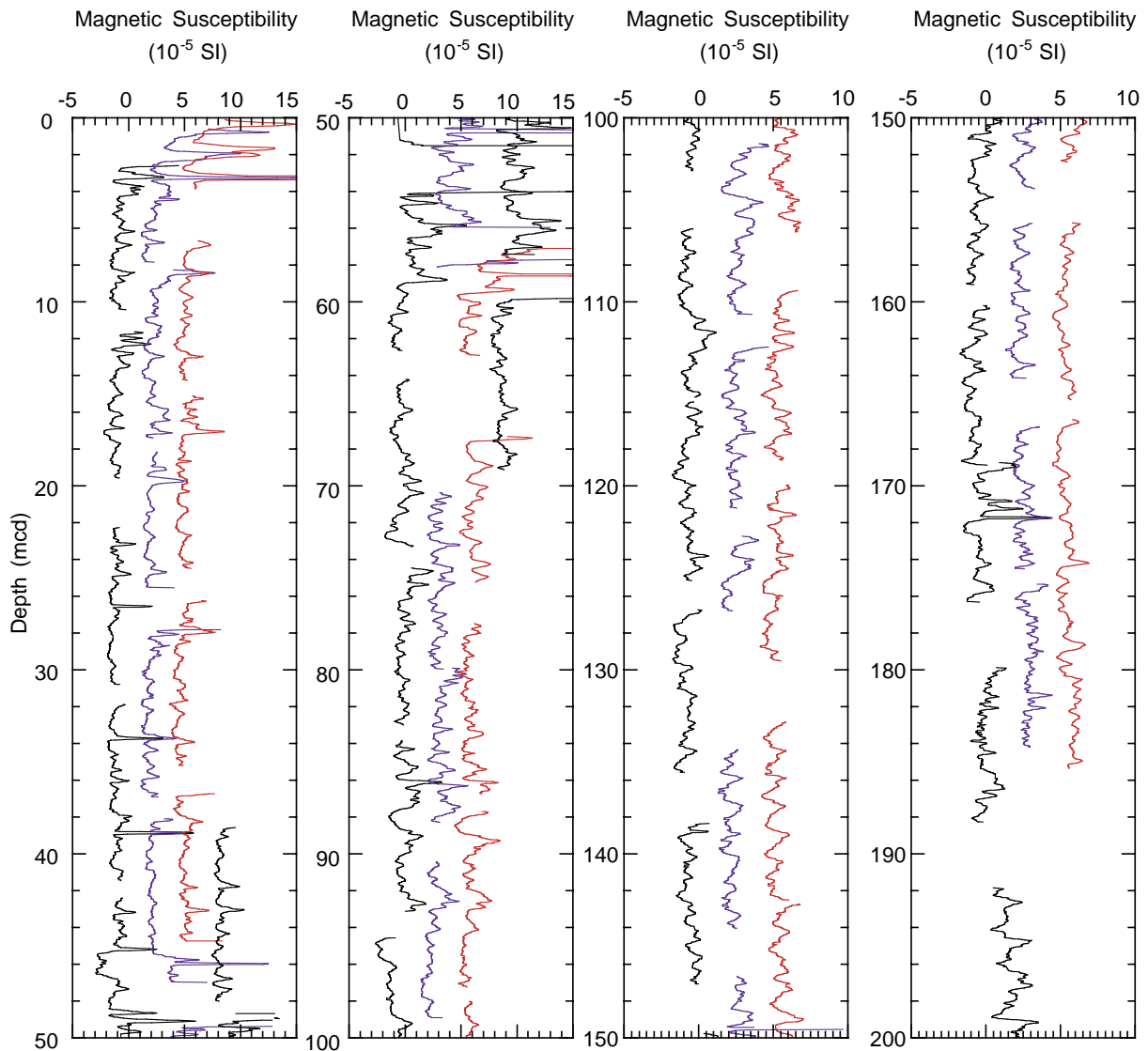


Figure F8. Smoothed (5-point average) color reflectance data (650–750 nm) for Site 1092. Holes 1092A (left curve), 1092B (second from left curve), 1092C (second from right curve), and 1092D (right curve) are horizontally offset from each other by a constant (15%). Data from the top 20 cm of each core have been removed.

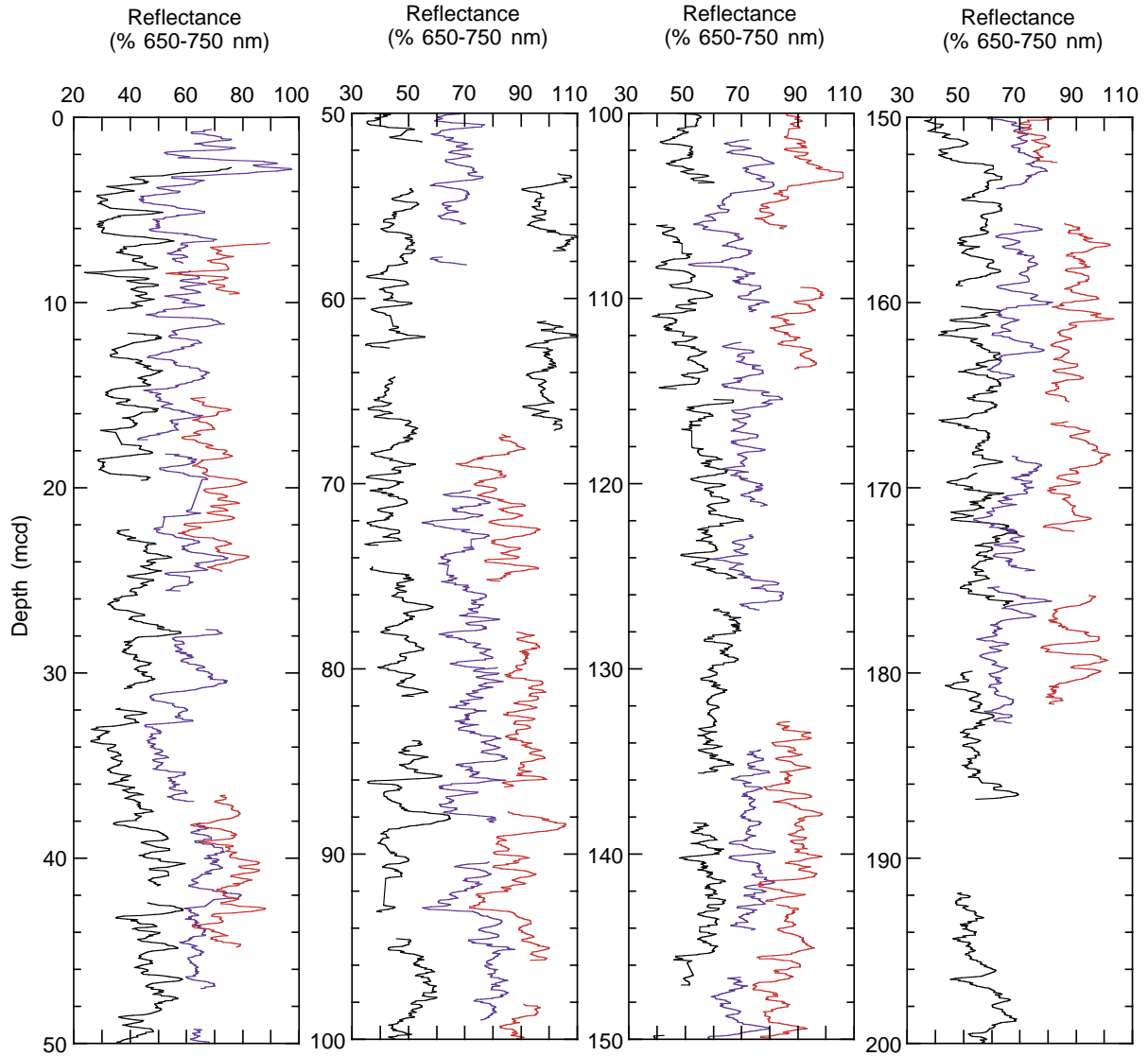


Figure F9. Spliced records of GRA bulk density and magnetic susceptibility for Site 1092. Both data sets were smoothed with a 5-point running mean. The horizontal lines in each plot identify the splice tie points (Table T3, p. 44).

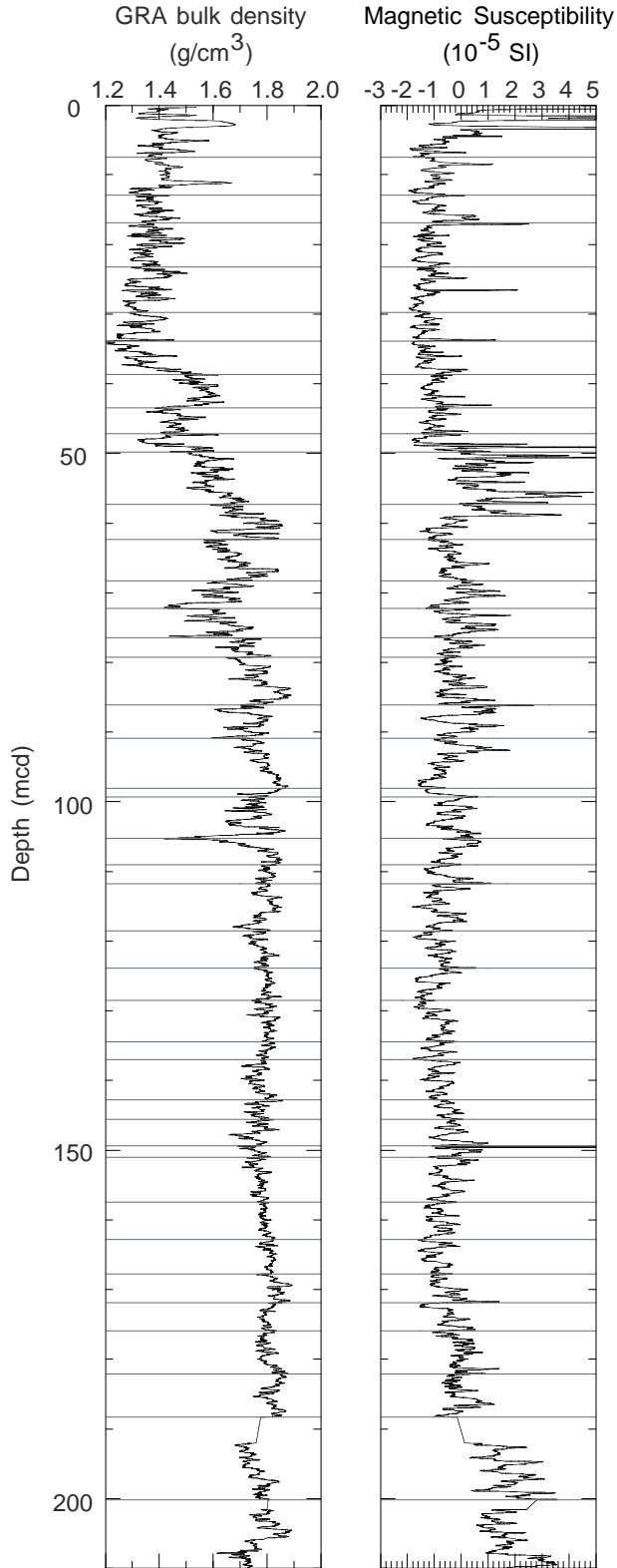


Figure F10. Biostratigraphic and magnetostratigraphic correlation chart for Site 1092, and selected absolute age designations. Shaded area indicates an interval with large stratigraphic uncertainties. Dashed lines indicate possible hiatuses.

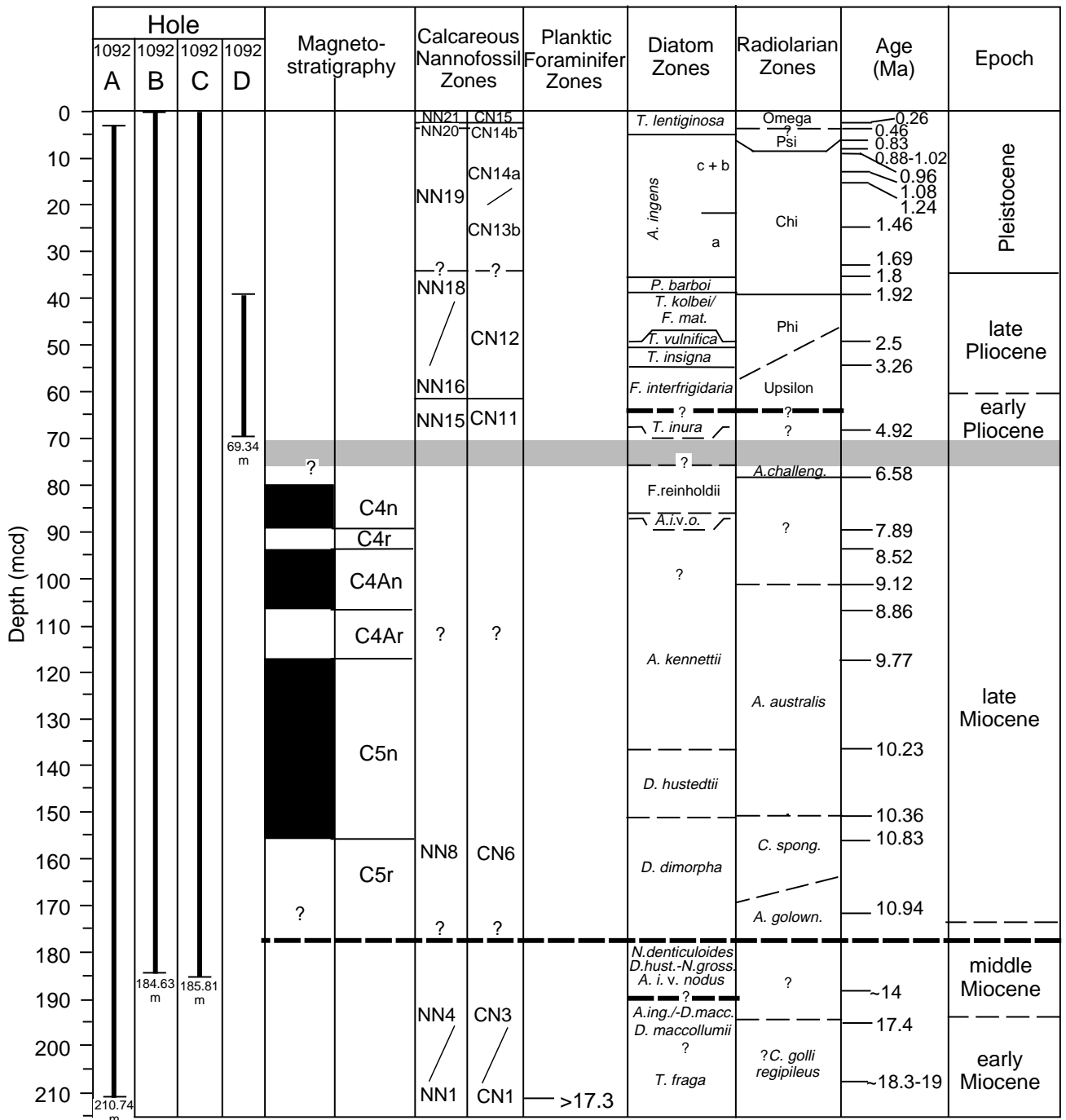




Figure F11. Age-depth plots of biostratigraphic and paleomagnetic events for (A) the entire sedimentary section and (B) a close up of the upper 80 mcd at Site 1092. Dashed lines indicate possible hiatuses. Shaded area indicates an interval with large stratigraphic uncertainties. Solid lines represent a visual best fit through the age-depth control points. Corresponding sedimentation rate averages are given in parentheses.

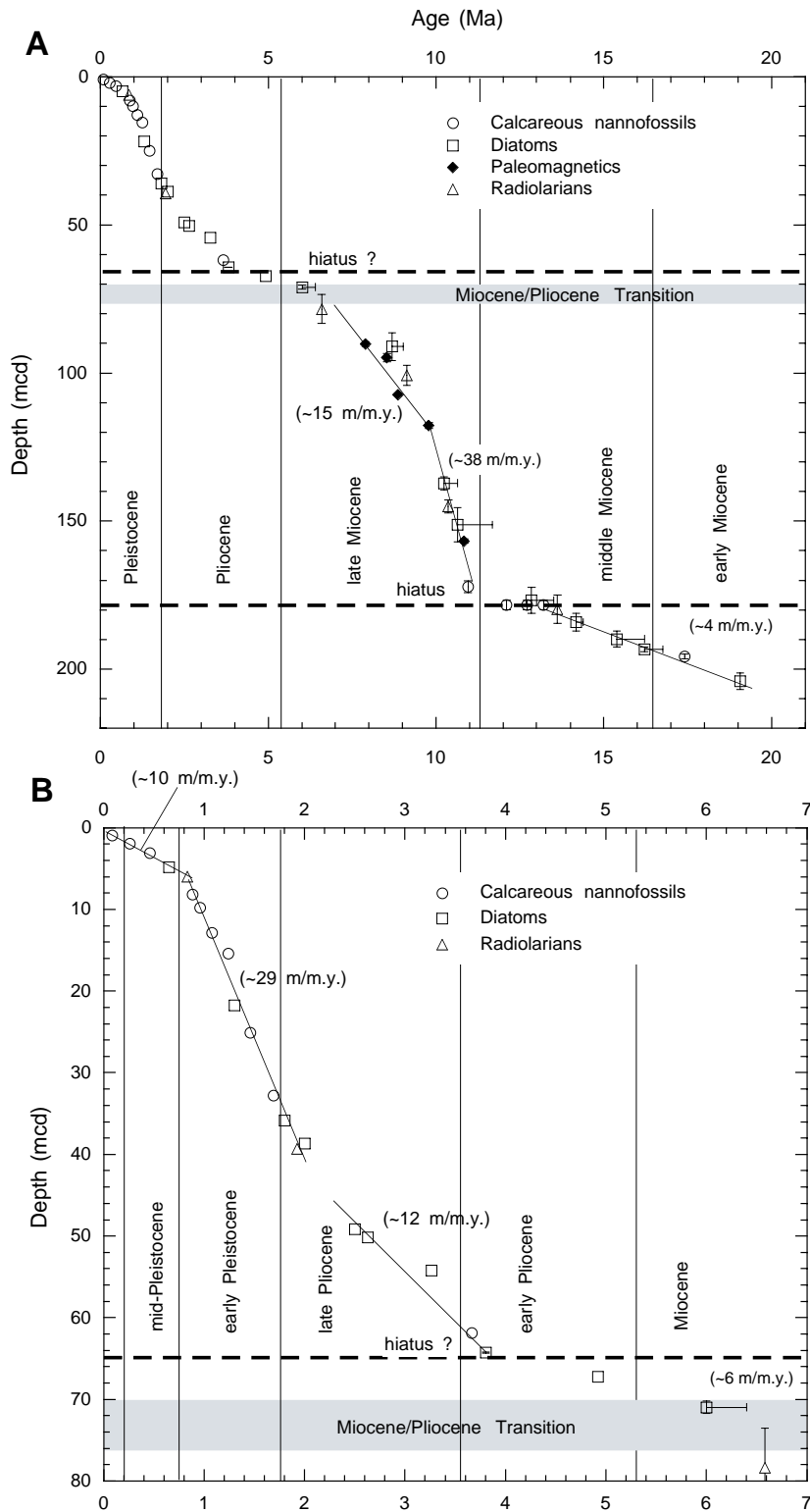


Figure F12. Inclination of the remanent magnetization after alternating-field demagnetization at peak fields of 20 or 25 mT at Holes 1092A–1092D. Magnetic polarity shading: black = normal, white = reversed; chrons are indicated by numbers.

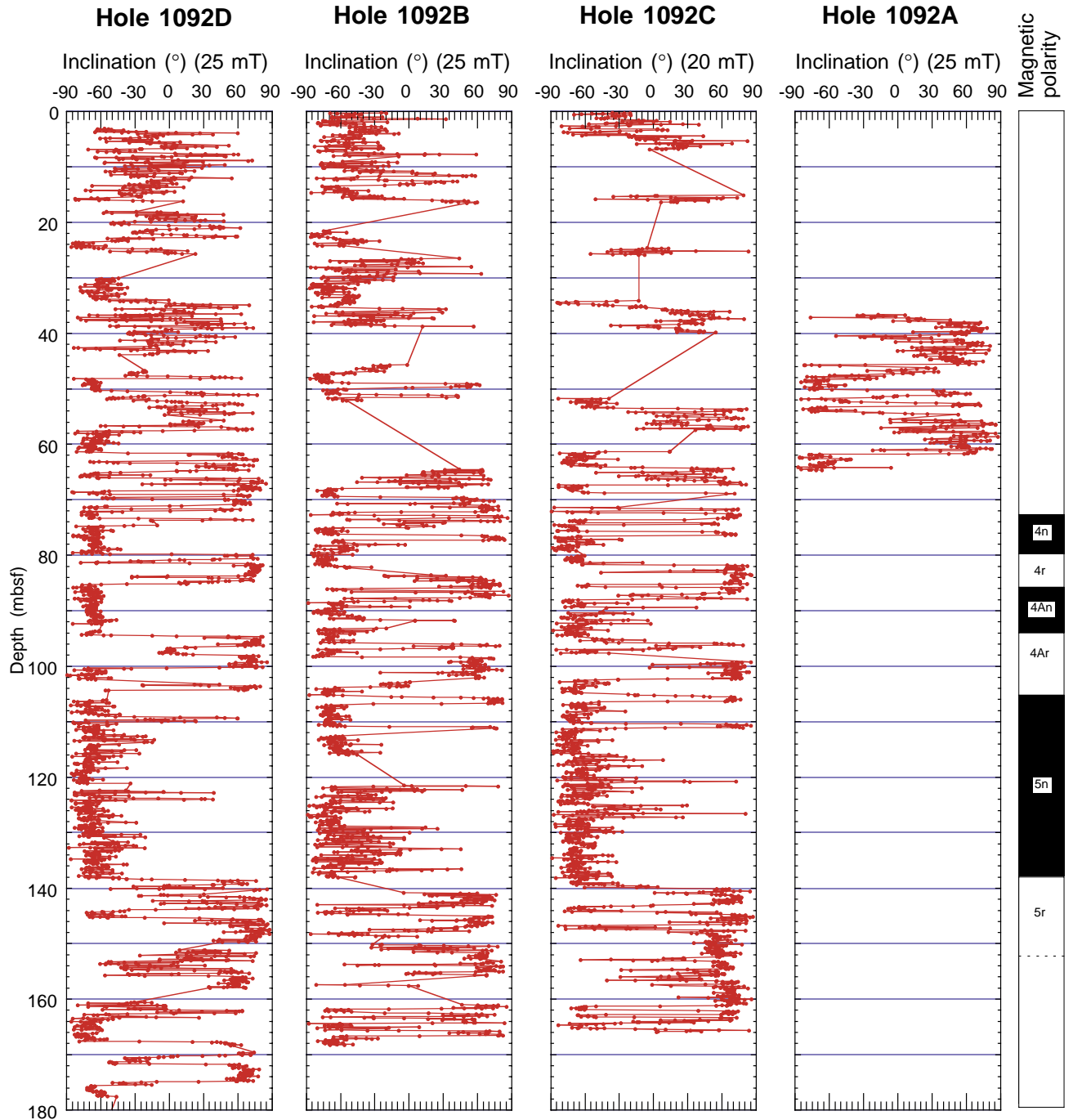


Figure F13. Concentration of methane vs. depth at Site 1092. The data are reported in Table T11, p. 76.

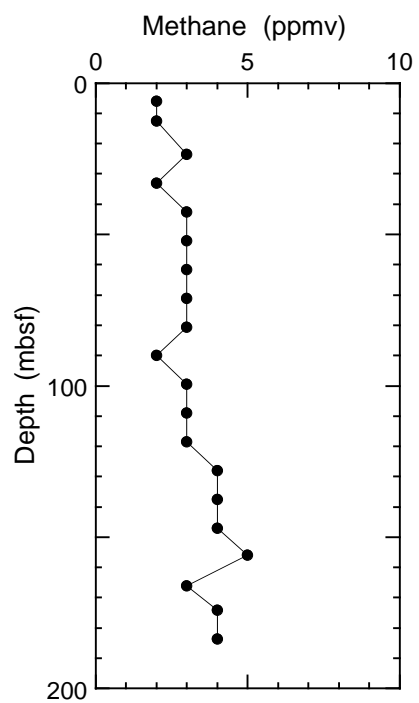


Figure F14. Interstitial water chemistry profiles vs. depth for chlorinity, alkalinity, pH, sodium, sulfate, calcium, magnesium, potassium, strontium, lithium, ammonium, phosphate, and silica at Site 1092. The data are reported in Table T12, p. 77.

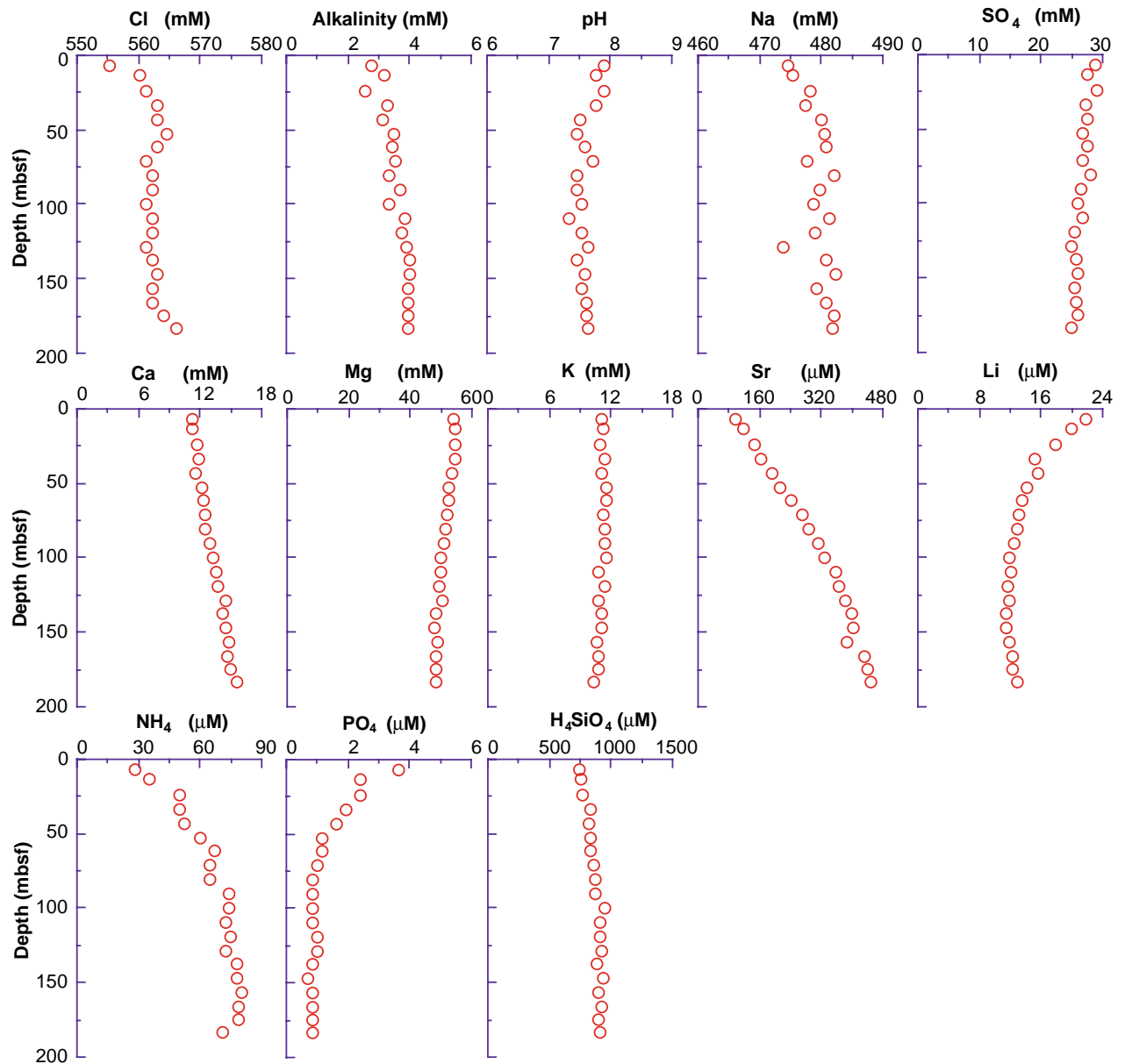


Figure F15. Concentration of calcium carbonate ( $\text{CaCO}_3$ ), total organic carbon (TOC), and TOC/TN vs. depth at Hole 1092A. The data are reported in Table T13, p. 79.

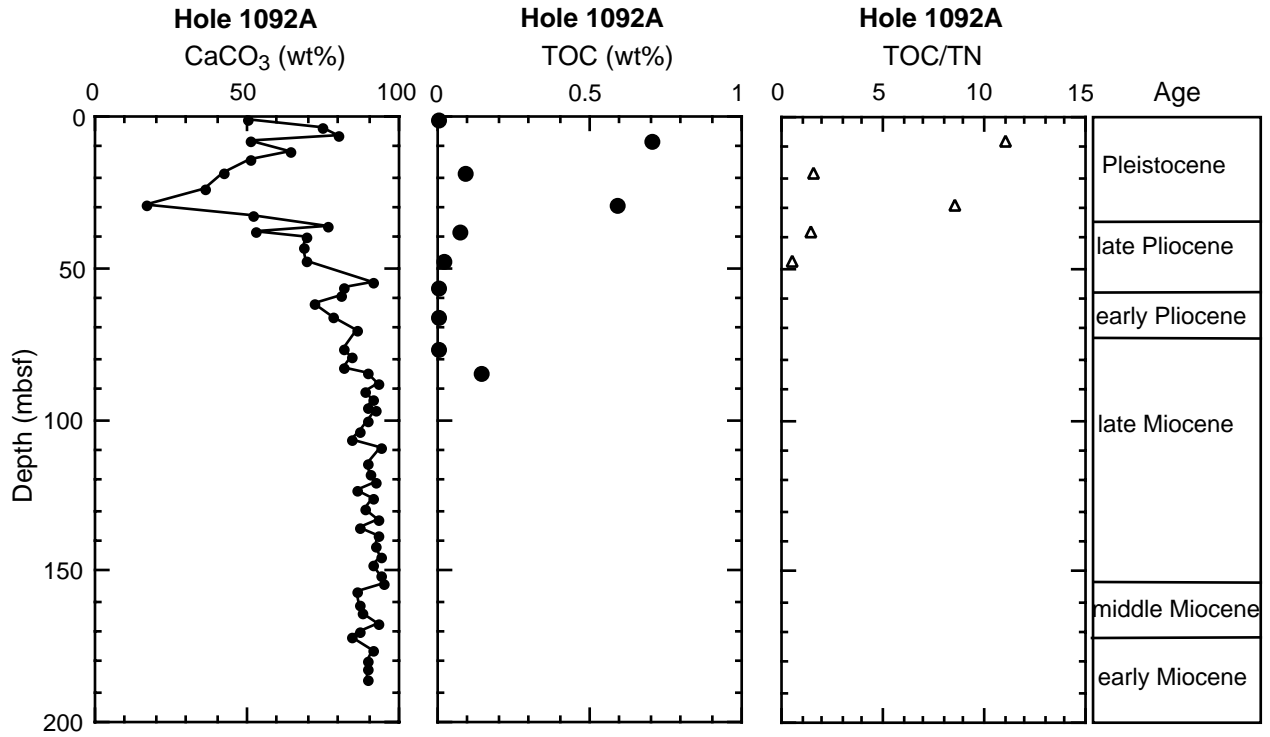


Figure F16. Site 1092 downhole variations of NGR (smoothed data), volume-specific magnetic susceptibility, porosity (open circles = MAD method) and OSU-SCAT resistivity (solid line), GRA bulk density (line = smoothed data) and MAD bulk density (open circles), and OSU-SCAT blue reflectance (450–550 nm). H = hiatus.

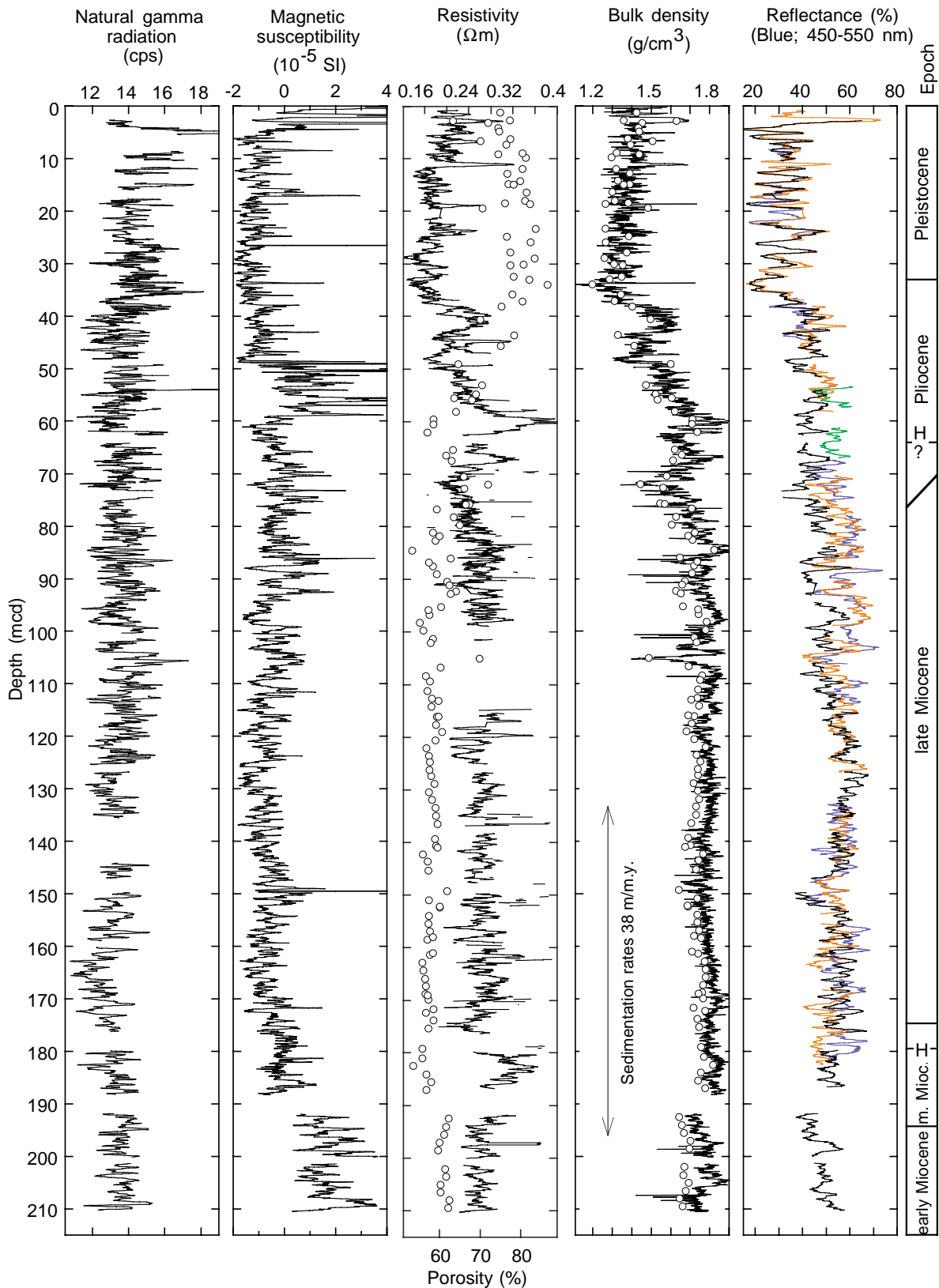




Figure F17. Relationship between GRA bulk density and gravimetric (MAD) bulk density at Site 1092.

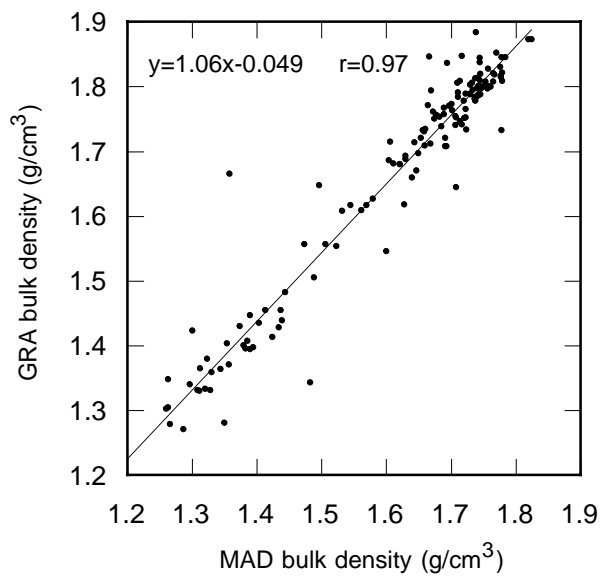


Figure F18. Variations in the upper 70 mcd of Site 1092 of volume-specific magnetic susceptibility, porosity (open circles) and OSU-SCAT resistivity (solid line = Hole 1092A, dashed line = Hole 1092B), GRA bulk density (solid line) and MAD bulk density (open circles), and OSU-SCAT reflectance from Hole 1092A plotted as red/blue value and individually for the blue (solid line) and red (dashed line) bands. H = hiatus.

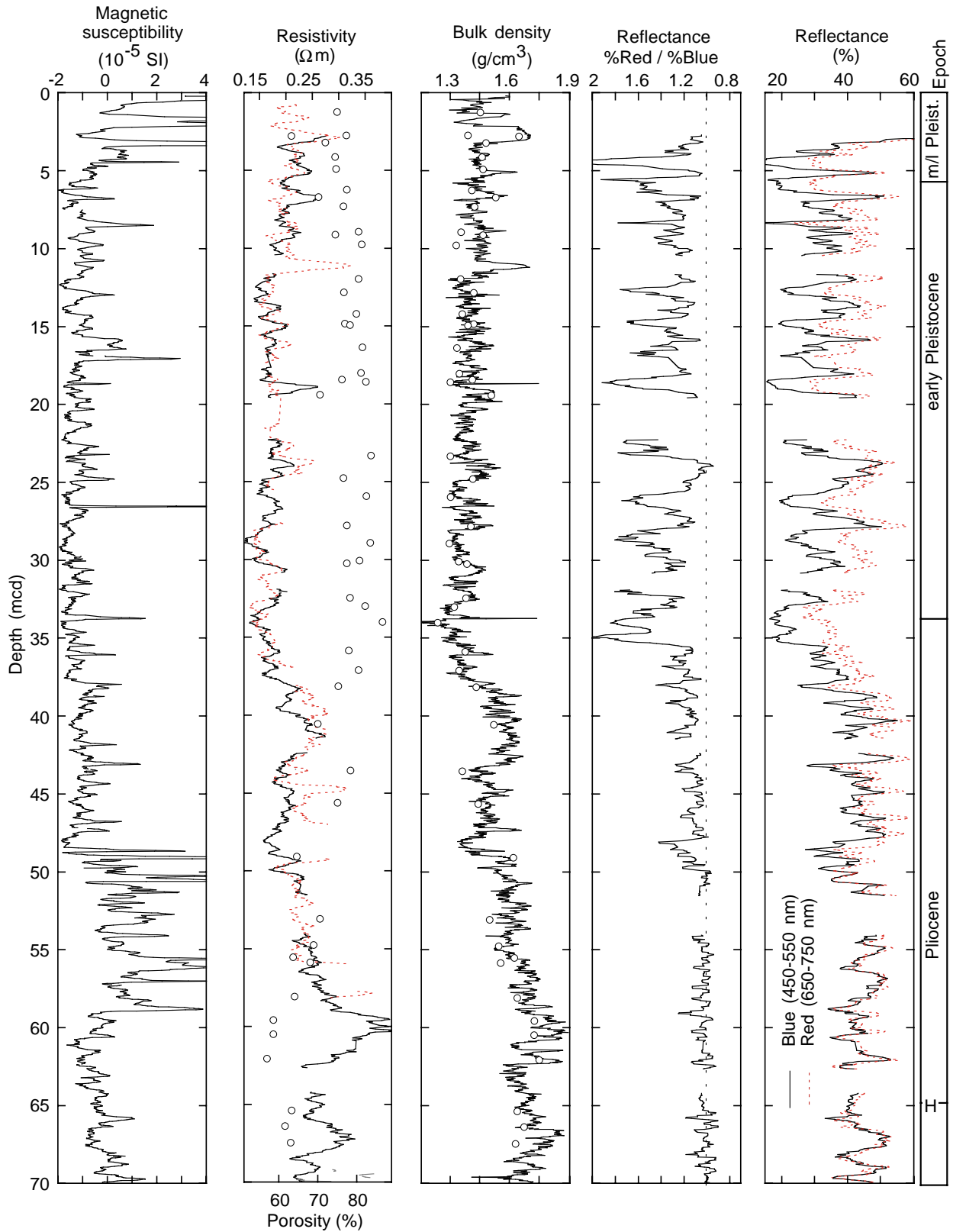


Figure F19. Variations in the 180–215 mcd of Site 1092 of volume-specific magnetic susceptibility, porosity (open circles) and OSU-SCAT resistivity (solid line = Hole 1092A, dashed line = Hole 1092B), GRA bulk density (solid line) and MAD bulk density (open circles), and OSU-SCAT reflectance from Hole 1092A plotted as red/blue value and individually for the blue (solid line) and red (dashed line) bands.

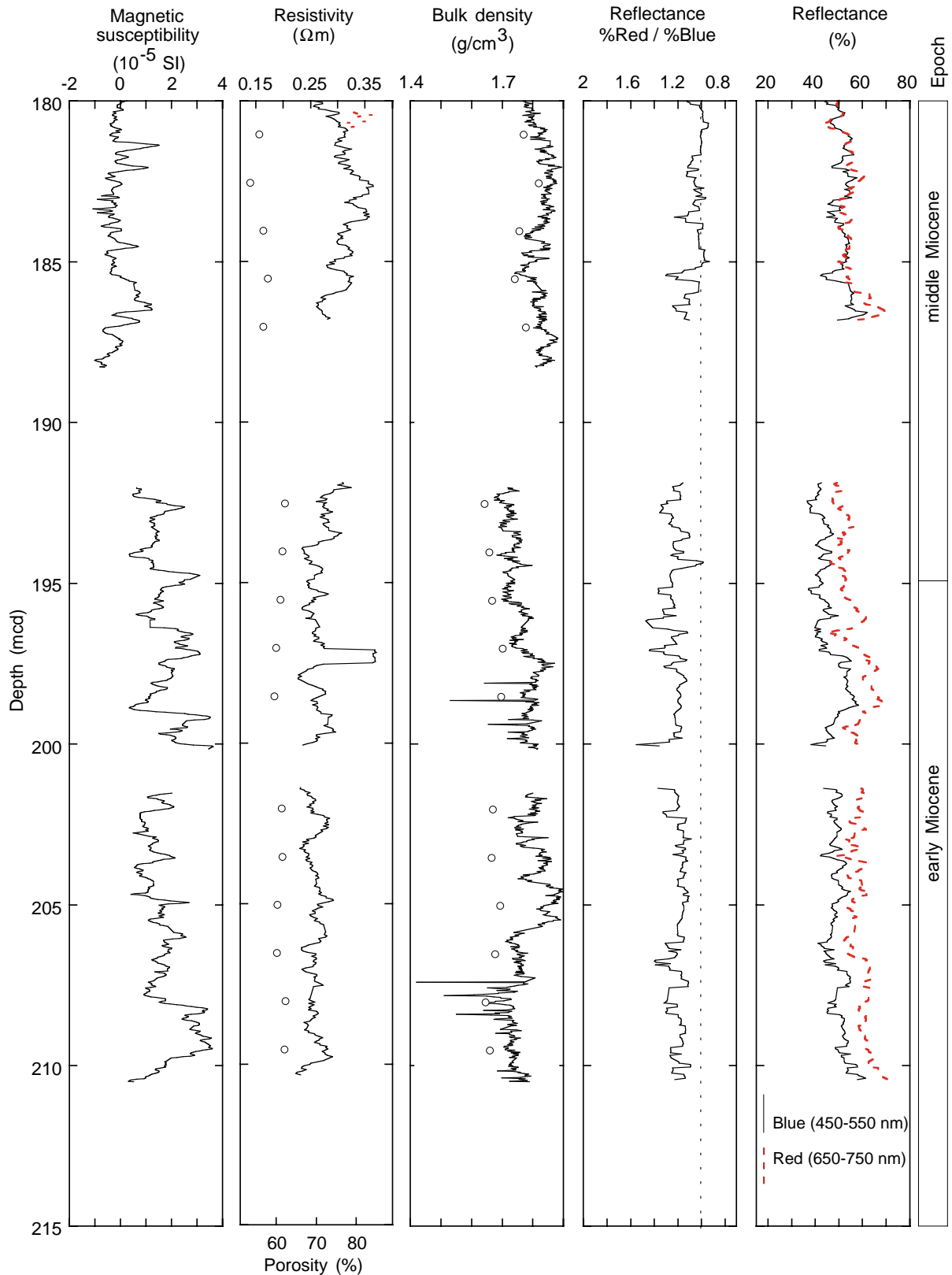


Figure F20. A. Distribution of PWL velocities. B. Downhole variation of *P*-wave velocities (dots = PWL, solid circles = PWS3).

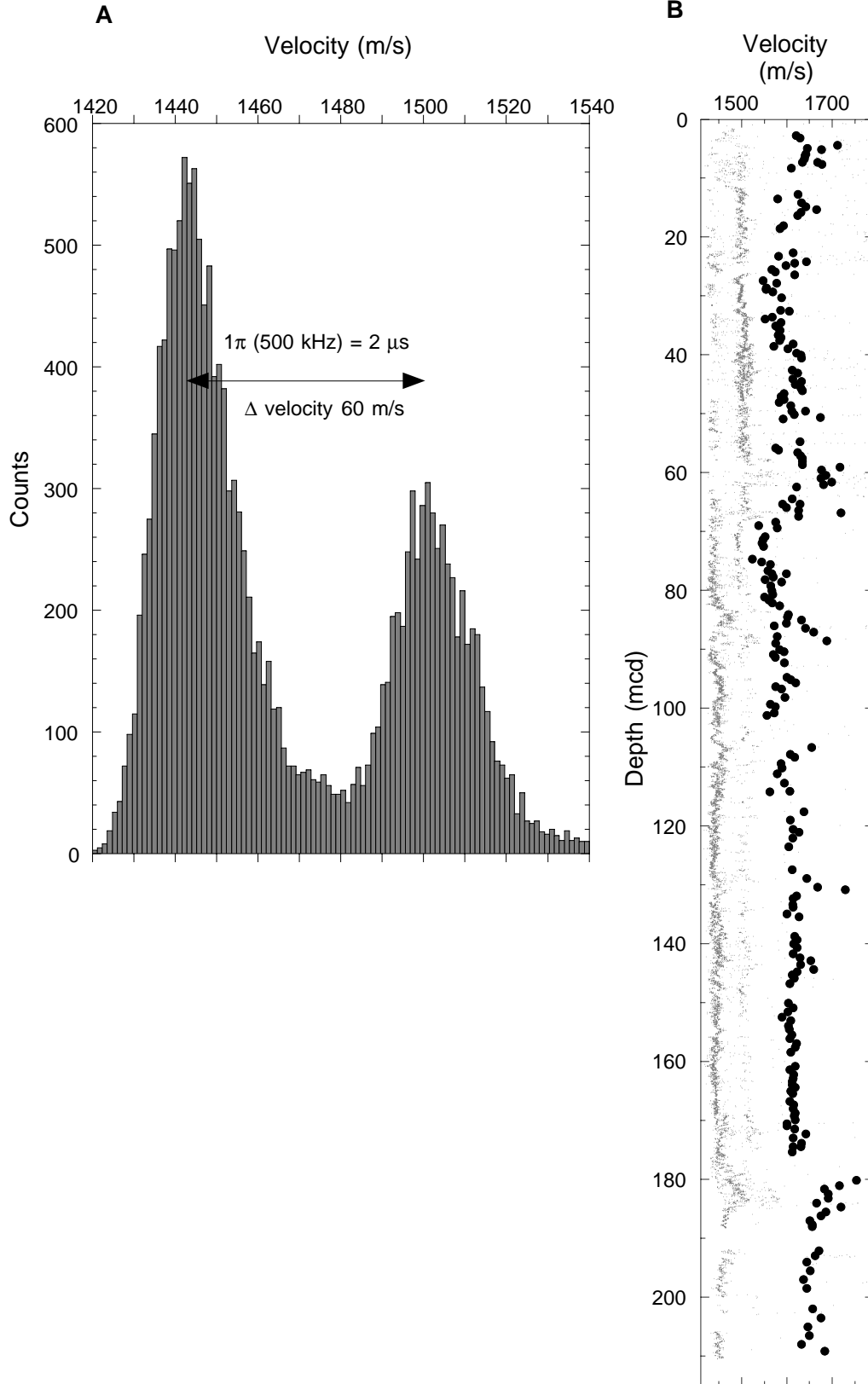


Figure F21. Thermal conductivity measurements at Site 1092. A. Frequency distribution of measured values. B. Correlation of measured values with interpolated GRA bulk density values. C. Thermal conductivity (solid circles) compared to interpolated GRA bulk density (open squares).

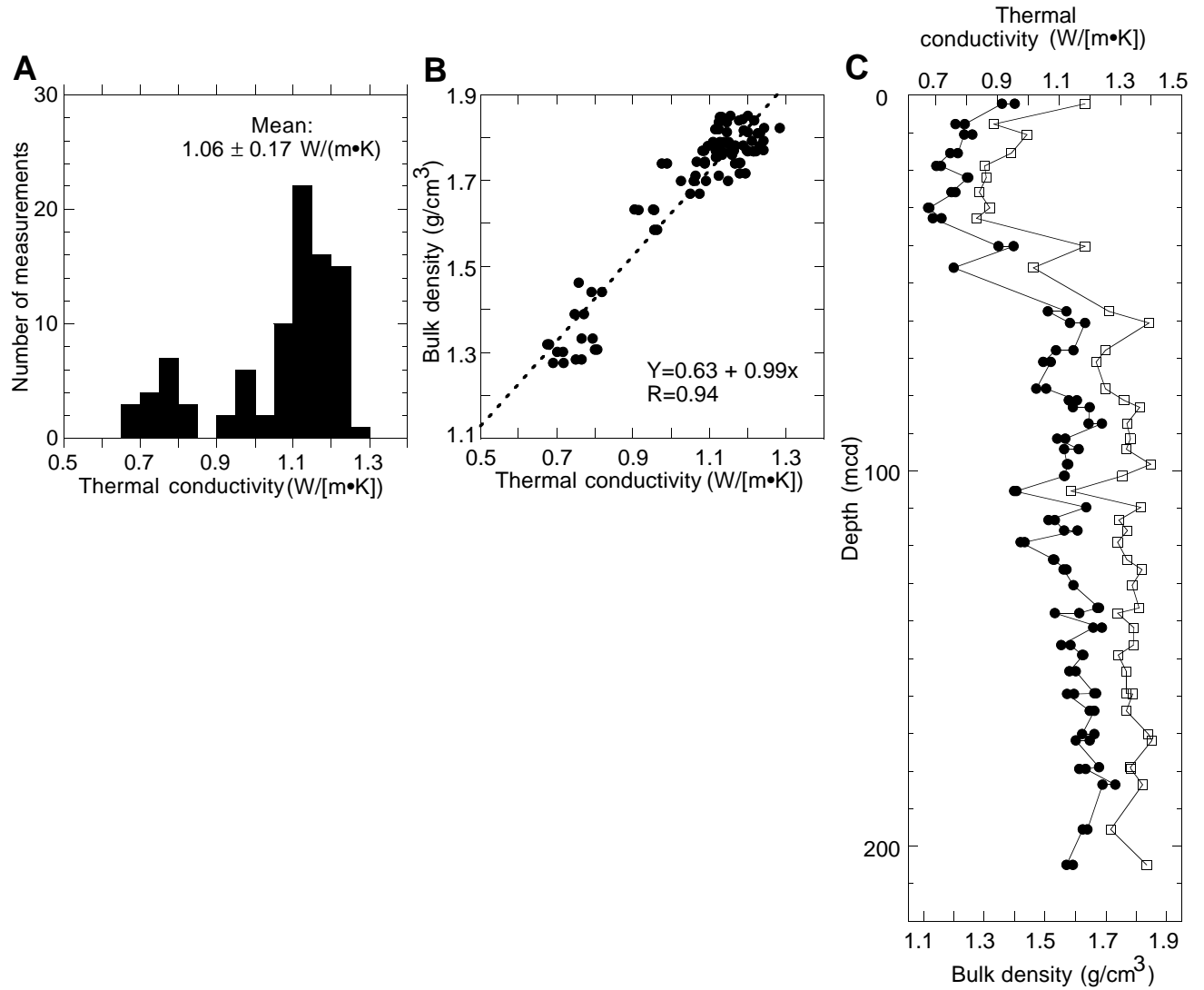


Table T1. X-ray diffraction data for Site 1092.

Core, section, interval (cm)	Depth (mbsf)	Depth (mcd)	Bulk carbonate (wt%; coulometry)	Calculated bulk opal (wt%)	Bulk silicates (wt%)	Opal carbonate-free fraction (wt%; XRD peak intensity)	Quartz/feldspar (XRD peak area ratio)	Clay/(quartz + feldspar) (XRD peak area ratio)
177-1092A-								
1H-5, 62-63	6.625	9.18	80.1	14	5.9	70.5	6.87	0.048
2H-1, 37-39	8.38	12	50.9	35.3	13.8	71.9	0.78	0.236
2H-3, 26-27	11.26	14.89	64.2	28.3	7.5	79.1	6.04	0.105
2H-5, 42-44	14.43	18.05	51.1	36	12.9	73.6	1.76	
3H-1, 109-111	18.6	23.33	42.1	46.2	11.7	79.8	1.25	18.6
3H-2, 110-112	20.11	24.84					2.18	0.106
3H-5, 70-72	24.21	28.94	36.3	57.6	6.1	90.4	2.77	
4H-2, 61-62	29.12	33.99	16.7	79.6	3.7	95.6	2.16	
4H-4, 70-71	32.21	37.08	52	37.1	10.9	77.4	1.97	0.083
5H-1, 117-119	37.68	43.55	52.6	30.3	17.1	64	3.31	
5H-5, 69-71	43.2	49.07	68	14.9	17.1	46.5	2.87	0.064
6H-2, 46-48	47.97	55.86	69.4	14	16.6	45.8	2.26	0.083
6H-6, 66-68	54.17	62.06	91.1	4.5	4.4	50.3	1.74	0.133
7H-1, 120-122	56.71	65.4	81.3	7.4	11.3	39.7	1.74	0.107
7H-5, 30-32	61.81	70.5	71.6	11.9	16.5	42.1	1.95	0.073
8H-1, 120-122	66.21	75.66	78.1	8.5	13.4	38.6	1.34	0.104
8H-4, 71-73	70.22	79.67	85.7	6.6	7.7	45.8	1.47	0.134
9H-2, 71-73	76.72	86.05	81.3				1.64	0.148
9H-4, 71-73	79.67	89	84.1					
10H-1, 73-75	84.74	95.28	89.6				1.09	0.224
10H-5, 73-75	90.74	101.3	88.8				1.78	0.112
11H-2, 89-91	95.9	108.4	89.3	1.7	9	15.5	1.64	0.181
11H-5, 71-73	100.2	112.7	89.9	1.7	8.4	17.2	1.76	0.175
12H-1, 73-75	103.7	116.2	86.7	2.2	11.1	16.6	2.08	0.172
12H-5, 71-73	109.7	122.1	94	1.3	4.7	21.4	1.93	0.149
13H-2, 69-71	114.7	128.9	89.2	5.2	5.6	48.2	1.77	0.101
13H-6, 71-73	120.7	134.9	91.9	2.3	5.8	28.5	1.69	0.126
14H-1, 118-120	123.2	139.3	86	7.3	6.7	52.3	1.9	0.136
14H-5, 120-122	129.2	145.3	88.8	2.4	8.8	21.4	1.72	0.124
15H-5, 120-122	138.7	157	93.4	1.7	4.9	25.6	1.65	0.174
16H-5, 120-123	148.2	167.4	91.3	2.3	6.4	26.2	1.65	0.189
17H-3, 116-119	154.1	172.3	94.6	1.2	4.2	22.6	1.89	0.195
17H-5, 116-119	157.1	175.3	86.4	1.2	12.4	8.9	1.92	0.19
18H-1, 120-123	161.2	181.1	87.2	2	10.8	15.5	2.08	0.258
18H-5, 120-123	167.2	187.1	93.3	0.8	5.9	12.5	1.9	0.298
19H-1, 65-68	170.2	192.5	86.8	3.1	10.1	23.2	1.69	0.288
19H-2, 65-68	171.7	194	84.2	3.6	12.2	22.6	2.46	0.32
19H-5, 65-68	176.2	198.5	91.3	2.1	6.6	24.4	1.48	0.267
20H-1, 66-69	179.7	202	89.4	2	8.6	18.4	1.64	0.283
20H-6, 66-69	187.2	209.5	89.2	2.3	8.5	21.4	1	0.212

Note: XRD = X-ray diffraction. This table is also available in ASCII format in the [TABLES](#) directory.



**Table T2.** Composite depths for Site 1092.

Core	Depth (mbsf)	Offset (mbsf)	Depth (mcd)
177-1092A-			
1H	0.00	2.55	2.55
2H	8.00	3.62	11.62
3H	17.50	4.73	22.23
4H	27.00	4.87	31.87
5H	36.50	5.87	42.37
6H	46.00	7.89	53.89
7H	55.50	8.69	64.19
8H	65.00	9.45	74.45
9H	74.50	9.33	83.83
10H	84.00	10.54	94.54
11H	93.50	12.49	105.99
12H	103.00	12.41	115.41
13H	112.50	14.22	126.72
14H	122.00	16.12	138.12
15H	131.50	18.24	149.74
16H	141.00	19.18	160.18
17H	150.50	18.22	168.72
18H	160.00	19.85	179.85
19H	169.50	22.34	191.84
20H	179.00	22.34	201.34
177-1092B-			
1H	0.00	0.55	0.55
2H	7.40	0.85	8.25
3H	16.90	1.24	18.14
4H	26.40	1.21	27.61
5H	35.90	2.17	38.07
6H	45.40	3.79	49.19
7H	54.90	2.65	57.55
8H	64.40	5.95	70.35
9H	73.90	5.98	79.88
10H	83.40	7.00	90.40
11H	92.90	8.49	101.39
12H	102.40	9.93	112.33
13H	111.40	10.82	122.22
14H	121.40	12.92	134.32
15H	130.90	15.72	146.62
16H	140.40	15.32	155.72
17H	149.90	16.86	166.76
18H	159.40	15.91	175.31
177-1092C-			
1H	0.00	0.00	0.00
2H	4.00	2.65	6.65
3H	13.50	1.60	15.10
4H	23.00	3.23	26.23
5H	32.50	4.05	36.55
7H	51.50	5.47	56.97
8H	61.00	6.31	67.31
9H	70.50	6.95	77.45
10H	80.00	7.68	87.68
11H	89.50	8.50	98.00
12H	99.00	10.35	109.35
13H	108.50	11.43	119.93
14H	118.00	14.82	132.82
15H	127.50	15.20	142.70
16H	137.00	18.70	155.70
17H	146.50	19.88	166.38
18H	156.00	19.79	175.79
177-1092D-			
1H	36.40	2.07	38.47
2H	45.90	2.75	48.65
3H	55.40	4.31	59.71

Note: This table is also available in ASCII format in the **TABLES** directory.

**Table T3.** Site 1092 splice tie points.

Core, section, interval (cm)	Depth (mbsf)	Depth (mcd)		Core, section, interval (cm)	Depth (mbsf)	Depth (mcd)
177-				177-		
1092C-1H-3, 52	3.52	3.52	tie to	1092B-1H-2, 147	2.97	3.52
1092B-1H-5, 94	6.94	7.49	tie to	1092C-2H-1, 84	4.84	7.49
1092C-2H-5, 30	10.30	12.95	tie to	1092B-2H-4, 20	12.1	12.95
1092B-2H-7, 16	16.06	16.91	tie to	1092C-3H-2, 30	15.31	16.91
1092C-3H-6, 62	21.62	23.22	tie to	1092A-3H-1, 99	18.49	23.22
1092A-3H-6, 4	25.04	29.77	tie to	1092B-4H-2, 66	28.56	29.77
1092B-4H-5, 30	32.70	33.91	tie to	1092A-4H-2, 54	29.04	33.91
1092A-4H-5, 82	33.82	38.69	tie to	1092C-5H-2, 64	34.64	38.69
1092C-5H-5, 88	39.38	43.43	tie to	1092D-1H-4, 46	41.36	43.43
1092D-1H-6, 124	45.14	47.21	tie to	1092A-5H-4, 34	41.34	47.21
1092A-5H-5, 142	43.92	49.79	tie to	1092D-2H-1, 114	47.04	49.79
1092D-2H-7, 32	54.52	57.27	tie to	1092A-6H-3, 38	49.38	57.27
1092A-6H-6, 98	54.48	62.37	tie to	1092D-3H-2, 116	58.06	62.37
1092D-3H-6, 106	63.96	68.27	tie to	1092A-7H-3, 108	59.58	68.27
1092A-7H-6, 54	63.54	72.23	tie to	1092B-8H-2, 38	66.28	72.23
1092B-8H-5, 12	70.52	76.47	tie to	1092A-8H-2, 52	67.02	76.47
1092A-8H-4, 34	69.84	79.29	tie to	1092C-9H-2, 34	72.34	79.29
1092C-9H-6, 116	79.16	86.11	tie to	1092A-9H-2, 78	76.78	86.11
1092A-9H-5, 106	81.56	90.89	tie to	1092B-10H-1, 48	83.89	90.89
1092B-10H-6, 12	91.02	98.02	tie to	1092A-10H-3, 48	87.48	98.02
1092A-10H-4, 24	88.74	99.28	tie to	1092C-11H-1, 128	90.78	99.28
1092C-11H-6, 32	96.75	105.25	tie to	1092B-11H-3, 86	96.76	105.3
1092B-11H-6, 16	100.56	109.05	tie to	1092A-11H-3, 6	96.56	109.1
1092A-11H-4, 122	99.22	111.71	tie to	1092C-12H-2, 86	101.4	111.7
1092C-12H-7, 22	108.22	118.57	tie to	1092A-12H-3, 16	106.2	118.6
1092A-12H-6, 94	111.44	123.85	tie to	1092C-13H-3, 92	112.4	123.9
1092C-13H-6, 107	117.07	128.50	tie to	1092A-13H-2, 28	114.3	128.5
1092A-13H-6, 18	120.18	134.40	tie to	1092C-14H-2, 8	119.6	134.4
1092C-14H-3, 120	122.20	137.02	tie to	1092B-14H-2, 120	124.1	137
1092B-14H-6, 93	129.84	142.76	tie to	1092A-14H-4, 13	126.6	142.8
1092A-14H-5, 145	129.46	145.58	tie to	1092C-15H-2, 137	130.4	145.6
1092C-15H-5, 65	134.16	149.36	tie to	1092B-15H-3, 81	133.6	149.4
1092B-15H-4, 98	135.30	151.02	tie to	1092A-15H-1, 127	132.8	151
1092A-15H-6, 24	139.24	157.48	tie to	1092B-16H-2, 26	142.2	157.5
1092B-16H-5, 112	147.52	162.84	tie to	1092A-16H-2, 115	143.7	162.8
1092A-16H-6, 10	148.60	167.78	tie to	1092B-17H-1, 102	150.9	167.8
1092B-17H-4, 70	155.05	171.91	tie to	1092A-17H-3, 76	153.7	171.9
1092A-17H-6, 30	157.73	175.95	tie to	1092B-18H-1, 64	160	176
1092B-18H-5, 84	166.24	182.15	tie to	1092A-18H-2, 80	162.3	182.2
1092A-18H-6, 94	168.44	188.29	append	1092A-19H-1, 0	169.5	191.8
1092A-19H-6, 84	177.84	200.18	append	1092A-20H-1, 0	179	201.3
1092A-20H-7, 69	188.20	210.54				

Note: This table is also available in ASCII format in the **TABLES** directory.



Table T4 (continued).

Core, section, interval (cm)	Depth (mbsf)	Depth (mcd)	Abundance	Preservation	<i>Dictyococites antarcticus</i>	<i>Coccolithus miopelagicus</i>	<i>Cyclcaragolithus abisectus</i>	<i>Cyclcaragolithus floridanus</i>	<i>Calcidiscus premacintyreii</i>	<i>Coronocilius nitescens</i>	<i>Dictyococites productus</i>	<i>Reticulofenestra pseudoumbilicus</i>	<i>Reticulofenestra minutula</i>	<i>Reticulofenestra minuta</i>	<i>Discoaster brouweri</i>	<i>Discoaster pentaradiatus</i>	<i>Coccolithus pelagicus</i>	<i>Pseudoemiliania lacunosa</i>	<i>Calcidiscus leptaporus</i>	<i>Calcidiscus macintyreii</i>	<i>Helicosphaera carteri</i>	<i>Gephyrocapsa smalli</i>	<i>Gephyrocapsa caribbeanica</i>	<i>Gephyrocapsa medium</i> (4-5.5 µm)	<i>Gephyrocapsa large</i> (> 5.5 µm)	<i>Gephyrocapsa</i> sp. 3	<i>Reticulofenestra asanoi</i>	<i>Emiliania huxleyi</i>	Comments	
9H-1, 70-70	75.20	84.53	A M								D	F				C														
9H-2, 70-70	76.70	86.03	A M								D	R				A														
9H-3, 70-70	78.20	87.53	A M	C						R	D					R														
9H-4, 70-70	79.70	89.03	A M	D							F					C														
9H-5, 70-70	81.20	90.53	A M	A											R	A														
9H-6, 70-70	82.55	91.88	A M	A							A					C														
9H-CC, 10-15	83.97	93.30	A M	A							F					A				R										
10H-CC, 15-20	93.63	104.17	A M	A							F					A				R										
11H-CC, 0-10	102.77	115.26	A M	A							C					A														
12H-CC, 28-33	113.08	125.49	A M	A							C					A				F										
13H-CC, 10-15	121.55	135.77	A M	D							C					A			R	R										
14H-CC, 10-15	131.11	147.23	A M	C							F	D				C			F	R										
15H-CC, 14-19	141.03	159.27	A M	D							F	A				F														
16H-CC, 14-19	149.91	169.09	A M	D							C	C				C			F											
17H-1, 0-0	150.50	168.72	A M	D							C					A			F											
17H-2, 0-0	152.00	170.22	A M	D							A					C			F											
17H-5, 0-0	155.93	174.15	A M	A	F						A					A			R	R										
17H-6, 0-0	157.43	175.65	A M	A	F						C					A			F	R										
17H-CC, 32-37	158.51	176.73	A M	A	F						A					F			R											
18H-1, 0-0	160.00	179.85	A M		R		R	C		F	F	A				F			F											
18H-3, 0-0	163.00	182.85	C M				F	F		F	F	A				C			C											
18H-4, 0-0	164.50	184.35	C M		C		A	F	F	F		A				A			A											
18H-5, 0-0	166.00	185.85	C M		R		A	F			A					C			C											
18H-6, 0-0	167.50	187.35	A M			A	A		F	F						C														
18H-CC, 0-7	168.50	188.35	A M			A	C	F	F	F						A														
19H-1, 0-0	169.50	191.84	A M			A	C	R	R	C						A														
19H-2, 0-0	171.00	193.34	A M		R	A	F	R	R	F						A			C											
19H-3, 0-0	172.50	194.84	A M		C	A	R			F						A														
19H-4, 0-0	174.00	196.34	A M		R	C	D			F						C														
19H-5, 0-0	175.50	197.84	A M			C	A			C						C														
19H-CC, 72-77	178.63	200.97	A M		F	F	C		F										F											
20H-1, 0-0	179.00	201.34	F P			F				C	A					D														
20H-2, 0-0	180.50	202.84	F P			F	A			A						F														
20H-3, 0-0	182.00	204.34	C M			R	F		R	D						A														
20H-4, 0-0	183.50	205.84	C P			C				A	A					C														
20H-5, 0-0	185.00	207.34	C M			F	F			D						C														
20H-6, 0-0	186.50	208.84	C M		R	F	F			A	A																			
20H-CC, 13-18	188.35	210.69	A M			F	C																							
177-1092B-																														
1H-1, 10-10	0.10	0.65	A G																C	C	R			R		D				
1H-1, 60-60	0.60	1.15	A G																		C		F			A				
1H-1, 117-117	1.17	1.72	A M																	F	F	C	F			C				
1H-2, 10-10	1.60	2.15	F M																		A	C			C					
1H-2, 70-70	2.20	2.75	A G																		D	F								
1H-2, 126-126	2.76	3.31	A M													F	F	R			A	R			F					
1H-3, 50-50	3.50	4.05	C M													A	F	F			C	R			F					
1H-3, 100-100	4.00	4.55	A M																		A				F		F			
1H-4, 68-68	5.18	5.73	F M													F	F	C			R	A		R	F	?				
1H-4, 130-130	5.80	6.35	A M														F				D				C					
1H-5, 84-84	6.84	7.39	A M														F	F			F	D			R					
1H-5, 100-100	7.00	7.55	A M													R	F	C			D									
2H-1, 44-44	7.84	8.69	C M													A	F	F			A				F	F				
2H-2, 115-115	10.05	10.90	A G													A	F				D									
2H-3, 80-80	11.20	12.05	C M													C	F	F			R	D								

Contamination  
*E. huxleyi*?

Table T4 (continued).

Core, section, interval (cm)	Depth (mbsf)	Depth (mcd)	Abundance Preservation	<i>Dictyococcites antarcticus</i>	<i>Coccolithus miopelagicus</i>	<i>Cyclicargolithus abisectus</i>	<i>Cyclicargolithus floridanus</i>	<i>Calcidiscus premacintyreii</i>	<i>Coronociclus nitescens</i>	<i>Dictyococcites productus</i>	<i>Reticulofenestra pseudoumbilicus</i>	<i>Reticulofenestra minutula</i>	<i>Reticulofenestra minuta</i>	<i>Discoaster brouweri</i>	<i>Discoaster pentaradiatus</i>	<i>Coccolithus pelagicus</i>	<i>Pseudoemiliana lacunosa</i>	<i>Calcidiscus leptoporus</i>	<i>Calcidiscus macintyreii</i>	<i>Helicosphaera carteri</i>	<i>Gephyrocapsa small</i>	<i>Gephyrocapsa caribbeanica</i>	<i>Gephyrocapsa medium</i> (4-5.5 µm)	<i>Gephyrocapsa large</i> (> 5.5 µm)	<i>Gephyrocapsa</i> sp. 3	<i>Reticulofenestra asanoi</i>	<i>Emiliana huxleyi</i>	Comments				
2H-4, 80-80	12.70	13.55	C M													F	F	F		R	A											
2H-5, 40-40	13.80	14.65	C M								C	F				D	C	F		R												
2H-6, 30-30	15.20	16.05	C M								C	A				F	F	C		R	C											
2H-7, 30-30	16.20	17.05	C M													D	F	R			R											
3H-1, 40-40	17.30	18.54	A M									F	F			A	C	C			C		A		A					Reworking		
3H-2, 120-120	19.60	20.84	C P								C	C				A	C	F			C		C		C							
3H-3, 40-40	20.30	21.54	A M													A	F	C		R			C		A							
3H-4, 40-40	21.80	23.04	A M													A	F	R		R			F		F							
3H-5, 40-40	23.30	24.54	A M													A	C	C		F			F		F							
3H-5, 140-140	24.30	25.54	A M													A	C	F		R			C		F							
4H-1, 40-40	26.80	28.01	A M													D	F				A		F									
4H-1, 90-90	27.30	28.51	A M										F			D	C	C			C		C									
4H-2, 140-140	29.30	30.51	A M													D	F	R					F									
4H-3, 40-40	29.80	31.01	A M													A	R				F		C									
4H-3, 140-140	30.80	32.01	A M													D	R				C		R									
4H-4, 40-40	31.30	32.51	A M													A	F	R			F											
4H-3, 140-140	30.80	32.01	C M									C				A	F	F			F											
4H-4, 140-140	32.30	33.51	C M									C				A	F	F			F											
4H-6, 60-60	34.50	35.71	C M									A	A			D	F															
5H-1, 130-130	37.20	39.37	C M						R			F	F			D	F				F											
5H-2, 30-30	37.70	39.87	C M								C	R				D	C	F			F											
5H-3, 140-104	40.30	42.47	C M									R	R			D	F	R			F											
5H-5, 40-40	42.30	44.47	C M									F	F			D	F	R			R											
6H-1, 30-30	45.70	49.49	C M							C		C	F			A	R															
7H-1, 60-60	55.50	58.15	C M									R	R			D	?				F											

Notes: Abundance abbreviations: D = dominant, A = abundant, C = common, F = few, R = rare. Preservation abbreviations: G = good, M = moderate, P = poor. For more specific definitions, refer to **"Biostratigraphy,"** p. 10, in the "Explanatory Notes" chapter. The distributions of the species are mainly described in stratigraphic intervals where events are identified. This table is also available in ASCII format in the **TABLES** directory.

**Table T5.** Summary of biostratigraphic age assignments for Site 1092. (See table note. Continued on next seven pages.)

Core, section, interval (cm)	Depth (mbsf)	Depth (mcd)	Calcareous nannofossil zone	Calcareous nannofossil age (Ma)	Diatom zone	Diatom age (Ma)	Comments
177-1092A-							
1H-1, 30-30	0.30	2.85	G		<i>T. lentiginosa</i>	0-0.65	
1H-2, 1-1	1.51	4.06			<i>T. lentiginosa</i>	0-0.65	<i>A. ingens</i> rare to trace abundance
1H-3, 1-1	3.01	5.56			middle/upper <i>A. ingens</i>	0.65-1.3	
1H-4, 1-1	4.51	7.06		<0.88			
1H-CC, 7-12	8.00	10.55	NN19	>0.46	middle/upper <i>A. ingens</i>	0.65-1.3	
2H-1, 1-1	8.01	11.63		>1.08			
2H-2, 1-1	9.51	13.13		<1.24			
2H-3, 1-1	11.01	14.63		>1.24	middle/upper <i>A. ingens</i>	0.65-1.3	
2H-5, 1-1	14.01	17.63		>0.88	middle/upper <i>A. ingens</i>	0.65-1.3	
2H-CC, 9-14	16.11	19.73		1.24-1.46	middle/upper <i>A. ingens</i>	0.65-1.3	<i>A. ingens</i> acme
3H-1, 1-1	17.51	22.24		<1.46			
3H-2, 1-1	19.01	23.74		>1.46	lower <i>A. ingens</i>	1.3-1.8	<i>Thalassiothrix</i> ooze
3H-5, 1-1	23.51	28.24			lower <i>A. ingens</i>	1.3-1.8	<i>A. ingens</i> ooze
3H-CC, 9-14	26.24	30.97	NN19	1.46-1.69	lower <i>A. ingens</i>	1.3-1.8	<i>A. ingens</i> acme
4H-1, 1-1	27.01	31.88		>1.69	lower <i>A. ingens</i>	1.3-1.8	
4H-3, 1-1	30.01	34.88			lower <i>A. ingens</i>	1.3-1.8	
4H-4, 1-1	31.51	36.38			<i>P. barboi</i>	1.8-2.0	
4H-5, 1-1	33.01	37.88			<i>P. barboi</i>	1.8-2.0	
4H-6, 1-1	34.51	39.38			<i>T. kolbei/F. matuyamae</i>	2.0-2.5	
4H-7, 1-1	35.96	40.83			<i>T. kolbei/F. matuyamae</i>	2.0-2.5	
4H-CC, 9-14	36.69	41.56	late Pliocene	>1.69	<i>T. kolbei/F. matuyamae</i>	2.0-2.5	
5H-1, 1-1	36.51	42.38			<i>T. kolbei/F. matuyamae</i>	2.0-2.5	
5H-4, 1-1	41.01	46.88			<i>T. kolbei/F. matuyamae</i>	2.0-2.5	
5H-5, 1-1	42.51	48.38			<i>T. kolbei/F. matuyamae</i>	2.0-2.5	
5H-6, 1-1	44.01	49.88			<i>T. vulnifica</i>	2.5-2.6	
5H-CC, 10-15	45.65	51.52	late Pliocene	<3.66	<i>T. insigna</i>	2.6-3.3	
6H-1, 1-1	46.01	53.90			<i>T. insigna</i>	2.6-3.3	
6H-2, 1-1	47.51	55.40			<i>F. interfrigidaria</i>	3.3-3.8	
6H-3, 1-1	49.01	56.90			<i>F. interfrigidaria</i>	3.3-3.8	
6H-5, 1-1	52.01	59.90			<i>F. interfrigidaria</i>	3.3-3.8	
6H-6, 1-1	53.51	61.40			<i>F. interfrigidaria</i>	3.3-3.8	
6H-CC, 1-10	54.84	62.73	late Pliocene	<3.66	<i>F. interfrigidaria</i>	3.3-3.8	
7H-1, 1-1	55.51	64.20			<i>F. interfrigidaria</i>	3.3-3.8	
7H-1, 120-122	56.70	65.39			<i>T. inura</i>	4.4-4.9	
7H-3, 1-1	58.51	67.20			<i>T. inura</i>	4.4-4.9	
7H-4, 1-1	60.01	68.70			?	?	No <i>T. oestrupii</i> found
7H-5, 1-1	61.51	70.20			?	?	No <i>T. oestrupii</i> found
7H-6, 1-1	63.01	71.70			<i>F. reinholdii</i>	5.6-6.4	
7H-7, 1-1	64.31	73.00			<i>F. reinholdii</i>	5.6-6.4	
7H-CC, 15-20	64.82	73.51	early Pliocene	>3.66	<i>F. reinholdii</i>	5.6-6.4	
8H-1, 120-122	66.20	75.65			<i>F. reinholdii</i>	5.6-6.4	
8H-4, 71-73	70.21	79.66			<i>F. reinholdii</i>	5.6-6.4	
8H-CC, 11-16	73.68	83.13	late Miocene	?	<i>F. reinholdii</i>	5.6-6.4	



Table T5 (continued).

Core, section, interval (cm)	Depth (mbsf)	Depth (mcd)	Radiolarian zone	Radiolarian age (Ma)	Planktic foraminifers	Benthic foraminifers	Comments
177-1092A-							
1H-1, 30-30	0.30	2.85					
1H-2, 1-1	1.51	4.06					
1H-3, 1-1	3.01	5.56					
1H-4, 1-1	4.51	7.06					
1H-CC, 7-12	8.00	10.55	Chi	0.83-1.92			
2H-1, 1-1	8.01	11.63					
2H-2, 1-1	9.51	13.13					
2H-3, 1-1	11.01	14.63					
2H-5, 1-1	14.01	17.63					
2H-CC, 9-14	16.11	19.73	?	?			
3H-1, 1-1	17.51	22.24					
3H-2, 1-1	19.01	23.74					
3H-5, 1-1	23.51	28.24					
3H-CC, 9-14	26.24	30.97					
4H-1, 1-1	27.01	31.88					
4H-3, 1-1	30.01	34.88					
4H-4, 1-1	31.51	36.38					
4H-5, 1-1	33.01	37.88					
4H-6, 1-1	34.51	39.38					
4H-7, 1-1	35.96	40.83					
4H-CC, 9-14	36.69	41.56					CN: no zone markers
5H-1, 1-1	36.51	42.38					
5H-4, 1-1	41.01	46.88					
5H-5, 1-1	42.51	48.38					
5H-6, 1-1	44.01	49.88					
5H-CC, 10-15	45.65	51.52	Upsilon	2.61-3.5			CN: no zone markers
6H-1, 1-1	46.01	53.90					
6H-2, 1-1	47.51	55.40					
6H-3, 1-1	49.01	56.90					
6H-5, 1-1	52.01	59.90					
6H-6, 1-1	53.51	61.40					
6H-CC, 1-10	54.84	62.73	Upsilon	3.5-4.57			CN: no zone markers
7H-1, 1-1	55.51	64.20					
7H-1, 120-122	56.70	65.39					
7H-3, 1-1	58.51	67.20					
7H-4, 1-1	60.01	68.70					
7H-5, 1-1	61.51	70.20					
7H-6, 1-1	63.01	71.70					
7H-7, 1-1	64.31	73.00					
7H-CC, 15-20	64.82	73.51	<i>A. challengerae</i>	6.1-6.58			CN: no zone markers
8H-1, 120-122	66.20	75.65					
8H-4, 71-73	70.21	79.66					
8H-CC, 11-16	73.68	83.13	?	late Miocene			CN: no zone markers

Table T5 (continued).

Core, section, interval (cm)	Depth (mbsf)	Depth (mcd)	Calcareous nannofossil zone	Calcareous nannofossil age (Ma)	Diatom zone	Diatom age (Ma)	Comments
9H-2, 71-73	76.71	86.04			<i>F. reinholdii</i>	5.6-6.4	
9H-3, 1-1	77.46	86.79			<i>A. ingens</i> var. <i>ovalis</i>	6.4-8.7	
9H-CC, 10-15	83.92	93.25	late Miocene	?	?		Trace diatoms, no markers
10H-1, 73-75	84.73	95.27			?	8.7-9.0	
10H-5, 73-75	90.73	101.27			?	8.7-9.0	
10H-CC, 15-20	93.45	103.99	late Miocene	?		late Miocene	
11H-2, 89-91	95.89	108.38			?	8.7-9.0	
11H-5, 71-73	100.21	112.70			<i>A. kennettii</i>	9.0-10.2	
11H-CC, 0-10	102.77	115.26	late Miocene	?	?		Trace diatoms, no markers
12H-1, 73-75	103.73	116.14			<i>A. kennettii</i>	9.0-10.2	
12H-5, 71-73	109.66	122.07			<i>A. kennettii</i>	9.0-10.2	
12H-CC, 28-33	113.03	125.44	late Miocene	?			Trace diatoms, no markers
13H-2, 69-71	114.69	128.91			<i>A. kennettii</i>	9.0-10.2	
13H-6, 71-73	120.71	134.93			<i>A. kennettii</i>	9.0-10.2	
13H-CC, 10-15	121.55	135.77	late Miocene	?			Rare diatoms, no markers
14H-1, 118-120	123.18	139.30			<i>D. hustedtii</i>	10.2-10.6	
14H-5, 120-122	129.20	145.32			<i>D. hustedtii</i>	10.2-10.6	
14H-CC, 10-15	131.11	147.23	late Miocene	<12.3		late Miocene	
15H-5, 120-122	138.70	156.94			late <i>D. dimorpha</i>	10.6-10.9	
15H-CC, 14-19	141.04	159.28	late Miocene	>12.3?		late Miocene	Trace diatoms
16H-5, 120-123	148.20	167.38			late <i>D. dimorpha</i>	10.6-10.9	
16H-CC, 14-19	149.91	169.09	late Miocene	?		late Miocene	Trace diatoms
17H-3, 116-119	154.09	172.31			<i>D. dimorpha</i>	10.6-11.7	
17H-5, 116-119	157.09	175.31					No diatoms
17H-CC, 32-37	158.51	176.73	middle Miocene ?	>12.7, >13.2			No diatoms
18H-1, 120-123	161.20	181.05			<i>N. dentic.+D. hust./N. grossep.</i>	12.8-14.2	
18H-5, 120-123	167.20	187.05			<i>A. inges</i> var. <i>nodus</i>	14.2-14.4	
18H-CC, 0-7	168.50	188.35	middle Miocene	>13.2	?		Trace diatoms, no markers
19H-1, 65-68	170.15	192.49			<i>A. ingens/D. maccollumii</i>	15.4-16.2	
19H-2, 65-68	171.65	193.99			<i>D. maccollumii</i>	16.2-16.8	
19H-3, 1-1	172.51	194.85	middle Miocene	<17.4			No diatoms
19H-4, 1-1	174.01	196.35	early Miocene	>17.4			
19H-5, 65-68	176.15	198.49			Unzoned	early/middle Miocene	Trace diatoms
19H-CC, 72-77	178.63	200.97	early Miocene	17.4-23.9			No diatoms
20H-1, 66-69	179.66	202.00			<i>T. fraga</i>	17.7-20.8	Co-occurrence <i>T. fraga/N. maleinterp.</i>
20H-6, 66-69	187.16	209.50			<i>T. fraga</i>	17.7-20.8	
20H-CC, 13-18	188.35	210.69	early Miocene	17.4-23.9	?		Trace diatoms, no markers
177-1092B-							
1H-1, 10-10	0.10	0.65	NN21b	0-0.085	<i>T. lentiginosa</i>	0-0.65	
1H-1, 60-60	0.60	1.15			<i>T. lentiginosa</i>	0-0.65	
1H-1, 117-117	1.17	1.72	NN21a	0.085-0.26			
1H-2, 10-10	1.60	2.15	NN20	0.26-0.46			
1H-2, 22-22	1.72	2.27			<i>T. lentiginosa</i>	0-0.65	
1H-2, 28-28	1.78	2.33			<i>T. lentiginosa</i>	0-0.65	MIS 11?

Table T5 (continued).

Core, section, interval (cm)	Depth (mbsf)	Depth (mcd)	Radiolarian zone	Radiolarian age (Ma)	Planktic foraminifers	Benthic foraminifers	Comments
9H-2, 71-73	76.71	86.04					
9H-3, 1-1	77.46	86.79					
9H-CC, 10-15	83.92	93.25	?	late Miocene			CN: no zone markers
10H-1, 73-75	84.73	95.27					
10H-5, 73-75	90.73	101.27					
10H-CC, 15-20	93.45	103.99	<i>A. australis</i>	9.12-10.36			CN: no zone markers
11H-2, 89-91	95.89	108.38					
11H-5, 71-73	100.21	112.70					
11H-CC, 0-10	102.77	115.26					CN: no zone markers
12H-1, 73-75	103.73	116.14					
12H-5, 71-73	109.66	122.07					
12H-CC, 28-33	113.03	125.44	?	middle-late Miocene			CN: no zone markers
13H-2, 69-71	114.69	128.91					
13H-6, 71-73	120.71	134.93					
13H-CC, 10-15	121.55	135.77					CN: no zone markers
14H-1, 118-120	123.18	139.30					
14H-5, 120-122	129.20	145.32					
14H-CC, 10-15	131.11	147.23	?	middle-late Miocene			CN: no zone markers
15H-5, 120-122	138.70	156.94					
15H-CC, 14-19	141.04	159.28					CN: no zone markers
16H-5, 120-123	148.20	167.38					
16H-CC, 14-19	149.91	169.09	<i>C. spongothorax</i> - <i>A. glownini</i>	10.36-13.61	<i>R. senni</i> (P22-N10) and <i>Bolboforma compressispinosa</i> = middle Miocene.		CN: no zone markers; hiatus?
17H-3, 116-119	154.09	172.31					
17H-5, 116-119	157.09	175.31					
17H-CC, 32-37	158.51	176.73					Hiatus?
18H-1, 120-123	161.20	181.05					
18H-5, 120-123	167.20	187.05					
18H-CC, 0-7	168.50	188.35	?	<19.11			CN: no zone markers
19H-1, 65-68	170.15	192.49					
19H-2, 65-68	171.65	193.99					
19H-3, 1-1	172.51	194.85					
19H-4, 1-1	174.01	196.35					
19H-5, 65-68	176.15	198.49					
19H-CC, 72-77	178.63	200.97					CN: no zone markers
20H-1, 66-69	179.66	202.00					
20H-6, 66-69	187.16	209.50					
20H-CC, 13-18	188.35	210.69	?	<19.11	>17.3 Ma		CN: no zone markers
177-1092B-							
1H-1, 10-10	0.10	0.65					
1H-1, 60-60	0.60	1.15					
1H-1, 117-117	1.17	1.72					
1H-2, 10-10	1.60	2.15					
1H-2, 22-22	1.72	2.27					
1H-2, 28-28	1.78	2.33					

Table T5 (continued).

Core, section, interval (cm)	Depth (mbsf)	Depth (mcd)	Calcareous nannofossil zone	Calcareous nannofossil age (Ma)	Diatom zone	Diatom age (Ma)	Comments
1H-2, 70-70	2.20	2.75	NN19	0.26-0.46			
1H-2, 126-126	2.76	3.31	NN19	0.46-0.88			
1H-3, 10-10	3.10	3.65			<i>T. lentiginosa</i>	0-0.65	<i>A. ingens</i> rare to trace abundance
1H-4, 75-75	5.25	5.80			middle/upper <i>A. ingens</i>	0.65-1.3	
1H-5, 100-100	7.00	7.55	NN19	0.46-0.88			
1H-CC, 0-7	7.35	7.90	NN19	>0.46	middle/upper <i>A. ingens</i>	0.65-1.3	
2H-1, 44-44	7.84	8.69	NN19	0.88-0.96			
2H-2, 115-115	10.05	10.90	NN19	0.96-1.08			
2H-3, 80-80	11.20	12.05	NN19	0.96-1.08			
2H-4, 80-80	12.70	13.55	NN19	1.08-1.24			
2H-5, 40-40	13.80	14.65	NN19	1.08-1.24			
2H-6, 30-30	15.20	16.05	NN19	1.24-1.46			
2H-CC, 6-11	16.66	17.51	NN19	1.24-1.46	middle/upper <i>A. ingens</i>	0.65-1.3	
3H-5, 40-40	23.30	24.54	NN19	1.24-1.46			
3H-5, 140-140	24.30	25.54	NN19	1.46-1.69			
3H-CC, 7-14	24.44	25.68	NN19	1.46-1.69	lower <i>A. ingens</i>	1.3-1.8	
4H-3, 140-140	30.80	32.01	NN19	1.46-1.69			
4H-4, 140-140	32.30	33.51	NN19	>1.69			
4H-CC, 5-10	35.82	37.03		>1.69	<i>P. barboi</i>	1.8-2.0	
5H-CC, 0-10	44.90	47.07		<3.66	<i>T. kolbei/F. matuyamae</i>	2.0-2.5	
6H-CC, 11-16	52.36	56.15		<3.66	<i>F. interfrigidaria</i>	3.3-3.8	
7H-CC, 0-10	55.56	58.21	NN14-NN15	>3.66	<i>F. interfrigidaria</i>	3.3-3.8	
8H-CC, 9-14	74.16	80.11	late Miocene	?	?		No diatom markers
9H-CC, 17-22	82.53	88.51	late Miocene	?	?		Trace diatoms, no markers
10H-CC, 11-16	92.09	99.09	late Miocene	?	?		<i>H. karstenii</i> = C
11H-CC, 17-22	102.44	110.93	late Miocene	?	late Miocene?		Rare diatoms, no markers
12H-CC, 8-13	111.38	121.31	late Miocene	?	?		Rare diatoms, no markers
13H-CC, 10-15	116.15	126.97	late Miocene	?	?		Trace diatoms, no markers
14H-CC, 18-23	131.38	144.30	late Miocene	?	?		Rare diatoms, no markers
15H-CC, 20-25	138.37	154.09	late Miocene	?	?		Rare diatoms, no markers
16H-CC, 20-25	149.09	164.41	late Miocene	?	?		Rare diatoms, no markers
17H-CC, 23-28	157.92	174.78	middle Miocene	>10.94	?		Trace diatoms, no markers
18H-CC, 25-30	168.67	184.58	middle Miocene	>13.2	?		Trace diatoms, no markers
177-1092C-							
1H-CC, 7-12	3.99	3.99	NN19	>0.46	<i>T. lentiginosa</i>	0-0.65	<i>A. ingens</i> rare to trace abundance
2H-CC, 10-15	11.77	14.45	NN19	0.96-1.24	middle/upper <i>A. ingens</i>	0.65-1.3	
3H-CC, 11-16	23.07	24.67	NN19	>1.24	lower <i>A. ingens</i>	1.3-1.8	
4H-CC, 0-5	32.07	35.30		<3.36	lower <i>A. ingens</i>	1.3-1.8	
5H-CC, 11-16	40.88	44.93			<i>T. kolbei/F. matuyamae</i>	2.0-2.5	
6H-CC, 0-10	42.00	52.00	late Pliocene?	<4.0	<i>T. insigna</i>	2.6-3.3	
7H-CC, 8-15	57.55	63.05			<i>F. interfrigidaria</i>	3.3-3.8	
8H-CC, 13-20	69.14	75.45	NN14-NN15	>3.36	<i>F. reinholdii</i>	5.6-6.4	
9H-CC, 18-25	80.02	86.97	late Miocene	?	?		Trace diatoms, no markers
10H-CC, 14-19	89.74	97.42	late Miocene	?	?		Trace diatoms, no markers

Table T5 (continued).

Core, section, interval (cm)	Depth (mbsf)	Depth (mcd)	Radiolarian zone	Radiolarian age (Ma)	Planktic foraminifers	Benthic foraminifers	Comments
1H-2, 70-70	2.20	2.75					
1H-2, 126-126	2.76	3.31					
1H-3, 10-10	3.10	3.65					
1H-4, 75-75	5.25	5.80					
1H-5, 100-100	7.00	7.55					
1H-CC, 0-7	7.35	7.90	Chi	0.83-1.92			
2H-1, 44-44	7.84	8.69					
2H-2, 115-115	10.05	10.90					
2H-3, 80-80	11.20	12.05					
2H-4, 80-80	12.70	13.55					
2H-5, 40-40	13.80	14.65					
2H-6, 30-30	15.20	16.05					
2H-CC, 6-11	16.66	17.51					
3H-5, 40-40	23.30	24.54					
3H-5, 140-140	24.30	25.54					
3H-CC, 7-14	24.44	25.68	Chi	0.83-1.92			
4H-3, 140-140	30.80	32.01					
4H-4, 140-140	32.30	33.51					
4H-CC, 5-10	35.82	37.03	Chi	0.83-1.92			
5H-CC, 0-10	44.90	47.07	Upsilon	2.61-3.5			
6H-CC, 11-16	52.36	56.15					
7H-CC, 0-10	55.56	58.21					
8H-CC, 9-14	74.16	80.11					
9H-CC, 17-22	82.53	88.51	?				
10H-CC, 11-16	92.09	99.09					
11H-CC, 17-22	102.44	110.93					
12H-CC, 8-13	111.38	121.31					
13H-CC, 10-15	116.15	126.97	<i>A. australis</i>	9.12-10.36			
14H-CC, 18-23	131.38	144.30					
15H-CC, 20-25	138.37	154.09					
16H-CC, 20-25	149.09	164.41					
17H-CC, 23-28	157.92	174.78	<i>C. spongothorax</i> - <i>A. glownini</i>	10.36-13.61			
18H-CC, 25-30	168.67	184.58	?	early-middle Miocene			
177-1092C-							
1H-CC, 7-12	3.99	3.99	Psi	0.46-0.83			
2H-CC, 10-15	11.77	14.45	Chi	0.83-1.92			
3H-CC, 11-16	23.07	24.67	Chi	0.83-1.92			
4H-CC, 0-5	32.07	35.30					
5H-CC, 11-16	40.88	44.93					CN: dissolution
6H-CC, 0-10	42.00	52.00	Upsilon	2.61-3.5			
7H-CC, 8-15	57.55	63.05					
8H-CC, 13-20	69.14	75.45					
9H-CC, 18-25	80.02	86.97					
10H-CC, 14-19	89.74	97.42	?	late Miocene			

Table T5 (continued).

Core, section, interval (cm)	Depth (mbsf)	Depth (mcd)	Calcareous nannofossil zone	Calcareous nannofossil age (Ma)	Diatom zone	Diatom age (Ma)	Comments
11H-CC, 51-56	98.28	106.64	late Miocene	?	?		Rare diatoms, no markers
12H-CC, 20-25	108.51	118.86	late Miocene	?	?		Rare diatoms, no markers
13H-CC, 9-16	118.23	129.66	late Miocene	?	?		Rare diatoms, no markers
14H-CC, 15-20	127.92	142.74	late Miocene	?	?		Trace diatoms, no markers
15H-CC, 16-23	137.43	152.63	late Miocene	?	?		Trace diatoms, no markers
16H-CC, 20-26	146.88	165.58	late Miocene	?	?		Trace diatoms, no markers
17H-CC, 21-26	156.28	176.16	middle Miocene	>10.94	?		Trace diatoms, no markers
18H-CC, 23-30	165.95	185.74	middle Miocene	>13.2	?		No diatoms
177-1092D-							
1H-2, 70-70	38.60	40.67			<i>T. kolbei/F. matuyamae</i>	2.0-2.5	
1H-4, 90-90	41.80	43.87			<i>T. kolbei/F. matuyamae</i>	2.0-2.5	
1H-6, 70-70	44.60	46.67			<i>T. kolbei/F. matuyamae</i>	2.0-2.5	
2H-2, 30-30	47.70	50.45			<i>T. insigna</i>	2.6-3.3	
2H-2, 80-80	48.20	50.95			<i>T. insigna</i>	2.6-3.3	
2H-3, 10-10	49.00	51.75			<i>T. insigna</i>	2.6-3.3	
2H-4, 10-10	50.50	53.25			<i>T. insigna</i>	2.6-3.3	
2H-5, 10-10	51.80	54.55			<i>F. interfrigidaria</i>	3.3-3.8	
2H-CC, 3-13	54.78	57.53					
3H-1, 50-50	55.90	60.21			<i>F. interfrigidaria</i>	3.3-3.8	
3H-3, 10-10	58.50	62.81			<i>F. interfrigidaria</i>	3.3-3.8	
3H-4, 10-10	60.00	64.31			<i>T. inura</i>	4.4-4.9	
3H-5, 10-10	61.50	65.81			Unzoned		
3H-6, 10-10	63.00	67.31			Unzoned		
3H-6, 120-120	64.10	68.41			Unzoned		Warm-water assemblage
3H-7, 10-10	64.50	68.81			?		No <i>T. oestrupii</i> found
3H-CC, 7-14	64.96	69.27			?		Contaminated?

Note: CN = calcareous nannofossil, MIS = marine isotope stage. This table is also available in ASCII format in the [TABLES](#) directory.

Table T5 (continued).

Core, section, interval (cm)	Depth (mbsf)	Depth (mcd)	Radiolarian zone	Radiolarian age (Ma)	Planktic foraminifers	Benthic foraminifers	Comments
11H-CC, 51-56	98.28	106.64					
12H-CC, 20-25	108.51	118.86					
13H-CC, 9-16	118.23	129.66					
14H-CC, 15-20	127.92	142.74	<i>A. australis</i>	9.12-10.36			
15H-CC, 16-23	137.43	152.63					
16H-CC, 20-26	146.88	165.58					
17H-CC, 21-26	156.28	176.16					
18H-CC, 23-30	165.95	185.74	?	early-middle Miocene			
177-1092D-							
1H-2, 70-70	38.60	40.67					
1H-4, 90-90	41.80	43.87					
1H-6, 70-70	44.60	46.67					
2H-2, 30-30	47.70	50.45					
2H-2, 80-80	48.20	50.95					
2H-3, 10-10	49.00	51.75					
2H-4, 10-10	50.50	53.25					
2H-5, 10-10	51.80	54.55					
2H-CC, 3-13	54.78	57.53	Upsilon	2.61-3.5			
3H-1, 50-50	55.90	60.21					
3H-3, 10-10	58.50	62.81					
3H-4, 10-10	60.00	64.31					
3H-5, 10-10	61.50	65.81					
3H-6, 10-10	63.00	67.31					
3H-6, 120-120	64.10	68.41					
3H-7, 10-10	64.50	68.81					
3H-CC, 7-14	64.96	69.27					

Table T6. Distribution of major planktic foraminifer species at Site 1092. (See table note. Continued on next page.)

Core, section, interval (cm)	Depth (mbsf)	Depth (mcd)	Abundance Preservation	<i>Catapsydrax</i> <i>dissimilis</i>	<i>Globigerina</i> <i>bulloides</i>	<i>Globigerina</i> <i>quinqueloba</i>	<i>Globigerinita</i> <i>glutinata</i>	<i>Globigerina</i> <i>woodi</i>	<i>Globigerinita</i> <i>uvula</i>	<i>Globobulimina</i> <i>dehiscens</i>	<i>Globobulimina</i> <i>venezuelana</i>	<i>Globobulimina</i> <i>cibaoensis</i>	<i>Globobulimina</i> <i>juanai</i>	<i>Globobulimina</i> <i>miozea</i>	<i>Globobulimina</i> <i>puncticulata</i>	<i>Globobulimina</i> <i>puncticuloides</i>	<i>Globobulimina</i> <i>scitula</i>	<i>Neoglobobulimina</i> <i>continua</i>	<i>Neoglobobulimina</i> <i>pachyderma</i> (sinistral)	<i>Orbulina</i> spp.
177-1092A-																				
1H-CC, 7-12	8.00	10.55	A G		F A				F						F F				D	
2H-CC, 9-14	16.11	19.73	A G		A				A						F F				D	
3H-CC, 9-14	26.24	30.97	A G		A										F F				D	
4H-CC, 9-14	36.74	41.61	A G		A F										F A				D	
5H-CC, 10-15	45.82	51.69	A G		F										A A				D	
6H-CC, 0-10	54.83	62.72	A G		A F										A				D	
7H-CC, 15-20	64.82	73.51	A M		A										R		R		D	
8H-CC, 11-16	73.72	83.17	A G		D			F										R		
9H-CC, 10-15	83.97	93.30	A M		F				F								D	D		
10H-CC, 15-20	93.63	104.17	A G														F	D		
11H-CC, 0-10	102.77	115.26	A G		D												A	A		
12H-CC, 28-33	113.08	125.49	A M		D												A	A		
13H-CC, 10-15	121.55	135.77	A G		D												A	A		
14H-CC, 10-15	131.11	147.23	A G		D												A	A		
15H-CC, 14-19	141.03	159.27	A G		D												A	A		
16H-CC, 14-19	149.91	169.09	A G		D													F		
17H-CC, 32-37	158.51	176.73	A M														D	D		
18H-CC, 0-7	168.50	188.35	A M					A					F	A						
19H-CC, 72-77	178.63	200.97																		
20H-CC, 13-18	188.35	210.69	A M	D					R	R										
177-1092B-																				
1H-CC, 0-7	7.35	7.90	A G		F D	F			A						F F				D	
2H-CC, 6-11	16.65	17.50	A G		D				F						F F				D	
3H-CC, 7-14	24.44	25.68	A G		F F										A A				D	
4H-CC, 5-10	35.82	37.03	A G		F A										A A				F	
5H-CC, 0-10	44.90	47.07	A G		A										F F				D	
6H-CC, 11-16	52.36	56.15	A G		A A										D D	P			F	
7H-CC, 0-10	55.56	58.21	A G		A										D	F				
8H-CC, 9-14	74.16	80.11	A G		D			F											R	
9H-CC, 17-22	82.53	88.51	A G	D				F		A								F		
10H-CC, 11-16	92.09	99.09	A G					F		F	F						F	D		
11H-CC, 17-22	102.44	110.93	A G		D			F									A			
12H-CC, 8-13	111.38	121.31	A M		F			F									F	A		
13H-CC, 10-15	116.15	126.97	A G		A			F									D			
14H-CC, 18-23	131.40	144.32	A G		D			D		A							F	F		
15H-CC, 20-25	138.37	154.09	A M		D			D		F							A	F		
16H-CC, 20-25	149.09	164.41	A M		D			D									F	A		
17H-CC, 23-28	157.96	174.82	A M		F			D									D			
18H-CC, 25-30	168.65	184.56	A M					D						D			F			
177-1092C-																				
1H-CC, 7-12	3.99	3.99	A G		A A			F	F						F F				D	
2H-CC, 10-15	11.77	14.42	A G		A				A						F F				D	
3H-CC, 11-16	23.07	24.67	A G		F F										D D					
4H-CC, 0-5	32.07	35.30	F G												F F				D	
5H-CC, 11-16	40.88	44.93	F M		D A				A						F				A	
6H-CC, 0-10	42.00	42.00	A G		D			F							D A					
7H-CC, 8-15	57.55	63.02	A G		D										D A	F				
8H-CC, 13-20	69.14	75.45	F G		D												D			
9H-CC, 18-25	80.02	86.97	A G		A			F				F					F	D		
10H-CC, 14-19	89.74	97.42	A G		A												A	D		
11H-CC, 51-56	98.28	106.78	A G		D			A									A	F		



Table T6 (continued).

Core, section, interval (cm)	Depth (mbsf)	Depth (mcd)	Abundance		Preservation	<i>Catapsydrax</i> <i>dissimilis</i>	<i>Globigerina</i> <i>bulloides</i>	<i>Globigerina</i> <i>quinqueloba</i>	<i>Globigerinita</i> <i>glutinata</i>	<i>Globigerina</i> <i>woodi</i>	<i>Globigerinita</i> <i>uvula</i>	<i>Globoquadrina</i> <i>dehiscens</i>	<i>Globoquadrina</i> <i>venezuelana</i>	<i>Globorotalia</i> <i>cibaoensis</i>	<i>Globorotalia</i> <i>juanai</i>	<i>Globorotalia</i> <i>miozea</i>	<i>Globorotalia</i> <i>punctulata</i>	<i>Globorotalia</i> <i>punctuloides</i>	<i>Globorotalia</i> <i>scitula</i>	<i>Neogloboquadrina</i> <i>continuosa</i>	<i>Neogloboquadrina</i> <i>pachyderma</i> (sinistral)	<i>Orbulina</i> spp.
			A	G																		
12H-CC, 20-25	108.51	118.86	A	G			A													R	D	
13H-CC, 9-16	118.23	129.66	A	G			F													D	D	
14H-CC, 15-20	127.92	142.74	A	G			D		F											D	D	
15H-CC, 16-23	137.43	152.63	A	M			D													D	R	
16H-CC, 20-26	146.88	165.58	A	G			D													F	R	
17H-CC, 21-26	156.28	176.16	A	P			D		F											D	D	
18H-CC, 23-30	165.95	185.74	A	G			A		A							D						
177-1092D-																						
1H-CC, 0-7	46.00	48.07	A	G			D	A		A							F	F			D	
2H-CC, 3-13	54.78	57.53	A	G			A										D	D			D	
3H-CC, 7-14	64.96	69.27	A	G			D		D										A		D	

Notes: Abundance abbreviations: D = dominant, A = abundant, F = few, R = rare, P = present. Preservation abbreviations: G = good, M = moderate, P = poor. For more specific definitions, refer to "Biostratigraphy," p. 10, in the "Explanatory Notes" chapter. This table is also available in ASCII format in the TABLES directory.



Table T7 (continued).

Core, section, interval (cm)	Depth (mbsf)	Depth (mcd)	Abundance Preservation	<i>Nodosaria</i> spp.	<i>Nonionella</i> sp.	<i>Nuttallides umbonifera</i>	<i>Oolina</i> spp.	<i>Ophthalimidium</i> sp.	<i>Oridorsalis umbonatus</i>	<i>Parafissurina</i> sp.	<i>Pleurostomella</i> sp.	<i>Polymorphinid</i> spp.	<i>Pullenia bulloides</i>	<i>Pullenia</i> sp.	<i>Pullenia quinqueloba</i>	<i>Pullenia subcarinata</i>	<i>Pyrgo murrhina</i>	<i>Pyrgo</i> spp.	<i>Quinqueloculina</i> sp.	<i>Rectuvigierina multicoستا</i>	<i>Rectuvigierina senni</i>	<i>Siphotextularia</i> sp.	<i>Sphaeroidina bulloides</i>	<i>Stainforthia</i> sp.	<i>Francesita</i> sp.	<i>Stilostomella lepidula</i>	<i>Stilostomella subspinosa</i>	<i>Stilostomella</i> sp.	<i>Textularia</i> sp.	<i>Trifarina angulosa</i>	<i>Uvigerina hispidocostata</i>	<i>Uvigerina peregrina</i>	<i>Uvigerina</i> sp.	Sample sum	Number of species	Abundance (specimens/cm <sup>3</sup> )					
177-1092A-																																									
1H-CC, 7-12	8	10.55	A M		1				1		40				1	1																				180	19	1265.6			
2H-CC, 9-14	16.11	19.73	A G								7													1												231	16	577.5			
3H-CC, 9-14	26.24	30.97	A M						1		1				1									2												78	13	780.0			
4H-CC, 9-14	36.69	41.61	A M							1		3												1	1											44	16	154.0			
5H-CC, 10-15	45.65	51.69	A M		1	1	1		8	1			10		2	1								1	1	1	2									64	21	240.0			
6H-CC, 0-10	54.83	62.72	A P						2		5	2			1		2							1	1					3						44	20	165.0			
7H-CC, 15-20	64.82	73.51	A M						4	1		1				5					1				3	1					3					96	21	200.0			
8H-CC, 11-16	73.68	83.17	A M	2							3	2	2		5	2									1	1			5		3					89	27	133.5			
9H-CC, 10-15	83.92	93.3	A M				1		1	1		3		1			1												7		3					109	21	218.0			
10H-CC, 15-20	93.45	104.17	A M	1		3			1			17			3							1			6	2										148	25	98.7			
11H-CC, 0-10	102.77	115.26	C M	1	1	5				1	1	1			1	1					1			1	2	1											75	21	30.0		
12H-CC, 28-33	113.03	125.49	A P		1	1			1						3	1	1					1			9													76	20	57.0	
13H-CC, 10-15	121.55	135.77	C M		1						3	1			1	4					1	1									1							64	25	32.0	
14H-CC, 10-15	131.11	147.23	A M			3			2	1	1				1	2						3				10	2			1	1							116	33	83.9	
15H-CC, 14-19	141.04	159.27	C M			1			1		4	3	3		1							1				5				64								147	28	51.5	
16H-CC, 14-19	149.91	169.09	C M						7	1	2	1		4	3			1	1						4	1			6	11								124	27	80.6	
17H-CC, 32-37	158.51	176.73	C M			2			5	1	5	2			1										2					3									136	29	283.3
18H-CC, 0-7	168.5	188.35	A M		6				3		1	5		1											9	4				2									95	25	237.5
19H-CC, 72-77	178.63	200.97	C M		1	2			9	6	8			1							3	1				20			7										172	32	430.0
20H-CC, 13-18	188.35	210.69	C M		1	9			3	1	2	1	12		5						1	1	1			28			4	8	1								201	37	586.3

















Table T8 (continued).

Core, section, interval (cm)	Depth (mbsf)	Depth (mcd)	Diatom abundance (uncleaned)			Diatom abundance (acid-cleaned)			Diatom preservation	<i>Thalassiosira insignis</i> <i>Thalassiosira inura</i> <i>Thalassiosira kolbei</i> <i>Thalassiosira lentiginosa</i> <i>Thalassiosira mahoodii</i> <i>Thalassiosira miocenica</i> <i>Thalassiosira oestrupii</i> <i>Thalassiosira oliverana</i> <i>Thalassiosira oliverana</i> var. <i>sparsa</i> <i>Thalassiosira praeconvexa</i> <i>Thalassiosira tetraoestrupii</i> var. <i>reimeri</i> <i>Thalassiosira vulnifica</i> <i>Thalassiothrix antarctica-longissima</i> gr.	Diatom zone	Diatom age (Ma)
			T	C	M	F	M-P	R				
12H-CC, 28-33	113.03	125.44	T							X		
13H-2, 69-71	114.69	128.91		C	M					A	<i>A. kennettii</i>	9.0-10.2
13H-6, 71-73	120.71	134.93		F	M-P					R	<i>A. kennettii</i>	9.0-10.2
13H-CC, 10-15	121.55	135.77	R							X		
14H-1, 118-120	123.18	139.30		A-C	M					R	<i>D. hustedtii</i>	10.2-10.6
14H-5, 120-122	129.20	145.32		C	M					R	<i>D. hustedtii</i>	10.2-10.6
14H-CC, 10-15	131.11	147.23	F-R		M-P					C		late Miocene
15H-5, 120-122	138.70	156.94		C	M-P						late <i>D. dimorpha</i>	10.6-10.9
15H-CC, 14-19	141.04	159.28	R-T		M					X		late Miocene
16H-5, 120-123	148.20	167.38		C	M						late <i>D. dimorpha</i>	10.6-10.9
16H-CC, 14-19	149.91	169.09	T									late Miocene
17H-3, 116-119	154.09	172.31		F	M-P							10.6-11.7
17H-5, 116-119	157.09	175.31		T								
17H-CC, 32-37	158.51	176.73	B									
18H-1, 120-123	161.20	181.05		R	P						<i>N. dentic.+D. hust./N. grossep.</i>	12.8-14.2
18H-5, 120-123	167.20	187.05		T	P						<i>A. ingens</i> var. <i>nodus</i>	14.2-14.4
18H-CC, 0-7	168.50	188.35	T							X	?	
19H-1, 65-68	170.15	192.49		F	M-P						<i>A. ingens/D. maccollumii</i>	15.4-16.2
19H-2, 65-68	171.65	193.99		F	P						<i>D. maccollumii</i>	16.2-16.8
19H-5, 65-68	176.15	198.49		R	M					X	Unzoned	early/middle Miocene
19H-CC, 72-77	178.63	200.97	B									
20H-1, 66-69	179.66	202.00		F	M						<i>T. fraga</i>	17.7-20.8
20H-6, 66-69	187.16	209.50		F	M-P						<i>T. fraga</i>	17.7-20.8
20H-CC, 13-18	188.35	210.69	T								?	
177-1092B-												
1H-1, 60-60	0.60	1.15	A	G		C					<i>T. lentiginosa</i>	0-0.65
1H-2, 22-22	1.72	2.27	A	G		F		R			<i>T. lentiginosa</i>	0-0.65
1H-2, 28-28	1.78	2.33	R	P		X					<i>T. lentiginosa</i>	0-0.65
1H-3, 10-10	3.10	3.65	A	G		C		R			<i>T. lentiginosa</i>	0-0.65
1H-4, 75-75	5.25	5.80	A	G		C					middle/upper <i>A. ingens</i>	0.65-1.3
1H-CC, 0-7	7.35	7.90	A	M		R		R			middle/upper <i>A. ingens</i>	0.65-1.3
2H-CC, 6-11	16.66	17.51	A	M		F					middle/upper <i>A. ingens</i>	0.65-1.3
3H-CC, 7-14	24.44	25.68	A	G-M		F		R R		R	lower <i>A. ingens</i>	1.3-1.8
4H-CC, 5-10	35.82	37.03	A	M		T R		R		R	<i>P. barboi</i>	1.8-2.0
5H-CC, 0-10	44.90	47.07	C	M		F R		F		F	<i>T. kolbei/F. matuyamae</i>	2.0-2.5
6H-CC, 11-16	52.36	56.15	F	M		R R		R			<i>F. interfrigidaria</i>	3.3-3.8
7H-CC, 0-10	55.56	58.21	C-F	M						C	<i>F. interfrigidaria</i>	3.3-3.8
8H-CC, 9.0-14	74.16	80.11	C-F	M						F	?	
9H-CC, 17.0-22	82.53	88.51	T							X	?	
10H-CC, 11.0-16	92.09	99.09	C-F	M							?	
11H-CC, 17.0-22	102.44	110.93	R							X	late Miocene?	
12H-CC, 8.0-13	111.38	121.31	R-T							X	?	
13H-CC, 10.0-15	116.15	126.97	T							X	?	
14H-CC, 18.0-23	131.38	144.30	R							X	?	
15H-CC, 20.0-25	138.37	154.09	R-T							X	?	
16H-CC, 20.0-25	149.09	164.41	R-T							X	?	
17H-CC, 23.0-28	157.92	174.78	T							X	?	
18H-CC, 25.0-30	168.67	184.58	T							X	?	









**Table T9.** Control points used to calculate sedimentation rates at Site 1092. (See table note. Continued on next page.)

Code	Event/Zone/Chron	Depth range of stratigraphic datums								Age (Ma)	Sedimentation rate (m/m.y.)
		Top			Base			Mean			
		Core, section, interval (cm)	Depth (mbsf)	Depth (mcd)	Core, section, interval (cm)	Depth (mbsf)	Depth (mcd)	Depth (mbsf)	Depth (mcd)		
		177-			177-						
CN	acme <i>E. huxleyi</i>	1092B-1H-1, 10-10	0.10	0.65	1092B-1H-1, 60-60	0.60	1.15	0.35	0.90	0.085	
CN	FO <i>E. huxleyi</i>	1092B-1H-1, 117-117	1.17	1.72	1092B-1H-2, 10-10	1.60	2.15	1.38	1.93	0.26	
CN	LO <i>P. lacunosus</i>	1092B-1H-2, 70-70	2.20	2.75	1092B-1H-2, 126-126	2.76	3.31	2.48	3.03	0.46	~10
DIAT	TOP <i>A. ingens</i> Zone	1092A-1H-2, 1-1	1.51	4.06	1092A-1H-3, 1-1	3.01	5.56	2.26	4.81	0.65	
RAD	BOT Psi Zone	1092C-1H-0, 7-12	3.99	3.99	1092B-1H-0, 0-7	7.35	7.90	5.67	5.95	0.46	
CN	LO <i>R. asanoi</i>	1092B-1H-5, 100-100	7.00	7.55	1092B-2H-1, 44-44	7.84	8.69	7.42	8.12	0.88	
CN	RE <i>Gephyrocapsa</i> medium (4-5.5 µm)	1092B-2H-1, 44-44	7.84	8.69	1092B-2H-2, 115-115	10.05	10.90	8.95	9.80	0.96	
CN	FO <i>R. asanoi</i>	1092B-2H-3, 80-80	11.20	12.05	1092B-2H-4, 80-80	12.70	13.55	11.95	12.80	1.08	
CN	LO <i>Gephyrocapsa</i> large (>5.5 µm)	1092B-2H-5, 40-40	13.80	14.65	1092B-2H-6, 30-30	15.20	16.05	14.50	15.35	1.24	
DIAT	TOP <i>A. ingens</i> Subzone a	1092A-2H-0, 9-14	16.11	19.73	1092A-3H-2, 1-1	19.01	23.74	17.56	21.73	1.30	~29
CN	FO <i>Gephyrocapsa</i> large (>5.5 µm)	1092B-3H-5, 40-40	23.30	24.54	1092B-3H-5, 140-140	24.30	25.54	23.80	25.04	1.46	
CN	FO <i>Gephyrocapsa</i> medium (4-5.5 µm)	1092B-4H-3, 140-140	30.80	32.01	1092B-4H-4, 140-140	32.30	33.51	31.55	32.76	1.69	
DIAT	TOP <i>P. barboi</i> Zone	1092C-4H-0, 0-5	32.07	35.30	1092A-4H-4, 1-1	31.51	36.38	31.79	35.84	1.80	
RAD	BOT Chi Zone	1092B-4H-0, 5-10	35.82	37.03	1092A-4H-0, 4-14	36.74	41.61	36.28	39.32	1.92	
DIAT	TOP <i>T. kolbei-F. matuyamae</i> Zone	1092A-4H-5, 1-1	33.01	37.88	1092A-4H-6, 1-1	34.51	39.38	33.76	38.63	2.00	
DIAT	TOP <i>T. vulnifica</i> Zone	1092A-5H-5, 1-1	42.51	48.38	1092A-5H-6, 1-1	44.01	49.88	43.26	49.13	2.50	
DIAT	TOP <i>T. insignia</i> Zone	1092A-5H-6, 1-1	44.01	49.88	1092D-2H-2, 30-30	47.70	50.45	45.86	50.17	2.63	
DIAT	TOP <i>F. interfrigidara</i> Zone	1092A-6H-1, 1-1	46.01	53.90	1092D-2H-5, 10-10	51.80	54.55	48.91	54.22	3.26	~12
CN	LO <i>R. pseudoumbilicus</i>	1092A-6H-6, 0-0	53.50	61.39	1092A-6H-6, 100-100	54.50	62.39	54.00	61.89	3.66	
DIAT	BOT <i>F. interfrigidara</i> Zone	1092A-7H-1, 1-1	55.51	64.20	1092D-3H-4, 10-10	60.00	64.31	57.75	64.25	3.80	
DIAT	FO <i>T. inura</i>	1092A-7H-3, 1-1	58.51	67.20	1092A-7H-4, 1-1	60.01	68.70	59.26	67.95	4.92	
DIAT	TOP <i>F. reinholdii</i> Zone	1092A-7H-5, 1-1	61.51	70.20	1092A-7H-6, 1-1	63.01	71.70	62.26	70.95	6.00	
RAD	BOT <i>A. challengerae</i> Zone	1092A-7H-0, 15-20	64.82	73.51	1092A-8H-0, 11-16	73.72	83.17	69.27	78.34	6.58	
PMAG	BOT C4n	1092A-9H-4, 80-80	79.80	81.60	1092A-9H-5, 110-110	89.30	90.93	90.115	90.12	7.89	
PMAG	BOT C4r	1092A-9H-7, 25-25	83.60	85.60	1092A-10H-2, 10-10	93.35	96.14	94.745	94.75	8.53	~15
DIAT	BOT <i>A. ing.</i> var. <i>ova.</i> Zone	1092A-9H-3, 1-1	77.46	86.79	1092A-10H-1, 73-75	84.73	95.27	81.10	91.03	8.68	
PMAG	BOT C4An	1092A-11H-1, 80-80	94.30	95.20	1092A-11H-2, 20-20	106.79	107.69	107.24	107.24	8.86	
RAD	LO <i>C. spongothorax</i>	1092C-10H-0, 14-19	89.74	97.42	1092A-10H-0, 15-20	93.63	104.17	91.69	100.80	9.12	
PMAG	BOT C4Ar	1092A-12H-1, 120-120	104.20	106.20	1092A-12H-3 20-20	116.61	118.61	117.61	117.61	9.78	
DIAT	TOP <i>D. hustedtii</i> Zone	1092A-13H-6, 71-71	120.71	134.93	1092A-14H-1, 118-118	123.18	139.30	121.95	137.12	10.23	
RAD	FO <i>A. australis</i>	1092C-14H-0, 15-20	127.92	142.74	1092A-14H-0, 10-15	131.11	147.23	129.52	144.98	10.36	~38
DIAT	TOP <i>D. dimorpha</i> Zone	1092A-14H-5, 120-122	129.20	145.32	1092A-15H-5, 120-122	138.70	156.94	133.95	151.13	10.63	
PMAG	BOT C5n	1092A-15H-5, 30-30	137.80	139.10	1092A-15H-6, 10-10	156	157.3	156.69	156.69	10.83	
CN	LO <i>C. miopelagicus</i>	1092B-17H-2, 0-0	152.00	170.22	1092A-17H-5, 0-0	155.93	174.15	153.97	172.18	10.94	
CN	LO <i>C. nitescens</i>	1092A-17H-0, 32-37	158.51	176.73	1092A-18H-1, 0-0	160.00	179.85	159.26	178.29	12.10	
CN	LO <i>C. premacintyreii</i>	1092A-17H-0, 32-37	158.51	176.73	1092A-18H-1, 0-0	160.00	179.85	159.26	178.29	12.70	
DIAT	TOP <i>N. denticuloides</i> Zone	1092A-17H-3, 116-119	154.09	172.31	1092A-18H-1, 120-123	161.20	181.05	157.65	176.68	12.84	
CN	LCO <i>C. floridanus</i>	1092A-17H-0, 32-37	158.51	176.73	1092A-18H-1, 0-0	160.00	179.85	159.26	178.29	13.20	~4
RAD	FO <i>A. golownini</i>	1092B-17H-0, 23-28	157.96	174.82	1092B-18H-0, 25-30	168.65	184.56	163.31	179.69	13.61	
DIAT	TOP <i>A. ingens</i> var. <i>nodus</i> Zone	1092A-18H-1, 120-120	161.20	181.05	1092A-18H-5, 120-120	167.20	187.05	164.20	184.05	14.17	



**Table T9 (continued).**

Code	Event/Zone/Chron	Depth range of stratigraphic datums								Age (Ma)	Sedimentation rate (m/m.y.)
		Top		Base		Mean					
		Core, section, interval (cm)	Depth (mbsf)	Depth (mcd)	Core, section, interval (cm)	Depth (mbsf)	Depth (mcd)	Depth (mbsf)	Depth (mcd)		
DIAT	TOP <i>A.ingens/D.maccollum</i> Zone	1092A-18H-5, 120-123	167.20	187.05	1092A-19H-1, 65-68	170.15	192.49	168.68	189.77	15.38	
DIAT	TOP <i>D. maccollumii</i> Zone	1092A-19H-1, 65-65	170.15	192.49	1092A-19H-2, 65-65	171.65	193.99	170.90	193.24	16.20	
CN	FO <i>C. premacintyreii</i>	1092A-19H-3, 0-0	172.50	194.84	1092A-19H-4, 0-0	174.00	196.34	173.25	195.59	17.40	

Notes: Code abbreviations: CN = calcareous nannofossil, DIAT = diatom, RAD = radiolaria, PMAG = magnetic polarity. Event abbreviations: FO = first occurrence, LO = last occurrence, LCO = last common occurrence, RE = reentrance, TOP = top of zone, BOT = bottom of zone. This table is also available in ASCII format in the **TABLES** directory.





**Table T11.** Concentrations of methane obtained by the headspace technique at Site 1092.

Core, section, interval (cm)	Depth (mbsf)	C <sub>1</sub> (ppmv)
177-1092A-		
1H-5, 0-5	6.02	2
2H-4, 0-5	12.52	2
3H-5, 0-5	23.52	3
4H-5, 0-5	33.02	2
5H-5, 0-5	42.52	3
6H-5, 0-5	52.02	3
7H-5, 0-5	61.52	3
8H-5, 0-5	71.03	3
9H-5, 0-5	80.53	3
10H-5, 0-5	90.02	2
11H-5, 0-5	99.52	3
12H-5, 0-5	109.02	3
13H-5, 0-5	118.52	3
14H-5, 0-5	128.02	4
15H-5, 0-5	137.52	4
16H-5, 0-5	147.02	4
17H-5, 0-5	155.96	5
18H-5, 0-5	166.02	3
19H-4, 0-5	174.02	4
20H-4, 0-5	183.52	4

Note: C<sub>1</sub> = methane.

**Table T12.** Interstitial water chemistry from shipboard measurements at Site 1092. (Continued on next page.)

Core, section, interval (cm)	Depth (mbsf)	pH	Method	Alkalinity (mM)	Method	Salinity	Method	Cl (mM)	Method	SO <sub>4</sub> (mM)	Method	Na (mM)	Method	Mg (mM)	Method
177-1092A-															
1H-4, 145-150	5.98	7.89	ISE	2.739	T	35.5	R	555	T	28.7	I	474	CB	53.7	I
2H-3, 145-150	12.48	7.76	ISE	3.162	T	35.5	R	560	T	27.3	I	475	CB	54.3	I
3H-4, 145-150	23.48	7.90	ISE	2.514	T	35.5	R	561	T	28.8	I	478	CB	54.3	I
4H-4, 145-150	32.98	7.77	ISE	3.238	T	35.5	R	563	T	27.2	I	477	CB	54.2	I
5H-4, 145-150	42.48	7.50	ISE	3.125	T	35.5	R	563	T	27.5	I	480	CB	53.4	I
6H-4, 145-150	51.98	7.46	ISE	3.478	T	35.5	R	564	T	26.6	I	480	CB	52.3	I
7H-4, 140-150	61.45	7.57	ISE	3.394	T	35.5	R	563	T	27.5	I	481	CB	52.1	I
8H-4, 140-150	70.95	7.72	ISE	3.535	T	35.5	R	561	T	26.8	I	478	CB	52.0	I
9H-4, 140-150	80.45	7.44	ISE	3.304	T	35.5	R	562	T	27.9	I	482	CB	51.3	I
10H-4, 140-150	89.95	7.45	ISE	3.695	T	35.5	R	562	T	26.4	I	480	CB	50.6	I
11H-4, 140-150	99.45	7.53	ISE	3.304	T	35.5	R	561	T	26.0	I	479	CB	49.6	I
12H-4, 140-150	108.95	7.31	ISE	3.816	T	35.5	R	562	T	26.6	I	481	CB	49.7	I
13H-4, 140-150	118.45	7.53	ISE	3.751	T	35.0	R	562	T	25.4	I	479	CB	49.1	I
14H-4, 140-150	127.95	7.62	ISE	3.871	T	35.5	R	561	T	24.9	I	474	CB	50.3	I
15H-4, 140-150	137.45	7.45	ISE	3.987	T	35.5	R	562	T	25.6	I	481	CB	48.2	I
16H-4, 140-150	146.95	7.57	ISE	3.987	T	35.5	R	563	T	25.8	I	482	CB	47.8	I
17H-4, 140-150	155.88	7.53	ISE	3.952	T	35.5	R	562	T	25.5	I	479	CB	48.4	I
18H-4, 140-150	165.95	7.60	ISE	3.915	T	35.5	R	562	T	25.6	I	481	CB	47.9	I
19H-3, 140-150	173.95	7.60	ISE	3.914	T	35.5	R	564	T	25.8	I	482	CB	48.0	I
20H-3, 140-150	183.45	7.63	ISE	3.931	T	35.5	R	566	T	25.0	I	482	CB	47.9	I

Note: Method abbreviations: ISE = ion selective electrode, T = titration, R = refractometer, I = ion chromatography, CB = charge balance calculation, S = spectrophotometry, AAS = atomic absorption spectrometry, AES = atomic emission spectrometry.

Table T12 (continued).

Core, section, interval (cm)	Depth (mbsf)	Ca (mM)	Method	K (mM)	Method	H <sub>4</sub> SiO <sub>4</sub> (μM)	Method	NH <sub>4</sub> (μM)	Method	HPO <sub>4</sub> (μM)	Method	Sr (μM)	Method	Mn (μM)	Method	Li (μM)	Method
177-1092A-																	
1H-4, 145-150	5.98	11.1	I	11.0	I	744	S	28	S	3.6	S	97	AAS	0	AAS	21.7	AES
2H-3, 145-150	12.48	11.2	I	11.2	I	748	S	35	S	2.4	S	116	AAS	0	AAS	19.9	AES
3H-4, 145-150	23.48	11.6	I	10.9	I	764	S	49	S	2.4	S	146	AAS	0	AAS	17.8	AES
4H-4, 145-150	32.98	11.7	I	11.3	I	833	S	49	S	1.9	S	160	AAS	0	AAS	15.1	AES
5H-4, 145-150	42.48	11.5	I	11.0	I	820	S	52	S	1.6	S	191	AAS	0	AAS	15.5	AES
6H-4, 145-150	51.98	12.1	I	11.6	I	833	S	60	S	1.1	S	213	AAS	0	AAS	14.1	AES
7H-4, 140-150	61.45	12.2	I	11.5	I	826	S	67	S	1.1	S	242	AAS	0	AAS	13.5	AES
8H-4, 140-150	70.95	12.4	I	11.1	I	854	S	64	S	1.0	S	269	AAS	0	AAS	13.0	AES
9H-4, 140-150	80.45	12.4	I	11.4	I	861	S	64	S	0.8	S	287	AAS	0	AAS	12.8	AES
10H-4, 140-150	89.95	12.9	I	11.4	I	863	S	73	S	0.8	S	310	AAS	0	AAS	12.5	AES
11H-4, 140-150	99.45	13.2	I	11.4	I	942	S	73	S	0.8	S	328	AAS	0	AAS	11.9	AES
12H-4, 140-150	108.95	13.5	I	10.7	I	905	S	72	S	0.8	S	356	AAS	0	AAS	12.0	AES
13H-4, 140-150	118.45	13.7	I	11.3	I	909	S	75	S	1.0	S	366	AAS	0	AAS	11.6	AES
14H-4, 140-150	127.95	14.4	I	10.8	I	923	S	72	S	1.0	S	380	AAS	0	AAS	11.9	AES
15H-4, 140-150	137.45	14.2	I	11.0	I	879	S	77	S	0.8	S	397	AAS	0	AAS	11.3	AES
16H-4, 140-150	146.95	14.4	I	11.0	I	928	S	77	S	0.7	S	400	AAS	0	AAS	11.3	AES
17H-4, 140-150	155.88	14.8	I	10.5	I	898	S	80	S	0.8	S	384	AAS	0	AAS	11.9	AES
18H-4, 140-150	165.95	14.6	I	10.6	I	923	S	79	S	0.8	S	430	AAS	0	AAS	12.2	AES
19H-3, 140-150	173.95	14.9	I	10.7	I	886	S	79	S	0.8	S	439	AAS	0	AAS	12.2	AES
20H-3, 140-150	183.45	15.6	I	10.2	I	900	S	71	S	0.8	S	446	AAS	0	AAS	12.8	AES

**Table T13.** Analytical results of inorganic carbon, calculated calcium carbonate, total carbon, total organic carbon, total nitrogen, total sulfur, and TOC/TN at Site 1092.

Core, section, interval (cm)	Depth (mbsf)	IC (wt%)	CaCO <sub>3</sub> (wt%)	TC (wt%)	TOC (wt%)	TN (wt%)	TS (wt%)	TOC/ TN
177-1092A-								
1H-1, 67-68	0.68	5.96	49.6	5.81	0.00	0.03	0.0	
1H-3, 69-70	3.70	8.94	74.5					
1H-5, 59-60	6.60	9.61	80.0					
2H-1, 35-36	8.36	6.10	50.8	6.80	0.70	0.06	0.0	11.0
2H-3, 23-24	11.24	7.70	64.2					
2H-5, 39-40	14.40	6.13	51.1					
3H-1, 109-110	18.60	5.05	42.1	5.14	0.09	0.06	0.0	1.6
3H-5, 69-70	24.20	4.36	36.3					
4H-2, 62-63	29.13	2.00	16.7	2.59	0.59	0.07	0.0	8.6
4H-4, 72-73	32.23	6.24	52.0					
4H-6, 119-120	35.70	9.17	76.4					
5H-1, 119-120	37.70	6.32	52.6	6.38	0.07	0.05	0.0	1.5
5H-3, 27-28	39.78	8.32	69.3					
5H-5, 71-72	43.22	8.16	68.0					
6H-2, 49-50	48.00	8.34	69.4	8.36	0.02	0.04	0.0	0.5
6H-6, 69-70	54.20	10.94	91.1					
7H-1, 120-121	56.71	9.76	81.3	9.72	0.00	0.06	0.0	
7H-3, 28-29	58.79	9.67	80.5					
7H-5, 29-30	61.80	8.60	71.6					
8H-1, 120-121	66.21	9.38	78.1	9.29	0.00	0.06	0.0	
8H-4, 71-72	70.22	10.29	85.7					
9H-2, 69-70	76.70	9.76	81.3	9.58	0.00	0.00	0.0	
9H-4, 69-70	79.70	10.10	84.1					
9H-6, 119-120	83.05	9.85	82.0					
10H-1, 72-73	84.73	10.75	89.6	10.89	0.14	0.00	0.0	
10H-3, 72-73	87.73	11.20	93.3					
10H-5, 72-73	90.73	10.66	88.8					
10H-7, 72-73	93.13	10.92	91.0					
11H-2, 86-87	95.87	10.72	89.3					
11H-3, 38-39	96.89	11.06	92.1					
11H-5, 69-70	100.20	10.79	89.9					
12H-1, 71-72	103.72	10.41	86.7					
12H-3, 69-70	106.70	10.15	84.5					
12H-5, 68-69	109.69	11.29	94.0					
13H-2, 68-69	114.69	10.71	89.2					
13H-4, 72-73	117.73	10.85	90.4					
13H-6, 71-72	120.72	11.03	91.9					
14H-1, 118-119	123.19	10.32	86.0					
14H-3, 124-125	126.25	10.98	91.5					
14H-5, 120-121	129.21	10.66	88.8					
15H-1, 121-122	132.72	11.12	92.6					
15H-3, 122-123	135.73	10.40	86.6					
15H-5, 122-123	138.73	11.21	93.4					
16H-1, 121-122	142.22	11.07	92.2					
16H-3, 120-121	145.21	11.29	94.0					
16H-5, 120-121	148.21	10.96	91.3					
17H-1, 121-122	151.72	11.29	94.1					
17H-3, 115-116	154.09	11.35	94.6					
17H-5, 118-119	157.12	10.37	86.4					
18H-1, 121-122	161.22	10.46	87.2					
18H-3, 120-121	164.21	10.58	88.1					
18H-5, 123-124	167.24	11.20	93.3					
19H-1, 68-69	170.19	10.42	86.8					
19H-2, 68-69	171.69	10.10	84.2					
19H-5, 68-69	176.19	10.96	91.3					
20H-1, 72-73	179.73	10.73	89.4					
20H-3, 67-68	182.68	10.71	89.2					
20H-5, 67-68	185.68	10.79	89.9					

Note: IC = inorganic carbon, CaCO<sub>3</sub> = calcium carbonate, TC = total carbon, TOC = total organic carbon, TN = total nitrogen, TS = total sulfur.

**Table T14.** Summary of physical properties measurements conducted at Site 1092.

Measurement	Core 177-1092A-	Core 177-1092B-	Core 177-1092C-	Core 177-1092D-
GRA sample spacing	1H-20H: 2 cm	1H-2H, 3H4-18H: 2 cm; 3H1-3H3: 4 cm	2H4-7H, 9H-15H4: 2 cm; 1H-2H3, 8H, 15H5-18H: 4 cm	1H-3H: 2 cm
MS sample spacing	1H-20H: 2 cm	1H-2H, 3H4-18H: 2 cm; 3H1-3H3: 4 cm	2H4-7H, 9H-15H4: 2 cm; 1H-2H3, 8H, 15H5-18H: 4 cm	1H-3H: 2 cm
NGR sample spacing	1H-7H:2cm; 8H-20H: 4 cm	3H-18H: 4 cm	2H-5H, 9H-14H: 4cm; 15H: 8 cm	—
PWL sample spacing	1H-20H: 2 cm	3H4-18H: 2 cm; 3H1-3H3: 4 cm	2H4-5H, 9H-15H4: 2 cm; 1H-2H3, 15H5-18H: 4 cm	2H-3H: 2 cm
OSU-SCAT sample spacing	1H-20H: 4 cm	1H-18H: 4 cm	1H-3H, 5H, 8H-12H, 14H-18H: 4 cm	2H-3H: 4 cm
PWS3	N = 243	N = 96	—	—
MAD	N = 115	N = 31	—	—
TC	N = 19	N = 11	N = 17	—

Notes: GRA = gamma-ray attenuation, MS = magnetic susceptibility, NGR = natural gamma radiation, PWL = P-wave logger, OSU-SCAT = Oregon State University Split Core Analysis Track, PWS3 = P-wave velocity sensor 3 for split cores, MAD = moisture and density, TC = thermal conductivity.



**Table T15.** Thermal conductivity measurements at Site 1092. (See table note. Continued on next page.)

Core, section, interval (cm)	Depth (mbsf)	Depth (mcd)	TC (W/[m-K])	Start (s)	Length (s)	End (s)
177-1082A-						
1H-4, 75	5.25	7.80	0.795	31.5	30.0	61.5
1H-4, 75	5.25	7.80	0.765	62.0	25.0	87.0
2H-3, 80	11.80	15.42	0.772	45.5	25.0	70.5
2H-3, 80	11.80	15.42	0.747	92.5	25.0	117.5
3H-3, 60	21.10	25.83	0.765	61.0	25.0	86.0
3H-3, 60	21.10	25.83	0.751	68.0	25.0	93.0
5H-3, 55	40.05	45.92	0.758	108.0	25.0	133.0
6H-3, 75	49.75	57.64	1.064	124.5	25.0	149.5
6H-3, 75	49.75	57.64	1.125	84.0	25.0	109.0
7H-3, 75	59.25	67.94	1.148	29.5	25.0	54.5
7H-3, 75	59.25	67.94	1.091	118.5	25.0	143.5
8H-3, 75	68.75	78.20	1.059	41.0	30.5	71.5
8H-3, 75	68.75	78.20	1.026	103.0	25.0	128.0
9H-3, 75	78.20	87.53	1.241	98.0	26.0	124.0
9H-3, 75	78.20	87.53	1.198	103.5	25.0	128.5
10H-3, 75	87.75	98.29	1.127	121.5	25.0	146.5
10H-3, 75	87.75	98.29	1.132	88.0	25.0	113.0
11H-3, 75	97.25	109.74	1.190	38.5	25.0	63.5
12H-3, 75	106.70	119.11	0.989	106.5	25.0	131.5
12H-3, 75	106.70	119.11	0.976	120.0	26.0	146.0
13H-3, 75	116.25	130.47	1.148	101.0	25.0	126.0
14H-3, 75	125.75	141.87	1.211	117.0	26.0	143.0
14H-3, 75	125.75	141.87	1.241	25.0	31.5	56.5
15H-3, 75	135.25	153.49	1.135	88.0	25.0	113.0
15H-3, 75	135.25	153.49	1.156	53.5	25.0	78.5
16H-3, 75	144.75	163.93	1.216	48.0	25.0	73.0
16H-3, 75	144.75	163.93	1.201	78.5	25.0	103.5
17H-3, 75	153.68	171.90	1.155	122.0	25.0	147.0
17H-3, 75	153.68	171.90	1.201	53.0	25.0	78.0
18H-3, 75	163.75	183.60	1.243	87.5	25.0	112.5
18H-3, 75	163.75	183.60	1.284	49.5	29.0	78.5
19H-3, 70	173.20	195.54	1.179	116.0	27.5	143.5
19H-3, 70	173.20	195.54	1.194	54.0	25.0	79.0
20H-3, 70	182.70	205.04	1.125	86.0	25.0	111.0
20H-3, 70	182.70	205.04	1.146	30.0	33.0	63.0
177-1092B-						
3H-3, 75	20.65	21.89	0.801	97.5	25.0	122.5
3H-3, 75	20.65	21.89	0.806	94.5	25.0	119.5
4H-4, 75	31.65	32.86	0.719	77.5	25.0	102.5
4H-4, 75	31.65	32.86	0.691	116.0	33.5	149.5
9H-3, 75	77.10	83.08	1.201	120.0	25.0	145.0
9H-3, 75	77.10	83.08	1.146	76.5	25.0	101.5
10H-3, 90	87.30	94.30	1.164	41.5	25.0	66.5
10H-3, 90	87.30	94.30	1.117	108.5	25.0	133.5
11H-3, 100	96.90	105.39	0.955	72.0	28.5	100.5
11H-3, 100	96.90	105.39	0.963	32.5	26.0	58.5
12H-3, 60	106.00	115.93	1.117	102.5	25.0	127.5
12H-3, 60	106.00	115.93	1.162	27.5	25.0	52.5
13H-3, 60	115.50	126.32	1.116	115.0	25.0	140.0
13H-3, 60	115.50	126.32	1.125	118.5	25.0	143.5
14H-3, 60	125.00	137.92	1.167	51.5	25.0	76.5
14H-3, 60	125.00	137.92	1.087	119.5	30.0	149.5
15H-3, 60	133.42	149.14	1.180	35.5	27.0	62.5
15H-3, 60	133.42	149.14	1.177	34.5	25.0	59.5
16H-3, 60	144.00	159.32	1.222	49.5	30.5	80.0
16H-3, 60	144.00	159.32	1.216	72.0	29.0	101.0
18H-3, 60	163.00	178.91	1.231	101.0	25.0	126.0
18H-3, 60	163.00	178.91	1.231	123.0	25.0	148.0
177-1092C-						
1H-2, 75	2.25	2.25	0.915	73.0	25.0	98.0
1H-2, 75	2.25	2.25	0.956	45.0	25.0	70.0
2H-3, 75	7.75	10.40	0.818	62.0	28.0	90.0
2H-3, 75	7.75	10.40	0.792	108.0	26.0	134.0
3H-3, 75	17.25	18.85	0.716	74.0	28.5	102.5
3H-3, 75	17.25	18.85	0.702	99.0	25.0	124.0

Table 15 (continued).

Core, section, interval (cm)	Depth (mbsf)	Depth (mcd)	TC (W/[m·K])	Start (s)	Length (s)	End (s)
4H-3, 75	26.75	29.98	0.680	105.5	26.5	132.0
4H-3, 75	26.75	29.98	0.676	116.5	25.0	141.5
5H-3, 75	36.25	40.30	0.952	37.5	29.0	66.5
5H-3, 75	36.25	40.30	0.904	110.5	25.5	136.0
7H-3, 75	55.25	60.72	1.137	120.5	29.0	149.5
7H-3, 75	55.25	60.72	1.186	72.5	25.0	97.5
8H-3, 75	64.75	71.06	1.075	47.0	27.5	74.5
8H-3, 75	64.75	71.06	1.049	88.0	33.5	121.5
9H-3, 75	74.25	81.20	1.159	55.0	25.0	80.0
9H-3, 75	74.25	81.20	1.133	79.0	28.0	107.0
10H-3, 75	83.75	91.43	1.095	98.5	25.0	123.5
10H-3, 75	83.75	91.43	1.121	69.5	25.5	95.0
11H-3, 80	92.90	101.40	1.117	87.5	25.0	112.5
11H-3, 80	92.90	101.40	1.119	26.5	25.5	52.0
12H-3, 75	102.75	113.10	1.067	113.0	25.5	138.5
12H-3, 75	102.75	113.10	1.087	116.5	26.0	142.5
13H-3, 75	112.25	123.68	1.086	67.5	25.5	93.0
13H-3, 75	112.25	123.68	1.082	70.5	25.0	95.5
14H-3, 75	121.75	136.57	1.226	43.5	25.0	68.5
14H-3, 75	121.75	136.57	1.232	25.0	27.0	52.0
15H-3, 75	131.25	146.45	1.138	120.5	25.0	145.5
15H-3, 75	131.25	146.45	1.109	114.0	25.0	139.0
16H-3, 75	140.75	159.45	1.127	102.5	26.0	128.5
16H-3, 75	140.75	159.45	1.150	92.5	25.0	117.5
17H-3, 75	150.25	170.13	1.177	109.5	26.0	135.5
17H-3, 75	150.25	170.13	1.217	28.5	25.0	53.5
18H-3, 75	159.75	179.54	1.188	62.5	26.0	88.5
18H-3, 75	159.75	179.54	1.167	109.0	26.0	135.0

Notes: TC = thermal conductivity. Start, Length, and End refer to the interval of the time-temperature series used for the determination of thermal conductivity. This table is also available in ASCII format in the **TABLES** directory.